

**Inhibition of the JAK2-STAT3 pathway using ruxolitinib as a  
therapeutic option for pulmonary hypertension**

**Doctoral thesis**

**For the degree of doctor of natural sciences**

**(Dr. rer. nat)**

**At the Faculty of Biology and Chemistry**

**Of the Justus Liebig University Giessen**

**Submitted by**

**Naga Dinesh Reddy Yerabolu**

**Of**

**Julurpad, India**

**Giessen, November 2020**

From the Institute of Pulmonary Pharmacotherapy

Faculty of Medicine

Justus Liebig University Giessen

Supervisor: Prof. Dr. Ralph Schermuly

First supervisor: Prof. Dr. Reinhard Dammann  
Institute of Genetics  
Justus-Liebig-University Giessen  
Heinrich-Buff-Ring 58-62, 35392 Giessen

Second supervisor: Prof. Dr. Ralph Schermuly  
Professor for Pulmonary Pharmacotherapy  
Justus-Liebig-University Giessen  
Aulweg 130, 35392 Giessen

Examiner: Prof. Dr. Norbert Weissmann  
Medical Clinic II  
Justus-Liebig-University Giessen  
Aulweg 130, 35392 Giessen

Examiner: Prof. Dr. Sandra Hake  
Institute of Genetics  
Justus-Liebig-University Giessen  
Heinrich-Buff-Ring 58-62, 35392 Giessen

Date of oral defense: November 6<sup>th</sup> 2020

## Table of Contents

1.1 PULMONARY HYPERTENSION .....	9
1.2 CLASSIFICATION OF PULMONARY HYPERTENSION .....	9
1.3 PATHOPHYSIOLOGY OF PULMONARY ARTERIAL HYPERTENSION (PAH) .....	10
1.4 MOLECULAR MEDIATORS OF PAH.....	13
1.5 TREATMENT APPROACHES FOR PAH .....	16
1.5.2 PROTEIN KINASE SIGNALING IN PH .....	19
1.5.3 TYROSINE KINASE INHIBITORS .....	21
1.6 JANUS KINASE-SIGNAL TRANSDUCER AND ACTIVATOR OF TRANSCRIPTION (JAK-STAT) SIGNALING PATHWAY .....	21
1.7 ANIMAL MODELS OF PH .....	26
2. AIM OF THE STUDY .....	28
3. MATERIALS AND METHODS .....	29
3.1 MATERIALS .....	29
3.1.1 CHEMICALS AND REAGENTS .....	29
3.1.2 EQUIPMENT.....	30
3.1.3 KITS.....	31
3.1.4 PRIMARY ANTIBODIES.....	31
3.1.5 OLIGONUCLEOTIDES.....	32
3.1.6 HUMAN PULMONARY ARTERY SMOOTH MUSCLE CELLS .....	33
3.2 METHODS .....	37
3.2.1 CELL CULTURE.....	37
3.2.2 TOTAL PROTEIN ISOLATION .....	37
3.2.3 PROTEIN ESTIMATION-BCA ASSAY .....	38
3.2.4 SDS-POLYACRYLAMIDE-GEL ELECTROPHORESIS (SDS-PAGE) AND IMMUNOBLOT .....	38
3.2.5 DENSITOMETRY ANALYSIS.....	40

3.2.6 KINOME PROFILING .....	41
3.2.7 KINOME DATA ANALYSIS.....	41
3.2.8 RNA ISOLATION .....	42
3.2.9 REVERSE TRANSCRIPTION .....	43
3.2.10 QUANTITATIVE REAL-TIME PCR (QRT-PCR).....	44
3.2.11 BROMODEOXYURIDINE (BRDU) INCORPORATION ASSAY .....	44
3.2.12 MEASUREMENT OF CELL CYTOTOXICITY.....	45
3.2.13 CASPASE-GLO 3/7 ASSAY.....	46
3.2.14 XTT-ASSAY .....	46
3.2.15 TRANSWELL MIGRATION ASSAY .....	47
3.2.16 ANIMAL EXPERIMENTS.....	47
3.2.17 ECHOCARDIOGRAPHY .....	48
3.2.18 HEMODYNAMIC AND RIGHT VENTRICULAR HYPERTROPHY MEASUREMENTS.....	49
3.2.19 HISTOLOGY AND PULMONARY VASCULAR MORPHOMETRY.....	49
3.2.20 STATISTICAL ANALYSIS .....	50
4. RESULTS.....	51
4.1 PULMONARY ARTERIAL SMOOTH MUSCLE CELLS (PASMC) FROM PAH-PATIENTS DISPLAY INCREASED JAK ACTIVITY .....	51
4.2 EXPRESSION ANALYSES FOR JAK2-STAT3 SIGNALING IN A HUMAN SPECIMEN AND EXPERIMENTAL MODELS OF PH.....	53
4.3 MOLECULAR ANALYSIS OF THE JAK2-STAT3 SIGNALING AXIS IN HPASMCS.....	56
4.3.2 INHIBITION OF JAK2-STAT3 SIGNALING USING JAK2 INHIBITOR RUXOLITINIB .....	57
4.4 EFFECTS OF RUXOLITINIB ON DOWNSTREAM TARGETS OF JAK2 IN HEALTHY HPASMCS	59
4.5 EFFECTS OF RUXOLITINIB ON IL-6 INDUCED PROLIFERATION OF HUMAN HPASMCS.....	61
4.6 EFFECTS OF JAK2 INHIBITOR RUXOLITINIB ON CYTOTOXICITY OF HUMAN HPASMCS.....	62

4.7 TREATMENT WITH RUXOLITINIB HAS NO EFFECT ON APOPTOSIS AND VIABILITY OF HUMAN PASMCS .....	63
4.8 EFFECTS OF RUXOLITINIB ON IL-6 INDUCED MIGRATION OF HUMAN PASMCS .....	64
4.9 RUXOLITINIB IMPROVES CARDIO-PULMONARY FUNCTIONS IN MCT-INDUCED PAH .....	64
4.10 MCT INDUCED PULMONARY VASCULAR REMODELING IN RATS.....	66
4.11 RUXOLITINIB RESTORES RIGHT VENTRICULAR FUNCTION IN CHRONIC HYPOXIA-INDUCED PH IN MICE .....	68
4.12 CHRONIC HYPOXIA-INDUCED PULMONARY VASCULAR REMODELING IN MICE .....	69
5. DISCUSSION .....	71
5.1 TYROSINE KINASE ANALYSIS OF HUMAN PASMCS.....	72
5.2 EXPRESSION OF JAK-STAT SIGNALING MOLECULES IN HUMAN AND EXPERIMENTAL PH	72
5.3 MOLECULAR ANALYSIS OF JAK2-STAT3 SIGNALING IN HUMAN PASMCS .....	73
5.4 EFFECT OF RUXOLITINIB ON IL-6 INDUCED PROLIFERATION AND MIGRATION OF HUMAN PASMCS .....	73
5.5 EFFECT OF RUXOLITINIB IN EXPERIMENTAL PH MODELS .....	74
6. SUMMARY .....	77
7. ZUSAMMENFASSUNG.....	78
8. REFERENCES .....	79
9. DECLARATION.....	86
10. ACKNOWLEDGEMENTS .....	87

## LIST OF FIGURES

- Figure 1 Clinical classification of pulmonary hypertension.
- Figure 2 Histology of the PAH.
- Figure 3 Emerging targets and therapies for PAH.
- Figure 4 The molecular targets, signaling pathways, and modes of action of approved pulmonary hypertension (PH) therapies.
- Figure 5 Targets of kinase inhibitors for the treatment of PH.
- Figure 6 Overview of JAK activation and regulation.
- Figure 7 Schematic representation of the canonical JAK-STAT signaling pathway.
- Figure 8 Setup of cell culture conditions used to perform peptide-based kinase activity profiling of PASMCs from healthy individuals and IPAH patients.
- Figure 9 Protein expression analyses for JAK2-STAT3 signaling molecules in a HPASMCs.
- Figure 10 mRNA expression of JAK2-STAT3 signaling molecules in HPASMCs and in lung homogenates of experimental PH models.
- Figure 11 Stimulation (by interleukins and PDGF) of JAK2-STAT3 signaling in HPASMCs.
- Figure 12 Targeted inhibition of JAK2-STAT3 signaling by ruxolitinib in HPASMCs.
- Figure 13 Effects of ruxolitinib on downstream targets of JAK2 in healthy HPASMCs.
- Figure 14 Effects of ruxolitinib on IL-6 induced proliferation of HPASMCs.
- Figure 15 JAK2 inhibitor ruxolitinib has not induced cytotoxicity of HPASMCs.
- Figure 16 Treatment with ruxolitinib has no effect on apoptosis and viability of HPASMCs.
- Figure 17 Effects of ruxolitinib on IL-6 induced migration of healthy HPASMCs.
- Figure 18 Effects of ruxolitinib on cardio-pulmonary functions in rats with monocrotaline (MCT) induced PAH.
- Figure 19 Effect of ruxolitinib on vascular remodeling in rats with MCT induced PAH.
- Figure 20 Effects of ruxolitinib on cardio-pulmonary functions in mice with chronic hypoxia (Hox) induced pulmonary hypertension.
- Figure 21 Effect of ruxolitinib on vascular remodeling in mice with Hox induced pulmonary hypertension.
- Figure 22 Schematic representation of the ruxolitinib mode of action in HPASMCs in PAH.

## LIST OF ABBREVIATIONS

ANOVA	Analysis of variance
BSA	Bovine Serum Albumin
BrdU	Bromodeoxyuridine
Bcl-2	B-cell lymphoma 2
cDNA	complementary DNA
Ct	Threshold cycle
CH	Chronic hypoxia
CTEPH	Chronic thrombo embolic pulmonary hypertension
DNA	Deoxyribo nucleic acid
DPBS	Dulbecco's Phosphate Buffer Saline
EC	Endothelial cell
ECM	Extra cellular matrix
EDTA	Ethylene diamine tetra acetic acid
FCS	Fetal calf serum
FGF	Fibroblast growth factor
FITC	Fluorescein iso thiocyanate
GAPDH	Glyceraldehyde 3-phosphate dehydrogenase
HCL	Hydrochloric acid
Hox	Hypoxia
HPASMCs	Human pulmonary artery smooth muscle cells
HRP	Horseradish peroxidase
IGF	Insulin growth factor
IgG	Immunoglobulin
IL-6	Interleukin-6
IPAH	Idiopathic pulmonary arterial hypertension
JAK	Janus activated kinase
MC	Monoclonal
M-PER	Mammalian protein extraction reagent
mRNA	Messenger ribo nucleic acid
MCT	Monocrotaline
PA	Pulmonary artery

PAH	Pulmonary arterial hypertension
PAP	Pulmonary arterial pressure
PASMC	Pulmonary artery smooth muscle cell
PBS	Phosphate buffered saline
PC	Polyclonal
PDGF-BB	Platelet-derived growth factor-BB
PDGFR- $\beta$	Platelet-derived growth factor receptor $\beta$
PCR	Polymerase chain reaction
PIAS	Protein inhibitor of activated STAT
PTK	Protein tyrosine kinase
PTPs	Protein tyrosine phosphatases
PVR	Pulmonary vascular resistance
RIPA	Radio immunoprecipitation Assay
RT	Reverse transcriptase
RT-PCR	Real-time Polymerase Chain Reaction
RNA	Ribonucleic acid
RVSP	Right ventricular systolic pressure
SAP	Systemic arterial pressure
STAT	Signal transducer and activator of transcription
STK	Serine/Threonine kinase
SEM	Standard error of the mean
SYBER	Green Asymmetrical cyanine dye used as a nucleic acid stain in molecular biology
TBS-T	Tris-buffered saline-Tween 20
TYK	Tyrosine kinase
UGMLC	Universities of Giessen and Marburg lung center
VEGF	Vascular endothelial growth factor

## **1. INTRODUCTION**

### **1.1 Pulmonary hypertension**

Pulmonary hypertension (PH) is a complex and chronic progressive disease of the pulmonary vasculature. PH is hemodynamically defined by a mean pulmonary artery pressure (mPAP) of  $\geq 20$  mmHg at rest, with the presence of a pulmonary arterial wedge pressure (PAWP) of  $\leq 15$  mmHg and a pulmonary vascular resistance (PVR)  $> 3$  Wood units (WU), as measured by right heart catheterization [1]. Normally, the pulmonary circulation is a low-pressure system of about 15 mmHg at rest.

PH consists of a group of severe clinical conditions, including pulmonary arterial hypertension (PAH). PAH is characterized by rise in pulmonary artery pressure and pulmonary vascular resistance (PVR) due to an increased vascular remodeling through proliferation, vasoconstriction and inflammation, which progressively leads to right ventricular hypertrophy (RVH), and further resulting in right heart failure and ultimately death [2]. PH has an estimated prevalence of about 1% of the global population [3].

### **1.2 Classification of pulmonary hypertension**

Based on the cause of the disease, the World Health Organization (WHO) provided a classification for PH in 1973 at the first world symposium on PH, to maintain and produce international health information standards. In 1973, the first classification of PH was published and consisted only of 2 groups. These were primary PH and secondary PH, based on the absence or presence of identifiable cause of the disease [4]. A specified classification was announced at the second World Symposium on PH in 1998, held in Evian, France. This classification was based on the new scientific aspects of shared pathophysiological conditions, similar clinical presentation and therapeutic options [1]. Since then, the classification was further refined and has seen multiple revisions, reflecting progress in disease understanding. The current clinical classification of PH was presented in 2018, at the 6<sup>th</sup> World Symposium on PH held in Nice, France [5]. Now it comprises of five groups, as shown in (Figure 1).

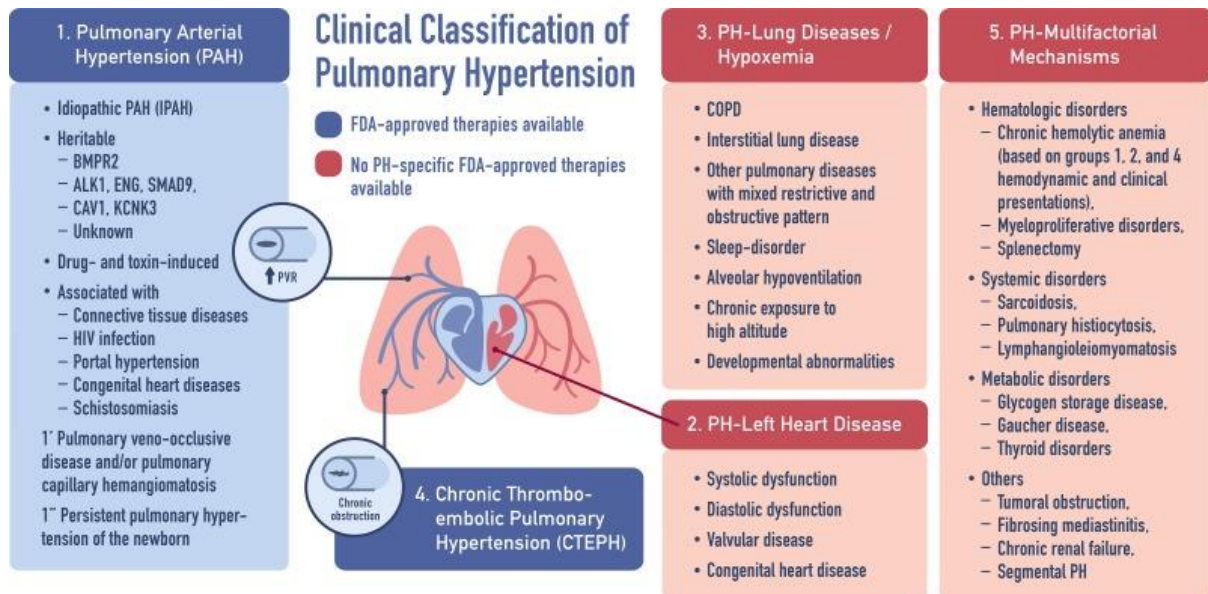


**Figure 1. Clinical classification of pulmonary hypertension.** BMPR2-bone morphogenetic protein receptor 2; PVR-pulmonary vascular resistance; FDA-Food and Drug Administration; COPD-chronic obstructive pulmonary disease [2].

### 1.3 Pathophysiology of pulmonary arterial hypertension (PAH)

The pathobiology of PAH is a multifactorial and involves a complex chain of mutually influencing cellular, molecular and physiological factors, and, despite scientific advances, it is still incompletely understood [6]. The increased pulmonary arterial pressure and vascular resistance are driven by a combination of thrombosis, vasoconstriction, proliferative and obstructive remodeling of small pulmonary arteries [7]. These factors are not exclusive to PAH but are present in most forms of PH [8].

#### 1.3.1 Pulmonary vasoconstriction

Vasoconstriction of pulmonary arteries is an important factor in the pathogenesis of PAH. Vasoconstriction is defined as constriction or narrowing of lumen of the blood vessel. It is a major contributor to PVR and, hence responsible for increased pulmonary arterial pressure (PAP) [9].

Under normal physiological conditions, the balance of endothelium released vasodilators such as a nitric oxide (NO), prostacyclin (PGI<sub>2</sub>), and vasoconstrictors like thromboxane, endothelin-1 (ET-1) is maintained [10].

Excessive vasoconstriction has been associated to endothelial dysfunction. Endothelial dysfunction caused due to inflammation or shear stress, can result in an imbalance of vasoactive mediators i.e. an overexpression of vasoconstrictors and impaired production of vasodilators. A decrease in circulating levels of the vasodilator, i.e. PGI<sub>2</sub>, as compared to

levels of the vasoconstrictor, i.e. thromboxane, has been reported in patients with PAH [11]. Hypoxia mediated pulmonary vasoconstriction plays a key role in high altitude-PH, high-altitude pulmonary edema (HAPE), and contributes to pulmonary hypertension in COPD [12].

### **1.3.2 *In-situ* thrombosis**

Thrombotic lesions are one of the common histopathological representations seen in PAH [13], however its role in PAH remains controversial. Endothelial dysfunction, an imbalance between prothrombotic and antithrombotic mechanisms might contribute to this pathological finding. Tissue factor (TF), a transmembrane glycoprotein, initiates the coagulation cascade through activation of Factor X, resulting in the generation of thrombin. Evidence for elevated thrombin activity by observing increased plasma levels of fibrinopeptide A (a byproduct and marker of fibrin generation) and plasminogen activator inhibitor 1 (PAI-1) (an inhibitor of fibrinolytic cascade) have been reported in IPAH patients [14]. Von Willebrand factor (vWF) is a protein which facilitates the interaction of platelets with endothelial cells and elevated activity has been reported in patients with IPAH [14]. The thrombotic lesions in pulmonary vasculature are present in all forms of PH. However, these lesions have never been associated with the severity of PH [15].

### **1.3.3 Pulmonary vascular remodeling**

Pulmonary vascular remodeling is a predominant pathological feature of PAH [16]. Remodeling is characterized by the structural changes involving all three layers of the pulmonary arterial wall that lead to adventitial proliferation and medial hypertrophy, intimal hyperplasia and plexiform lesions [17]. Under normal conditions, a fine balance between apoptosis and proliferation of PAEC, PASMC, and fibroblasts is maintained. In PAH, this balance is disturbed in favor of proliferation, results in thickening and narrowing of the pulmonary arterial wall and eventually obliteration of vessel lumen, and leading to elevated PVR [7]. Intimal lesions made up of eccentric intimal thickening, and fibrotic, concentric and plexiform lesions [18].

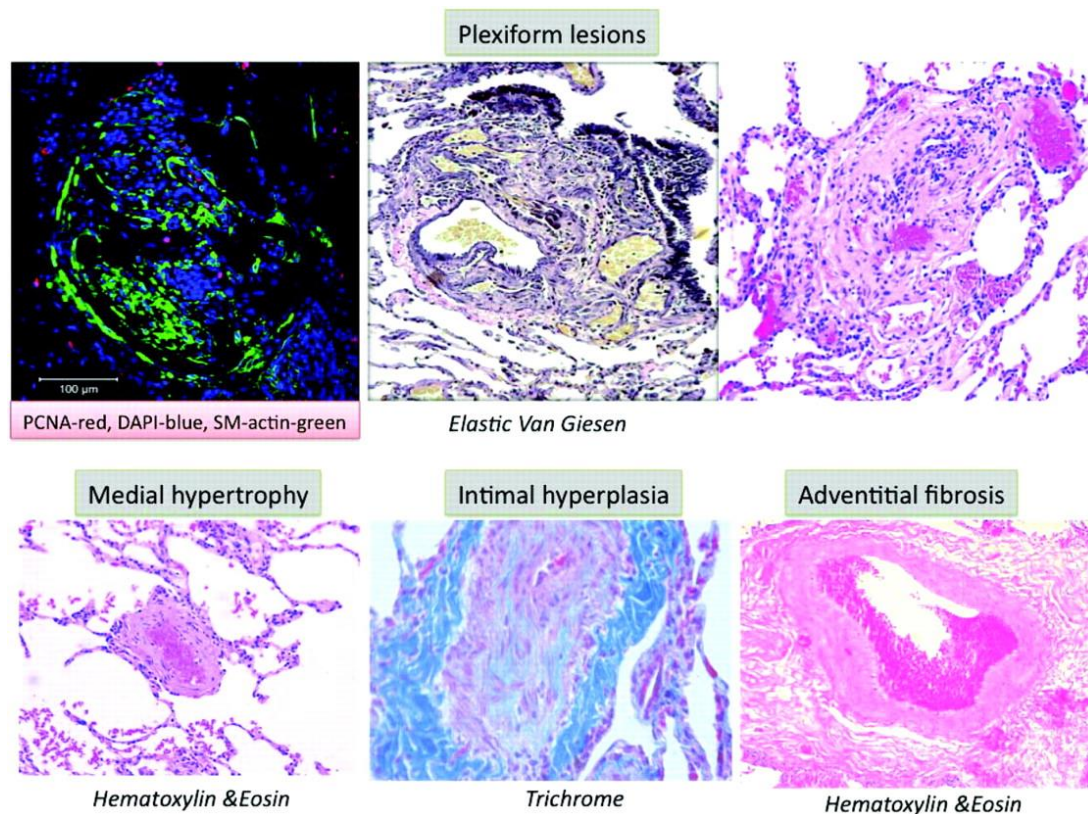


**Figure 2. Histology of the PAH.** Top: Plexiform lesions. Upper Left: Evidence of cell proliferation (red is proliferating cell nuclear antigen [PCNA], green is smooth muscle [SM] actin, and blue is DAPI). Bottom: Medial hypertrophy, intimal fibrosis, and adventitial proliferation [19].

### Intimal lesions

The intimal layer represents an endothelial cell-thick interface between the muscular media and the flowing blood. Intimal lesions account for most of the reduction of the luminal area of small pulmonary arteries and therefore influence the overall pulmonary vascular resistance [17]. Cells involved in intimal thickening show properties of SMC, fibroblasts, and myofibroblasts. Additional intimal lesions are characterized by excessive extracellular matrix deposition. Plexiform lesions are characteristic of IPAH morphology formed by the disorganized proliferation of endothelial cells. These are generally located at branching points of muscular arteries [18].

### Medial hypertrophy

The media layer composed mainly of smooth muscle cells. Medial hypertrophy is an important pathological feature of PH. It involves muscularized arteries (ranging between 70 and 500 µm in diameter), and precapillary vessels (below 70 µm in diameter) [18]. Medial thickening in previously muscularized vessels is caused by hypertrophy and hyperplasia of the existing SMCs [17]. Furthermore, SMCs and fibroblasts contribute to vascular remodeling

by an increase in proliferation, reduced apoptosis and formation of the extracellular matrix. The origin of SMCs which form the new media is not clear; however, it's believed to be derived from epithelium to mesenchymal transition and migration of adventitial fibroblasts present in the vessels [20].

### **Adventitial proliferation**

The adventitia layer is mostly composed of fibroblasts. The recent reports indicating that adventitia may play an important role in the regulation of pulmonary vascular function, apart from structural support for pulmonary vessels [21]. Adventitia thickening and infiltration of the adventitia layer by inflammatory cells are noted in animal models of hypoxia [20]. In hypoxia models of PH, the earliest and most significant structural changes are noted in the adventitial layer of the vascular wall, which further causes remodeling of intimal and medial layers [17, 21]. It has been proved that the heterogeneous population of pulmonary artery adventitial fibroblasts, can proliferate and release numerous cytokines and chemokines enable recruitment of inflammatory cells and differentiate into myofibroblasts in response to environmental stress such as hypoxia [21].

## **1.4 Molecular mediators of PAH**

Various pathological processes such as pulmonary vasoconstriction, followed by pulmonary arterial remodeling, growth factors and inflammation shown to contribute to the development and disease progression of PAH.

### **1.4.1 Vascular tone modulators and enhancers**

Imbalance in the synthesis of various endothelial vasoactive mediators, such as prostacyclin, nitric oxide, vasoactive intestinal peptide, endothelin-1, serotonin, thromboxane, etc. has been associated with the development of PAH by promoting vasoconstriction and vascular remodeling.

#### **Prostacyclin**

Prostacyclin (prostaglandin I<sub>2</sub>) is a very important endogenous pulmonary vasodilator synthesized by vascular endothelial cells [22]. Prostacyclin decreases platelet aggregation and inhibits vascular smooth muscle cell proliferation [23]. Prostacyclin production is decreased in endothelial cells from patients with PAH. This impaired synthesis is attributable to the reduction of prostacyclin synthase expression in small and medium-sized pulmonary arteries [16]. Prostacyclin was the first effective drug for the treatment of PAH.

### **Nitric oxide (NO)**

NO is a potent pulmonary vasodilator synthesized in endothelial cells by endothelial NO synthase (eNOS or NOS3) [23]. It exerts the vasodilatory and anti-proliferative effects by stimulation of soluble guanylate cyclase (sGS) to produce cyclic guanosine monophosphate (cGMP) in PSMCs [16]. It inhibits the proliferation of vascular smooth muscle cells. In patients with all forms of PH, reduced NO synthase expression reported in pulmonary endothelial cells [23]. NO, in particular, NOS3 plays an important role in the pulmonary circulation.

### **Vasoactive intestinal peptide (VIP)**

VIP, a neuropeptide primarily functioning as a neurotransmitter, acts as a potent pulmonary vasodilator and inhibitor of vascular smooth muscle cell proliferation as well as anti-apoptotic agent [23]. Low serum concentrations and reduced VIP immunoreactivity were reported in pulmonary arteries from IPAH patients [16].

### **Endothelin-1 (ET-1)**

ET-1 is a potent vasoconstrictor peptide. It is produced by the endothelial cells. ET-1 promotes smooth muscle cell proliferation and inflammation [9]. ET-1 activates via 2 GPCRs namely ET<sub>A</sub> and ET<sub>B</sub>. Both these receptors cause vasoconstriction in SMCs whilst in ECs, ET<sub>B</sub> releases vasodilation [24]. Hence, blockade of both ETA and ETB receptors are necessary to counteract the pathological alterations in this pathway in PH. ET-1 has been found to play a key role in vascular remodeling and pathophysiology of PAH [23].

### **Serotonin (5-Hydroxytryptamine, 5-HT)**

5-HT causes vasoconstriction and remodeling in PSMCs and pulmonary fibroblasts. It is produced by pulmonary artery endothelial cells [23]. 5-HT activates via serotonin transporter (5-HTT) and receptors. In patients with PAH, increased circulating levels of 5-HT and increase expression of 5-HTT are reported [25].

### **Thromboxane (TXA2)**

TXA2 is a vasoconstrictor and stimulates platelet aggregation. In IPAH patients, elevated urinary levels of a stable metabolite of TXA2 and increased total body synthesis of TXA2 observed [9]. This suggests that TXA2 may play a role in the development of vasoconstriction and vascular remodeling in patients with IPAH.

### **1.4.2 Pro-proliferative vasoactive mediators**

#### **PDGF**

PDGF acts as potent mitogen and chemoattractant for PSMCs and exerts their functions via PDGFR  $\alpha$ , PDGFR  $\beta$  receptors [23]. In PAH patients, the increased expression of PDGF and its receptors has been reported [26]. Additionally, increased activity of PDGFR  $\beta$  has been demonstrated in animal models of PAH, contributing mainly to the hyper proliferative and migratory phenotype of PSMCs [26]. In two animal models of PH, MCT, and hypoxia-induced, imatinib was found to dose-dependently reversed pulmonary hypertension [27].

#### **Other growth factors**

Various other growth factors are involved in the vascular remodeling and pathogenesis of PAH. Growth factors act as a potent mitogen for vascular cells and activate the tyrosine kinase receptors. Activation of these receptors leads to the initiation of complex intracellular signaling mechanisms causing cell proliferation, migration and apoptotic resistance [13].

TGF- $\beta$  superfamily consists of a big number of growth factors that control various cellular functions such as proliferation, migration, synthesis, and degradation of the extracellular matrix. Implications in members of TGF  $\beta$  family; BMPR2, ALK1, endoglin have been associated with the pathogenesis of PAH [13]. In patients with PH, increased expression of VEGF and its receptor has been reported in plexiform lesions [18].

Elevated urinary and plasma levels of basic FGF have been found in PAH patients. Recent studies demonstrate that pharmacological inhibition of FGF receptor 1 is a potential therapeutic target [23].

### **1.4.3 Inflammation**

Inflammation is an important component of the immune response to infectious agents. The presence of inflammatory cell infiltrates mainly consists of macrophages, dendritic cells, T and B cells are observed in most forms of PAH indicating an important role of pro-inflammatory cytokines and chemokines in the pathogenesis of PAH [28]. Lung vascular cells recruit the inflammatory cells by producing inflammatory mediators like cytokines and chemokines in response to inflammation and infection [29].

## **Cytokines**

Cytokines comprise a large group of signaling proteins that interact in an autocrine, paracrine and endocrine manner. Cytokines are produced and secreted by various vascular and immune cells [29]. Cytokines are classified as TNFs, ILs, IFNs, CSFs, TGFs, lymphokines and monokines [29]. Increased concentrations of circulating cytokines, TNFs, IL-1 $\beta$  and IL-6 are reported in patients with IPAH. Furthermore, overproduction of IL-6 in animal models of PAH, monocrotaline and chronic hypoxia suggests the potential role of IL-6 in the pathogenesis of PAH [13]. Elevated levels of IL-6 have been shown to contribute to vascular remodeling by activating the proliferation of PSMCs [28].

## **Chemokines**

Chemokines play a key role in the various steps of leukocyte recruitment like rolling, activation, adherence, and extravasation into the inflamed tissue [13]. A unique chemokine, Fractalkine (CX3CL1) detected at the membrane of ECs, may play a role in the recruitment of leukocytes expressing chemokine (C-X3-C motif) receptor 1 (CX3CR1) in the lungs of PAH patients. Other chemokines like CCL2, CXCL3, RANTES (CCL5), CXCL10 upregulated in IPAH patients [28].

## **1.5 Treatment approaches for PAH**

Pulmonary hypertension is a complex disease characterized by vascular remodeling and currently, the disease remains incurable. However, an advanced understanding of the disease mechanisms has resulted in the development of new therapies targeting specific abnormal signaling pathways. Currently, there are five classes of agents approved by the FDA for the treatment of PAH: ERAs bosentan, macitentan, and ambrisentan; PDE-5 inhibitors sildenafil, tadalafil; soluble guanylate cyclase stimulator riociguat; prostacyclin analogs epoprostenol, treprostinil, and iloprost; prostacyclin IP receptor agonist selexipag [30]. These medications have shown improvement in PAH management by targeting three main signaling pathways that are involved in the control of vascular cell proliferation and vascular tone. These are Prostacyclin, endothelin 1, and nitric oxide (NO) pathways. The treatment strategy for PAH has changed significantly over the last decade.

Current data indicate that combination therapies might delay disease progression and improve outcomes [24]. Several other drugs targeting novel signaling pathways are under investigation such as receptor tyrosine kinase inhibitors and serotonin.

# Emerging Targets & Strategies for the Treatment of PAH

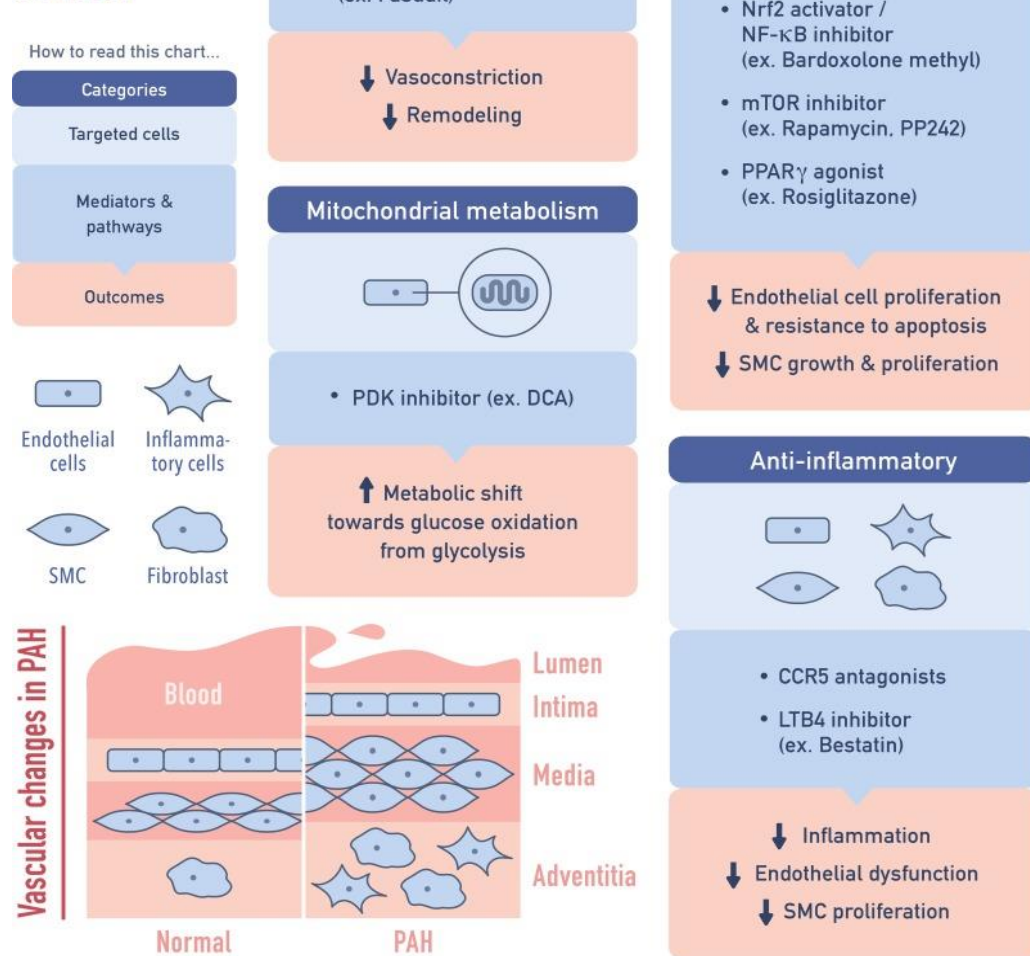


**Figure 3. Emerging targets and therapies for PAH.** TGF-β, transforming growth factor-β; SMC, smooth muscle cells; LTB4, leukotriene B4; mTOR, mammalian target of rapamycin [2].

## 1.5.1 Currently available therapies

### ERAs

ET-1 is a potent vasoconstrictor and contributes to PSMCs proliferation. ET-1 is produced by endothelial cells and expression level is increased in PAH patients [30]. Bosentan was the first orally non-selective ERA approved for the treatment of PAH and it targets both receptors ET<sub>A</sub> and ET<sub>B</sub>. However, abnormal liver function is the common side effect induced

by bosentan. Ambrisentan is an orally selective antagonist for the ET<sub>A</sub> receptor. Despite the receptor selectivity data did not show a significant difference in ambrisentan efficacy [31]. Macitentan is a novel ERA like bosentan, targets ET<sub>A</sub> and ET<sub>B</sub> receptors. A phase 3 clinical trial reported that macitentan was not associated with liver function abnormalities [24].

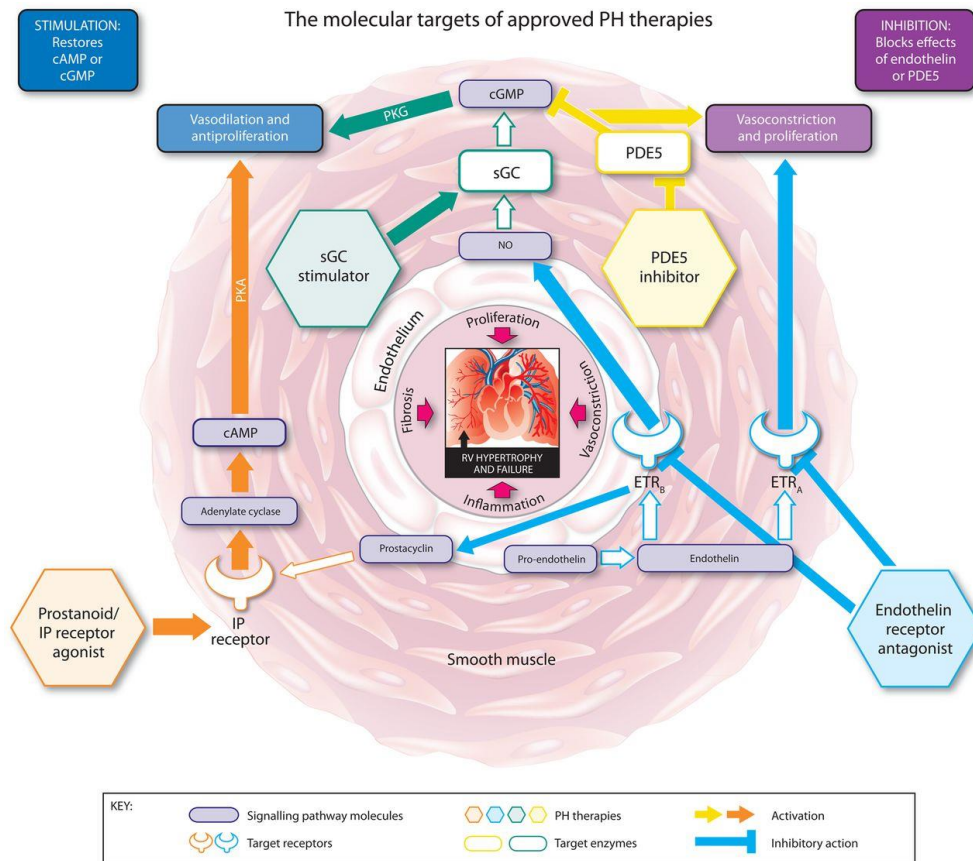


**Figure 4. The molecular targets, signaling pathways, and modes of action of approved pulmonary hypertension (PH) therapies.** cAMP, cyclic adenosine monophosphate; cGMP, cyclic guanosine monophosphate; ETR<sub>A</sub>, endothelin receptor A; ETR<sub>B</sub>, endothelin receptor B; IP, prostacyclin; NO, nitric oxide; PDE5, phosphodiesterase type 5; PKA, phosphate kinase A; PKG, cGMP-dependent protein kinase; sGC, soluble guanylate cyclase [31].

### PDE-5 inhibitors

PDE-5, an enzyme highly expressed in the vascular smooth muscle cells, inactivates cGMP and upregulated in the PAH patients [31]. PDE-5 inhibitors bind to the catalytic domain of this enzyme and increase the levels of cGMP and contribute to the anti-proliferative and vasodilatory effects of endogenous NO. Therefore, PDE-5 inhibitors like Sildenafil and tadalafil initially approved for the treatment of erectile dysfunction has evaluated as potential drug therapy for the management of PAH [32]. Tadalafil is structurally different

from sildenafil and longer half-life (17.5 hrs.), allows for once-daily dosing, while three times a day for sildenafil [30].

### **Soluble guanylate cyclase stimulator (sGC)**

sGC is a catalytic enzyme, expressed mainly in the VASMCs [31]. sGC mediates the conversion of GTP to cGMP by binding to NO, promotes vasodilation and inhibition of smooth muscle cell proliferation. Riociguat is the first oral sGC stimulator approved for the treatment of both PAH and CTEPH [30]. Riociguat has a dual mode of action, stabilizes the NO-sGC complex and can also directly stimulate sGC to promote cGMP production independent of NO [32].

### **Prostanoids**

The prostanoid drugs are synthetic forms of prostacyclin, developed to replace the endogenous prostacyclin that is reduced in PH patients. Prostacyclin is a potent vasodilator and produced by endothelial cells. Prostanoids' main target is the receptor of prostacyclin (IP), activation of which results in the production of cAMP from ATP and vasodilation [31]. Intravenous Epoprostenol was the first PAH targeted therapy approved by the US FDA. Due to some shortcomings, such as short half-life and lack of stability, new prostacyclin analogs were developed with a longer half-life and various routes of administration. They include: treprostinil (4.5 hrs.), iloprost and beraprost can be administered via intravenous, subcutaneous, orally or inhalation in patients with PAH [30].

### **Selexipag**

Selexipag is a novel agent, highly selective non-prostanoid IP receptor agonist. Selexipag might reduce the side effects associated with prostanoid therapy. It is approved for the treatment of PAH by FDA in 2015 [30].

## **1.5.2 Protein Kinase signaling in PH**

The human protein kinome contains 518 members and constitute about 1.7% of the human genome [33]. PTKs are enzymes that regulate the biological activity of proteins by phosphorylation of specific amino acids with ATP as the source of phosphate, which results in conformational change from an inactive to an active form of the protein [33]. The PTKs are classified into 3 main types, based on the amino acid side chain that they phosphorylate:

1. Tyrosine kinases (TKs)- Receptor and non-receptor TKs
2. Serine-threonine kinases (STKs)

### 3. Histidine kinases

The overexpression, dysregulation and mutations of PTKs play an important role in the pathogenesis of many diseases including pulmonary hypertension, cardiovascular, inflammatory, and as well as cancers [34]. Kinases have become one of the key drug targets in the past 20 years.

As discussed in section 3.1 and 3.2, growth factors signal via their respective receptors and initiate kinase-dependent signaling events [35]. Thereby, leading to an increased proliferation, resistance to apoptosis and metabolic changes in various vascular cell types including PSMCs, ECs and Fibroblasts [36]. The FDA has approved 52 small molecule protein kinase inhibitors as of June 2020. This demonstrates that the field of protein kinases and its inhibitors is a major research area in industry as well as in academic research. Rise in protein kinase research paralleled by the development of screening technologies dedicated to the evaluation and profiling of the candidate kinase inhibitors. A brief pictorial summary of the main signaling pathways targeted by kinase inhibitors in PH is given in Fig. 5.

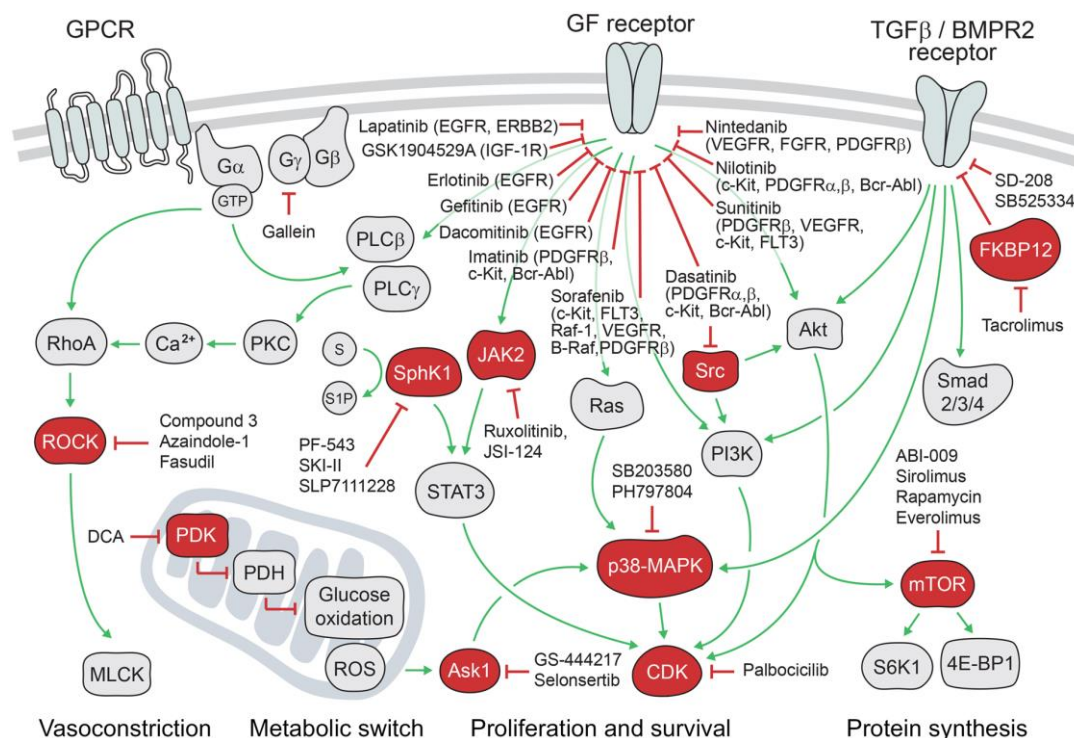


**Figure 5. Targets of kinase inhibitors for the treatment of pulmonary hypertension.** Kinases for targeted inhibition are represented in red and other intracellular signaling proteins are colored in grey. Membrane receptors are highlighted in beige. Colored connections reflect activating protein-protein interaction (green) or blockage of protein function (red) [37].

### 1.5.3 Tyrosine kinase inhibitors

Currently available therapies as well as above mentioned emerging treatment approaches for the treatment of PAH mainly focus on vasodilation. The role of growth factors in the pulmonary vascular remodeling indicates that inhibition of tyrosine kinase receptor might be a potential anti-proliferative approach in PAH [38]. The kinase inhibitors interfere with the kinase activity in the pulmonary vasculature which results in reduction of proliferation, vasoconstriction and inflammation which then promotes the reversal of the vascular remodeling process. RTKs such as PDGFR $\beta$  and Janus kinases (JAKs) have been involved in the pathogenesis of PAH in humans and in animal models of PH (as discussed in section 3.2 Pro-proliferative vasoactive mediators). Imatinib is an orally selective tyrosine kinase inhibitor of RTK BCR-ABL, c-kit, PDGFR $\alpha$ , and PDGFR $\beta$ . Imatinib is approved for the treatment of chronic myeloid leukemia (CML), gastrointestinal stromal tumor and myeloproliferative disorders [26]. Imatinib therapy was shown to reverse the experimental pulmonary hypertension via blocking PDGFR $\beta$  signaling in both *in vitro* and *in vivo* studies, supporting the rationale for a potential therapeutic role of imatinib [27, 34]. This proof of concept study has led to exploring the use of receptor tyrosine kinase inhibitors (RTKs) in PAH.

### 1.6 Janus kinase-signal transducer and activator of transcription (JAK-STAT) signaling pathway

Various growth factors, cytokines, and chemokines utilize the JAK-STAT pathway to transduce extracellular signals to the nucleus [39]. The JAK-STAT pathway activation leads to stimulation of cellular functions like proliferation, migration, and apoptosis [40]. JAKs were discovered in the early 1990s during the study related to interferon signaling in human cells [41]. JAKs belong to a class of protein tyrosine kinases (PTK) and evolutionarily conserved across species. In mammals, JAK family consists of 4 members, JAK1, JAK2, TYK2, which are ubiquitously expressed and JAK3, which is mainly expressed in cells of hematopoietic origin [42]. JAKs are relatively large proteins with a size of 120-140 KDa. The basic structural organization of JAKs made up of 4 structural domains consists of 7 homologous regions (JH1-7). Catalytically active kinase domain (JH1) is required for the JAK activation and target of the JAK inhibitors developed so far. Pseudo kinase domain (JH2) has been thought to play a role in regulatory function. Both JH1 and JH2 located at c-terminus. SH-3 domain (JH3-JH4)

mainly associated with stabilizing the structural confirmation. N-terminus FERM domain (JH5-JH7) is primarily involved in receptor association [43].

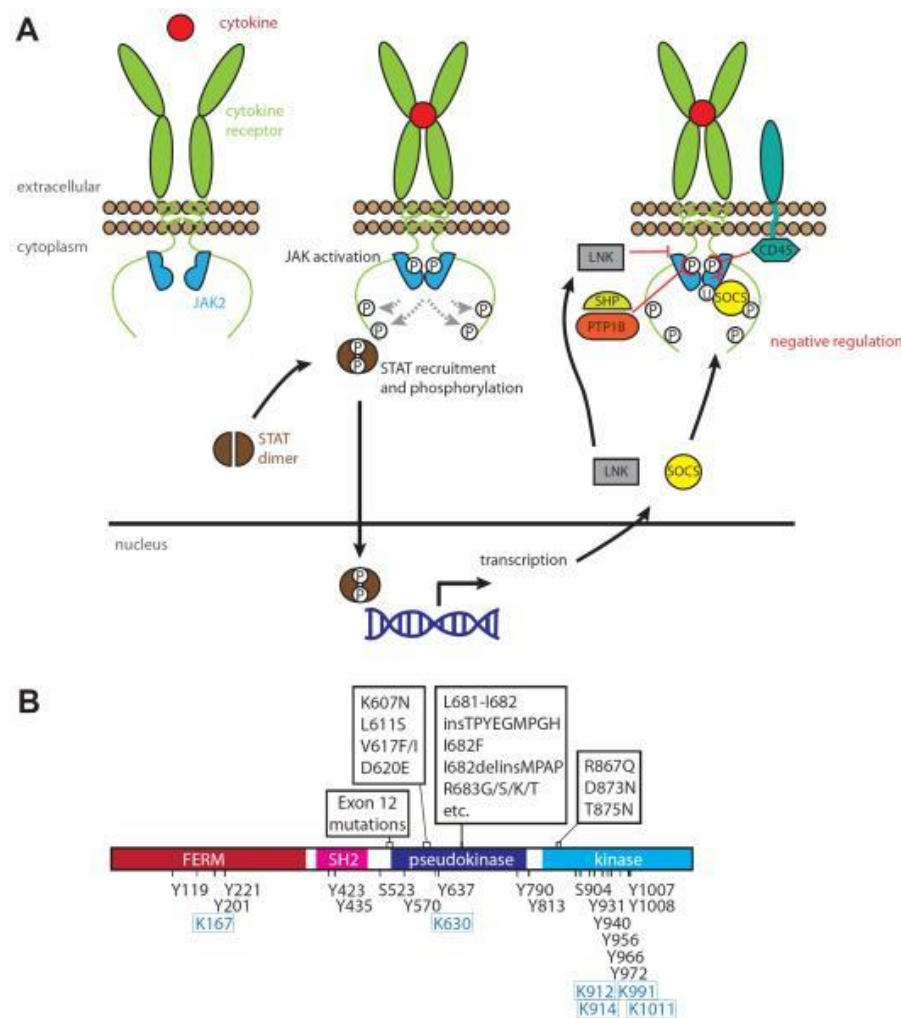


**Figure 6. Overview of JAK activation and regulation.** (A) Summary of the JAK-STAT signaling pathway and its negative regulation. Activated JAK is characterized by phosphorylation of activation loop residues within its kinase domain (encircled P; middle). Negative regulation (right), including phosphatases (CD45, PTP1B, SHP1 and SHP2) and SH2 domain containing regulators from the LNK and SOCS families. (B) The human JAK2 domain structure. Mutational sites associated with myeloproliferative neoplasms are annotated above. Residues subject to phosphorylation and sumoylation are annotated below in black text and blue boxed text, respectively [44].

STATs are classic transcription factors and main downstream targets of JAKs. STATs were discovered in 1992 and 7 family members (STAT 1-4, STAT5A, STAT5B and STAT6) were found in mammals [45]. The structural domain of STATs includes an amino-terminal, a coiled-coil, a DNA binding domain, a linker, SH2 domain, and a transcriptional activation domain. The highly conserved SH2 domain is a target of patented STAT inhibitors [45]. The linker and DBD located at the center, whereas TAD is located at the c-terminus and

undergoes serine phosphorylation and contributes to increasing transcriptional activity [46]. The JAK-STAT pathway consists of two intracellular subunits – the canonical and non-canonical part. The canonical JAK-STAT pathway is activated by the binding of an extracellular ligand (e.g. IL-6) to transmembrane receptors (e.g. gp130 homodimers), this leads to the dimerization of receptor subunits. This dimerization brings the two JAKs into close proximity and allows trans-phosphorylation of JAKs [43, 47]. These activated JAK complex, further phosphorylate and dimerize STAT proteins and subsequent translocation to the nucleus to initiate the transcription of target genes, such as Bcl-2, Cyclin D1, c-Myc, VEGF [48, 49]. In addition to the activation of canonical pathway, dimerization of IL-6 type cytokine receptors lead to the initiation of MAPK cascade, PI3k signaling, and activation of ERK 1/2 [47]. The canonical JAK-STAT pathway plays an important role in development and human diseases [50]. In non-canonical JAK-STAT signaling mode, JAKs regulate the transcription in the nucleus independently of STATs and unphosphorylated STATs in the nucleus maintains the genome stability in association with heterochromatin protein 1 (HP1) [51, 52]. The JAK-STAT pathway is inactivated by negative regulators such as SOC, PIAS, and PTPs.

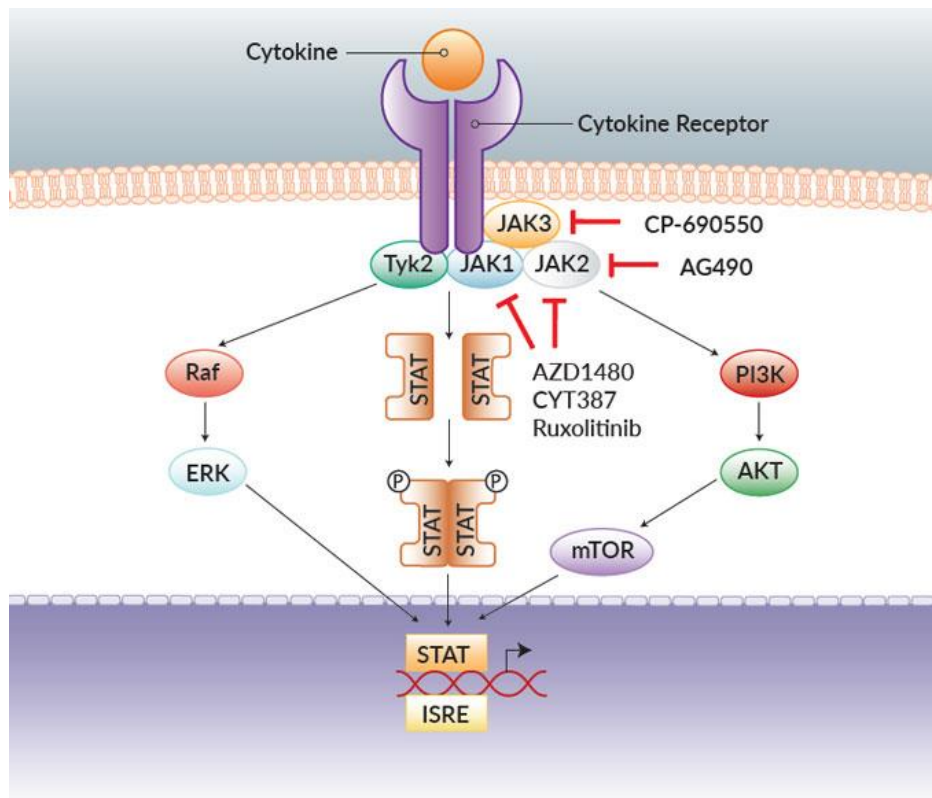


**Figure 7. Schematic representation of the canonical JAK-STAT signaling pathway.**  
(www.invivogen.com)

### 1.6.1 JAK-STAT signaling in human disease

The implications of JAK-STAT signaling and the continuous activation of STAT3 and STAT5 on tumor cell proliferation, survival, and invasion were demonstrated many years ago and have made the JAK-STAT pathway a potential target for drug development and cancer therapy [53]. This idea was further reinforced by the discovery of additional functions of STAT signaling in cancer [54]. Polymorphisms and mutations in JAK and STAT genes have been associated with several human diseases such as myelofibrosis, polycythemia Vera, essential thrombocythemia, etc. [43]. JAK1 and JAK2 with loss of function mutations are embryonically lethal in mice and mutations of JAK3 and TYK2 cause primary immunodeficiency in patients with immunodeficiencies [55]. A hyper-activation of STAT5 and its role in many hematopoietic tumors and chronic myeloid leukemia (CML) were reported [56]. The role of STAT3 in inflammation and cancer is extensively studied [57].

### **1.6.1.1 JAK-STAT signaling in vascular disease**

It is well established that growth factors and cytokine driven cellular events play an important role in the development of vascular diseases. Hence, increased level of circulating IL-6 can be observed in PAH patients [58].

#### **Atherosclerosis**

The elevation of pro-inflammatory cytokines like IL-1, IL-6, and TNF- $\alpha$  was reported in inflammatory diseases such as atherosclerosis. IL-6 is induced by Ang II through JAK-STAT signaling which is believed to play a key role in the pathogenesis of cardiovascular diseases [59].

#### **Pulmonary hypertension**

JAK-STAT signaling activates in response to growth factors such as PDGF and pro-inflammatory cytokines such as IL-6. The synthesis of these factors was dysregulated in PAH and their levels were elevated in the serum of patients with PAH [60]. The increased expression of JAKs mRNA has been reported in hypoxia-induced PAH rats [61]. The activity of JAK2 has been found by a microarray study in PAH associated with autoimmune disease [62]. The role of JAK2-STAT3 has been described in IPF patients with PAH [36]. The role of JAK-STAT, especially in the context of proliferative and anti-apoptotic phenotype, has been demonstrated and many downstream targets of the pathway have been identified. Overexpression of Pim-1 and survivin is associated with PSMCs proliferation in vascular remodeling and plays a major role in the pathogenesis of PAH [63, 64].

### **1.6.2 Targeting the JAK-STAT pathway**

A growing body of literature supports the role of JAK-STAT signaling in several diseases including PAH, which has led to an increased interest in therapeutic exploitation of the pathway. Many small molecule inhibitors are available to block the signaling at different levels. JAK is an upstream protein of STAT; hence JAK family members have been more popular drug targets than STATs [65]. In particular, JAK2-STAT3 suggests being the most popular drug targets in the treatment of cancer [66]. At present 3 JAK inhibitors; ruxolitinib, tofacitinib, baricitinib have been approved by the USA FDA for clinical use.

#### **Ruxolitinib**

Ruxolitinib (INCB018424) is a potent small-molecule inhibitor of both JAK1 and JAK2 with an IC<sub>50</sub> of 3.3 and 2.8nm respectively [67]. It is the first JAK kinase inhibitor approved by the FDA in 2011 for the treatment of myelofibrosis and in 2014 for polycythemia Vera [50].

Ruxolitinib has an equal inhibitory effect on both mutant (JAK2V617F) and wild-type JAK2. Ruxolitinib blocks the JAK activity by targeting the ATP-binding catalytic site of the kinase domain [66]. The pharmacokinetics of ruxolitinib was demonstrated in healthy volunteers and showed good oral bioavailability and a 3 hours plasma half-life [68]. Ruxolitinib can be administered orally at 25mg twice a day and 100 mg once a day [69]. The pharmacodynamics studies showed a dose and time-dependent inhibition of p-stat3 observed with ruxolitinib treatment [70]. The adverse effects associated with ruxolitinib treatment are neutropenia and thrombocytopenia along with more common side effects such as headache, fatigue, and nausea [71].

## **1.7 Animal models of PH**

The use of experimental animal models has contributed to a better understanding of underlying pathophysiological mechanisms of the pulmonary hypertensive process. Various animal models of PH are available to the researchers. The monocrotaline injury model and chronic hypoxia model are the commonly used animal models of PH. The animal models played an important role in discovery and testing of the possible therapeutic approaches.

### **1.7.1 Monocrotaline (MCT) induced PAH model**

MCT model is the oldest model used in the field of PAH, it was first described in laboratory rats over 40 years ago [72]. MCT is a toxic pyrrolizidine alkaloid found in the plant *Crotalaria Spectabilis*. MCT is injected once subcutaneously or intraperitoneally to induce PAH in rats. It is known that injected MCT is metabolized in liver by cytochrome P450 to the active form MCT pyrole [73]. Severe PH develops within a few days, followed by increased PAP and pulmonary vascular remodeling. Although the exact mechanism of MCT induced PAH is unknown, it is speculated that direct endothelial damage causes the development and progression of PH [73]. Response to MCT varies among strains and species of animals. Rats are the preferred species of choice for MCT induced PH, showing consistent and predictable response, and mice exhibited varied results to the effects of MCT.

### **1.7.2 Chronic hypoxia model of PH**

Normo- and hypo-baric hypoxia are frequently used to induce PH in wide variety of animal species [72]. Rats and mice are commonly used species in hypoxic model of PH.

In contrast to the MCT model, hypoxia induced PH is associated with very similar structural changes in most of the animals investigated so far [74]. Exposure of mice to chronic hypoxia results in increase in PAP and associated with minimal vascular remodeling. The common pathological observations are muscularization of previously non-muscularized walls and a moderate medial thickening of muscular resistance walls [74]. The main limitation of the hypoxia mice model is that hypoxia induced PH is reversed once the animals are exposed to normal oxygen concentrations [72].

## 2. AIM OF THE STUDY

Despite the scientific advances in the field of pulmonary hypertension, the available therapies can only improve the patient's symptoms and quality of life but cannot cure the disease. PH has an estimated prevalence of about 1% of the global population. In the pulmonary vascular system, cytokine driven JAK-STAT signaling regulates various processes of vascular remodeling including proliferation, migration, and apoptosis of pulmonary vascular smooth muscle cells. Hence, we hypothesized that JAK-STAT signaling especially the JAK2-STAT3 signaling pathway may be involved in the pathogenesis of PAH. The main focus of the work presented in this thesis is to investigate the role of JAK2-STAT3 signaling in PH which could be further subdivided into the following aims:

- Kinase analysis of HPASMCs from healthy individuals and patients with IPAH.
- Expression profiling of JAK2-STAT3 signaling components in HPASMCs from healthy individuals and IPAH patients.
- Study the expression profile of JAK2-STAT3 signaling components in the lungs isolated from different animal models of PH.
- Investigating the effect of ruxolitinib on cellular functions of HPASMCs *in vitro*.
- Investigating the effect of ruxolitinib on cardio-pulmonary functions in different animal models.

### 3. MATERIALS AND METHODS

#### 3.1 MATERIALS

##### 3.1.1 Chemicals and Reagents

Reagent	Manufacturer
Acrylamide/Bisacrylamide Solution (30%; 37,5:1)	Roth, Germany
Ammonium persulfate (APS)	Sigma-Aldrich, USA
Agarose	Roth, Germany
Bromophenol blue	Merck, Germany
Bovine serum albumin (BSA)	Roth, Germany
Chloroform	Roth, Germany
DAPI	Invitrogen, USA
Dimethylsulfoxide (DMSO)	Sigma-Aldrich, USA
DNA ladder (100bp,1Kb)	New England Biolabs, USA
Ethylenediamine tetraacetic acid (EDTA)	Roth, Germany
Ethanol	Roth, Germany
Fluorescence mounting medium	Dako, USA
Halt protease & phosphatase inhibitor cocktail	Thermo Scientific, USA
Methanol	Roth, Germany
Glycine	Roth, Germany
Mammalian protein extraction reagent (M- PER)	Thermo Scientific, USA
Milk powder	Roth, Germany
Nitrocellulose membrane	Roth, Germany
Pageruler prestained molecular weight marker	Thermo Scientific, USA

RIPA lysis buffer	Thermo Scientific, USA
Sodium Dodecyl Sulfate (SDS)	Roth, Germany
SYBR Green Supermix	BioRad, USA
Staurosporine	Millipore, USA
Stripping buffer	Thermo Scientific, USA
N´N´N´N Tetramethylethyldiamine (TEMED)	Sigma-Aldrich, USA
Tris-Base	Sigma-Aldrich, USA
Tween 20 (Polyoxyethylenesorbitan monolaurate)	Sigma-Aldrich, USA
Triton X-100	Sigma-Aldrich, USA
Trizol reagent	Sigma-Aldrich, USA

### 3.1.2 Equipment

Agarose gel electrophoresis system	Bio-Rad, USA
Cell culture incubator, Hera cell	Thermo scientific, USA
Centrifuge	VWR, Germany
SDS Gel system	Bio-Rad, USA
Spectrophotometer	Thermo Scientific, USA
Thermo cycler	Biometra, USA
Light microscope	Zeiss, Switzerland
Microplate reader Infinite 200	TECAN, Germany
Precellys Homogenizer	VWR, Germany
Realtime PCR machine (Mx3000P)	Agilent technologies, USA
Fluorescent microscope	Nikon, Germany
Luminescence detector	Intas, USA
Shaker	Biosan, Latvia
Water bath (cell culture)	Heraeus, Germany
Western blot chambers	Bio-Rad, USA

### 3.1.3 Kits

Caspase-Glo 3/7 Assay systems	Promega, Germany
Cell proliferation ELISA, BrdU (Colorimetric)	Roche, Switzerland
Cytotoxicity detection kit (LDH)	Roche, Switzerland
Pierce BCA Protein assay kit	Thermo Scientific, USA
iScript cDNA synthesis kit	Bio-Rad, USA
RNeasy mini kit	Qiagen, USA
Supersignal west Femto maximum sensitivity substrate kit	Thermo Scientific, USA
Cell proliferation kit II (XTT)	Roche, Switzerland

### 3.1.4 Primary antibodies

#### List of primary antibodies used for western blot

Antibody	Dilution	Manufacturer	Number	Secondary AB	MC/PC
β-Actin	1:2000	Abcam	Ab6276	Mouse	MC
c-Myc	1:1000	R&D Systems	MAB3696	Mouse	MC
Cyclin D1	1:1000	Cell Signaling	2978	Rabbit	MC
GAPDH	1:2000	Novus	NB600-502	Mouse	MC
Jak-2	1:1000	Cell Signaling	3230	Rabbit	MC
P-Jak-2	1:1000	Cell Signaling	3776	Rabbit	MC
Stat3	1:1000	Cell Signaling	4904	Rabbit	MC
P-Stat3	1:1000	Cell Signaling	9145	Rabbit	MC
P-PI3K	1:1000	Cell Signaling	4228	Rabbit	MC
PI3K	1:1000	Cell Signaling	4292	Rabbit	MC
Vinculin	1:2000	Abcam	Ab18058	Mouse	MC

## Secondary antibodies

### List of secondary antibodies used for western blot

Antibody	Dilution	Manufacturer	Number
HRP anti-rabbit	1:2500	Cell Signaling, USA	7074
HRP anti-mouse	1:2000	Cell Signaling, USA	7076

## 3.1.5 Oligonucleotides

### The list of primers used for real time-PCR analyses

Human JAK2 5'	5'-TAGATGGCTACTTCCGGCTC-3'
Human JAK2 3'	5'-CCTGCACCTGCTCAGACT-3'
Human STAT3 5'	5'-AGAAACAGTTGGGACCCCTG-3'
Human STAT3 3'	5'-ACTGCTGGTCAATCTCTCCC-3'
Human Cyclin D1 5'	5'-ACAGATCATCCGCAAACACG-3'
Human Cyclin D1 3'	5'-GAGGCAGTCCGGGTCAC-3'
Human Bcl-2 5'	5'-GCCTTCTTTGAGTTCGGTGG-3'
Human Bcl-2 3'	5'-GTTCCACAAAGGCATCCCAG-3'
Human c-MYC 5'	5'-CATCCACGAAACTTTGCCCA-3'
Human c-MYC 3'	5'-CGGGAGGCTGGTTTTCCA-3'
Human GAPDH 5'	5'-TTTTGCGTCGCCAGCCGAG-3'
Human GAPDH 3'	5'-TGACCAGGCGCCCAATACGA-3'
Rat JAK2 5'	5'-TACCTTTTTGCTCAGTGGCG-3'
Rat JAK2 3'	5'-ACCTTATCCGCTCCGAGTT-3'
Rat STAT3 5'	5'-ACCCTGACATTCCCAAGGAG-3'
Rat STAT3 3'	5'-TGCAGGTCGTTGGTGTCA-3'
Rat Cyclin D1 5'	5'-ATCATCCGCAAACATGCACA-3'
Rat Cyclin D1 3'	5'-GAGGCAGTCCGGGTCAC-3'
Rat Bcl-2 5'	5'-GGTGGTGGAGGAACTCTTCA-3'
Rat Bcl-2 3'	5'-CACAAAGGCATCCCAGCC-3'
Rat IL-1 $\beta$ 5'	5'-AGCTTTCGACAGTGAGGAGAA-3'
Rat IL-1 $\beta$ 3'	5'-CCACAGCCACAATGAGTGAC-3'

Rat IL-6 5'	5'-TTCTCTCCGCAAGAGACTTCC-3'
Rat IL-6 3'	5'-TTCTGACAGTGCATCATCGC-3'
Rat B2M 5'	5'-TCTGCAAGCCTGTGTGCGGT-3'
Rat B2M 3'	5'-TGGGGCCAGCACGTCTGAAA-3'
Mouse JAK2 5'	5'-TGTCGCCGGTTCCTGAAG-3'
Mouse JAK2 3'	5'-AGGCCATTCCCATCTAGAGC-3'
Mouse STAT3 5'	5'-CATCAGTGGCAAGACCCAGA-3'
Mouse STAT3 3'	5'-ACTTGGTCTTCAGGTACGGG-3'
Mouse Cyclin D1 5'	5'-CTCTCCAAAATGCCAGAGGC-3'
Mouse Cyclin D1 3'	5'-GAGGCAGTCCGGGTCAC-3'
Mouse Bcl-2 5'	5'-GGATAACGGAGGCTGGGATG-3'
Mouse Bcl-2 3'	5'-CAGGTATGCACCCAGAGTGA-3'
Mouse IL-1 $\beta$ 5'	5'-TGCCACCTTTTGACAGTGAT-3'
Mouse IL-1 $\beta$ 3'	5'-CACGGGAAAGACACAGGTAG-3'
Mouse IL-6 5'	5'-ATCCAGTTGCCTTCTTGGA-3'
Mouse IL-6 3'	5'-TTGCCATTGCACAACTCTTTTC-3'
Mouse HMBS 5'	5'-ACCTTGCCAGAGAAAAGTGCCGT-3'
Mouse HMBS 3'	5'-TTCCGGAGGCGGGTGTTGAG-3'

### 3.1.6 Human pulmonary artery smooth muscle cells

Lot number	Condition	Source
369143	Healthy	Lonza, USA
370750	Healthy	Lonza, USA
466718	Healthy	Lonza, USA
550178	Healthy	Lonza, USA
559495	Healthy	Lonza, USA
669096	Healthy	Lonza, USA
701036	Healthy	Lonza, USA
7F3560	Healthy	Lonza, USA
553	Healthy	UGMLC Biobank, Giessen
480D	Healthy	UGMLC Biobank, Giessen

200	Healthy	UGMLC Biobank, Giessen
364	IPAH	UGMLC Biobank, Giessen
453	IPAH	UGMLC Biobank, Giessen
488	IPAH	UGMLC Biobank, Giessen
515	IPAH	UGMLC Biobank, Giessen
536	IPAH	UGMLC Biobank, Giessen
626	IPAH	UGMLC Biobank, Giessen
673	IPAH	UGMLC Biobank, Giessen
817	IPAH	UGMLC Biobank, Giessen
Gi-9	IPAH	UGMLC Biobank, Giessen

Human PSMCs (HPASMCs) from healthy individuals were obtained from Lonza Ltd. (CC-2581, Basel, Switzerland), as well as from the UGMLC Giessen Biobank of the Justus-Liebig University Giessen (Germany) under an existing ethical approval (58/15). HPASMCs from IPAH patients were obtained from the UGMLC Giessen Biobank. Statements about the ethical approval (10/06) and the experimental details can be found in the appendix. The patients have been informed and given their written consent for the use of biomaterials for research purposes. Both, the collection as well as the storage of this biomaterial by the UGMLC/DZL biobank (AZ 58/15) and its further use for the herein mentioned investigations (AZ 10/06) were approved by the Ethics Committee of the Justus Liebig University. All studies and procedures to obtain human specimen were conducted according to the Declaration of Helsinki.

### 3.1.7 Buffer solutions

TAE (50x)	40 mM TRIS, 20 mM acetic acid, 1 mM EDTA, adjusted to pH 8,0 with NaOH
Electrode buffer (10x)	30,28g Tris, 144,12g Glycine, 10g SDS, adjusted to pH 8,3 with NaOH.
TBS (10x)	0.2M Tris HCl, 1,37 M Nacl adjusted to pH 8,5 with HCl.
5% Milk TBS-T	5g milk powder in 100 ml TBS-T

5% BSA	5g BSA in 100 ml PBS
--------	----------------------

### 3.1.8 Cell culture medium and reagents

Names	Company
Dulbecco's Phosphate Buffer saline (DPBS)	Thermo Scientific, USA
Fetal calf serum	Biowest, USA
Penicillin/Streptomycin	PAN Biotech, Germany
Smooth muscle cell basal medium (SmBM)	Lonza, USA
SmGM-2 Single quotes	Lonza, USA
Trypsin/EDTA	Lonza, USA

### Stimulants

PDGF-BB	Peptrotech, USA
rhIL-1 $\beta$	R&D Systems, USA
rhIL-6	R&D Systems, USA
rhIL-13	R&D Systems, USA
rhIL-21	R&D Systems, USA

### Inhibitors

Ruxolitinib	Selleckchem, USA
-------------	------------------

### 3.1.9 Other materials

Cell scrapers	BD Falcon, USA
Cell culture dishes (10cm, 3cm, 6well, 48well, 96well)	Greiner, Germany
Filter tips (10, 100, 1000 $\mu$ l)	Griener, Germany
Gel blotting paper	Whatman, USA
Microcentrifuge tubes	Eppendorf, USA
Needles	B.Braun, Germany
Nitrocellulose membrane	ROTH, Germany
Polypropylene tubes (15ml, 50ml)	Greiner bio one, Germany

PTK Chip	Pamgene, Netherlands
Precellys Tubes with beads	VWR International, Germany
Real-time PCR plates	VWR International, Germany
Syringes	B.Braun, Germany
STK Chip	Pamgene, Netherlands
Tips (10, 100, 1000 $\mu$ l)	Eppendorf, USA
$\mu$ -Dish 35mm	Corning, Germany

## **3.2 METHODS**

### **3.2.1 Cell culture**

All the cell culture experiments described in this thesis were conducted in human pulmonary artery smooth muscle cells (HPASMCs). Cells between passages 4 and 6 were used. Human pulmonary artery smooth muscle cells (HPASMCs) isolated from the lungs of healthy individuals was purchased from Lonza (Walkersville, MD) and also from UGMLC Giessen Biobank. HPASMCs from patients with IPAH were obtained from UGMLC Giessen Biobank. HPASMC monolayers were grown at 37°C in a 5% CO<sub>2</sub> atmosphere in smooth muscle cell growth medium-2 (SmGM-2) supplemented with 5% fetal calf serum and SmGM-2 SingleQuots (Lonza, USA) until it reaches confluency and then subcultures to expand the numbers. For sub-culturing, cells were then washed twice with DPBS and treated with Trypsin/EDTA and placed it in an incubator for 2 minutes. Trypsin/EDTA was inactivated by the addition of an equal volume of culture media. Cells were centrifuged; the resulting cell pellet was re-suspended in 1 ml culture media and cell number counted using hemocytometer. The cells were then seeded into new sterile culture dishes.

For cell culture experiments, HPASMCs monolayers were washed with 1x phosphate-buffered saline (PBS) and serum-starved for 24 hours in smooth muscle basal media (SmBM) to ensure synchronization of cell growth, before being stimulated with IL-6 (100ng/ml) under basal media for 24 hours.

### **3.2.2 Total protein isolation**

#### **3.2.2.1 Preparation of protein lysates from tissues**

30mg of tissue section was dissected and put into 300µl of RIPA lysis buffer (Thermo Scientific) containing protease and phosphatase inhibitor cocktail. Tissues were homogenized using Precellys homogenizer for 10 seconds at 5500 rpm until the solution is clear (no clumps), followed by lysates were passed through the needle. After that, Incubation on ice for 1 hour with constant agitation and then centrifuged for 15 minutes at 4°C (16.000xg). Supernatants were transferred to pre-cooled 1.5ml tubes and snap-freeze by liquid nitrogen before stored at -80°C.

### **3.2.2.2 Preparation of protein lysates from HPASMCs**

HPASMCs were taken out of the incubator after the appropriate incubation time, the dishes were placed on ice and the medium was aspirated. The cells were washed twice with 5 ml ice-cold 1x PBS on ice. M-PER lysis buffer (Thermo Scientific) containing protease and phosphatase inhibitor cocktail or RIPA lysis buffer (Thermo Scientific) containing protease inhibitor cocktail and EDTA was then added to each dish (200µl or 300µl per 100-mm dish). The lysates were scratched using cell scrapers and collected into pre-cooled 1.5ml tubes and incubated for 1 hour at 4 °C with constant agitation, followed by centrifugation for 15 minutes at 4 °C (16,000xg). The supernatants were aliquoted (100µl/tube) in 0.2ml PCR tubes and immediately flash-frozen in liquid nitrogen before stored at -80°C. Protein concentrations for each sample were determined using a bicinchoninic acid (BCA) protein assay kit (Thermo Scientific).

### **3.2.3 Protein estimation-BCA assay**

Protein concentration was measured using a Pierce BCA Protein assay kit (Thermo Scientific). It is used for the colorimetric detection and quantitation of total protein content. This method involving reaction of proteins with a chelation of two molecules of BCA with one cuprous ion and giving rise to purple color. This water-soluble complex exhibits a strong absorbance at 562 nm. Protein samples were diluted in PBS at a ratio of 1:10 and the absorbance was measured at 562 nm using a microplate reader (TECAN). The exact protein concentrations were determined using BSA as a standard (20-2000µg/ml).

### **3.2.4 SDS-Polyacrylamide-gel electrophoresis (SDS-PAGE) and immunoblot**

For SDS-PAGE, total protein lysates (30µg per sample) were mixed with 4x Rotiload buffer at a ratio of 4:1 to a final volume of 30 µl supplemented with PBS and incubated at 95°C for 5min. Equal amounts of total protein samples were loaded together with protein marker into the wells of 6 or 10% (depending on protein sizes to be separated) polyacrylamide gels. Gels were run in electrophoretic assembly with a 1x running buffer at 100V for 2 hours. Following buffers used:

### Resolving gel

Gel component	Percentage of gel	
	6%	10%
Acrylamide/Bis-acrylamide	2 ml	3.3 ml
Tris-HCl (1.5M, pH-8.8)	2.5 ml	2.5 ml
SDS 10% (w/v)	0.1 ml	0.1 ml
APS 10% (w/v)	0.1 ml	0.1 ml
TEMED	0.008 ml	0.004 ml
Water up to the final volume	of 10 ml	of 10 ml

### Stacking gel (5%)

Gel component	Volume
Acrylamide/Bis-acrylamide	0.67 ml
Tris-HCl (1M, pH-6.8)	0.5 ml
SDS 10% (w/v)	0.4 ml
APS 10% (w/v)	0.4 ml
TEMED	0.004 ml
Water up to the final volume	of 4 ml

1x SDS running buffer components	Final concentration (1 Liter Volume)
Tris (-Base)	25 mM
Glycine	192 mM
SDS 10% (w/v)	0.1% (w/v)

After proteins were separated on a gel, they were transferred to a nitrocellulose membrane by electrophoretic transfer (tank-blot) at 100V for 1.5 hour (depending on the protein size and % of gel) in a transfer buffer.

<b>Blotting buffer components</b>	<b>Weight and volume</b>
Tris (-Base)	3.03 g
Glycine	14.4 g
Methanol	200 ml
SDS 10% (w/v)	1 ml
Water up to the final volume	of 1 Liter

After the transfer process, membranes were blocked with blocking solution (5% milk in TBS-T or 5% BSA in TBS-T) for 1 hour on a shaker at room temperature and subsequently incubated with the primary antibodies diluted in blocking solution overnight at 4°C. After that, membranes were washed thrice with a 1xTBS-T buffer for 10 minutes and followed by incubation with appropriate HRP-coupled secondary antibody diluted in blocking solution for 1 hour at room temperature. After incubation, membranes were washed 3 times with 1x TBS-T for 10 min each. Protein bands were detected by chemiluminescence on a luminescence detector (Intas, Germany) using SuperSignal West Femto Kit (Thermo Fisher Scientific) or Immobilon Forte (Millipore). The exposure time was adjusted according to the signal intensity. In order to reuse the membranes and check the signal of housekeeping genes, membranes were incubated with a stripping buffer (Thermo Scientific) for 30 min at room temperature, washed thrice in 1x TBS-T buffer for 10min each and incubated again with primary antibody.

<b>Tris buffer saline (TBS-T) components</b>	<b>Weight and Volume</b>
Tris (-Base)	2.42 g
Nacl	8.76 g
0.05 % Tween 20	0.5 ml
pH	7.5
Water up to the final volume	of 1 Liter

### **3.2.5 Densitometry analysis**

Densitometry of western blots was performed using Image J software. Data were analyzed by Prism 5 software (GraphPad, USA).

### **3.2.6 Kinome profiling**

The HPASMCs were analyzed as biological replicates from the lungs of three healthy individuals and three IPAH patients, with each cell sample lysed independently and measured on an array of the PamChip® PTK. Kinomic profiling of HPASMC lysates (prepared as mentioned above) was conducted using the PamStation®12 platform (PamGene International, s-Hertogenbosch, Netherlands). Equal amounts of total protein lysates were dispensed onto the PamChip® PTK (7 µg) in standard kinase buffer (Pamgene).

The PamStation®12 platform uses a high throughput peptide microarray system analyzing 144 tyrosine peptides with known phosphorylation sites spotted in a 3D format to measure kinomic activity in cell or tissue lysates. A FITC conjugated antibody supplied within the reaction mix was used for visualization of phosphorylated Tyr to measure the phosphorylation signal during and after lysates are pumped through the array. A computer-controlled charge-coupled device (CCD) captures the peptide phosphorylation signal. The initial sample and array processing, as well as image capture, was analyzed using the Evolve 12 (PamGene) software and BioNavigator software (PamGene) for performing data analysis. Significantly deregulated peptide lists (phosphosubstrates) were generated for the HPASMC lysates based on differences between healthy and IPAH lysates using kinome render application (kinomerender.php).

### **3.2.7 Kinome Data analysis**

Initial image analysis was performed using the Bionavigator software v. 6.2 (PamGene) by following the standard protocol from PamGene. Then, the data is exported to a database for further processing. Kinase activity data were generated from the phosphorylatable peptide-specific reaction per 'spot' on the PamChip. After the lysates were washed off, the signal intensity of each of the 144 spots was captured over multiple exposure times (10, 20, 50, 100, 200 ms) by a CCD camera. Then the data were log-transformed for visualization and labeled as "log signal" by taking the slope of exposure times and multiplied by 100. Quality control was performed to remove saturated signal values from the raw data by applying filters. Unsupervised hierarchical clustering of kinomic profiles for the samples was done using Euclidean distance metrics and complete linkage in BioNavigator software and is displayed as heatmaps.

The log signal data were plotted in color corresponding to the pattern of their substrate peptide phosphorylation or with log change from control (the disease model). The peptide lists were then analyzed for upstream kinase analysis using the Kinome render application (<http://bcb.med.usherbrooke.ca/kinomerender.php>). The associated kinase activity measured according to the specificity and was indicated by colors. Briefly, data from samples that were run in singlicate from each cell line were grouped into either donor or IPA patient and then compared using the BioNavigator software.

### **3.2.8 RNA isolation**

#### **3.2.8.1 RNA isolation from tissues**

The isolation of total RNA from lung homogenates was carried out using the RNeasy mini kit (Qiagen). 30mg of tissue was excised and placed in 600µl of buffer RLT. Tissue was immediately disrupted and homogenized using a precllys homogenizer for 40sec at 5500 rpm in three repeats. The lysates were passed 5 times through a 20-gauge needle fitted onto a RNase-free syringe. After homogenization, lysates were centrifuged for 3min at 13,000 x g using an ultra-centrifuge. The supernatant was carefully removed and transferred into a new micro centrifuge tube. 600µl of 70% ethanol was added to the cleared lysate, mixed well and up to 700µl of lysate transferred to the RNeasy spin column. The column was centrifuged for 15sec at 8,000 x g and flow-through was discarded. The digestion of genomic DNA was carried out using the RNase-free DNase set (Qiagen) according to the protocol "On-Column DNase digestion". 500µl of buffer RPE was added to the column, followed by centrifugation for 2min at 8,000 x g and flow-through was removed.

To elute the RNA, 30µl of RNase free water was added directly to the spin column membrane and the column was placed in a new 1.5ml collection tube, followed by centrifugation for 1min at 8,000 x g.

#### **3.2.8.2 RNA isolation from HPASMCs**

The isolation of total RNA from HPASMCs was performed using the RNeasy mini kit (Qiagen). Cell culture media was aspirated from the dishes and cells were washed with ice-cold PBS. 600µl of Buffer RLT was directly added to the cell culture dish; lysates were collected using a cell scraper and transferred to micro centrifuge tubes. The lysates were passed 5 times through a 20-gauge needle fitted onto a RNase-free syringe followed by vortexing for 1min. 600µl of 70% ethanol was added to the homogenized lysate, mixed well by pipetting and up

to 700µl of lysate transferred to the RNeasy spin column. The column was centrifuged for 15sec at 8,000 x g and flow-through was removed. The digestion of genomic DNA was carried out using the RNase-free DNase set (Qiagen) according to the protocol “On-Column DNase digestion”. 500µl of buffer RPE was added to the column, followed by centrifugation for 2min at 8,000 x g and flow-through was discarded. To elute the RNA, 30µl of RNase free water was added directly to the spin column membrane and the column was placed in a new 1.5ml collection tube, followed by centrifugation for 1min at 8,000 x g.

The Nanodrop spectrophotometer (Thermal Scientific) was used to measure the concentration (A260) and purity (A260/280) of RNA. 1µl of the sample was pipetted onto a measurement pedestal and the ratio of 260/280 nm wavelengths was analyzed. RNA samples with a 260/280 ratio of around 1.8 were considered for further experiments.

### 3.2.9 Reverse transcription

Reverse transcription is an enzymatic method of generating complementary DNA (cDNA) from an mRNA template with the help of reverse transcriptase (RT) enzyme. The cDNA was synthesized from mRNA isolated from different samples by using the iScript cDNA synthesis kit (BioRad) according to the manufacturer’s instructions. Briefly, reverse transcription mix was prepared on ice as follows:

Components	Volume per reaction (in µl)
5x iScript reaction mix	4
iScript reverse transcriptase	1
Nuclease-free water	7
RNA template (1µg total RNA)	8
Total volume	20

The reaction mix was subjected to 25°C for 5min to allow annealing, followed by incubation at 42°C for 30min. Finally, the mix was subjected to 85°C for 5min to allow inactivation of the reverse transcriptase. The cDNA product was stored at -20°C for further use.

### 3.2.10 Quantitative real-time PCR (qRT-PCR)

Real-time PCR is a method that generates simultaneous amplification and quantification of target cDNA sequences by using target-specific primers.

Primers were designed using the Primer Blast program (NCBI) and the following criteria were used: product size 100-200bp must span exon-exon junction, intron spanning. Real-time PCR was performed using the iQ™ SYBR Green Supermix (BioRad). The reaction was prepared as follows:

Component	Volume added (in µl)
iTaq™ universal SYBR Green Supermix, 2X	12.5
Forward primer, 10µM	0.5
Reverse primer, 10µM	0.5
cDNA template	4
Nuclease-free water	7.5
Total volume	25

The reaction mix was pipetted into 96 well plate and centrifuged for 1min. Real-time PCR was carried out in a Stratagene Mx3000P (Agilent technologies) machine, using the following program:

Phase	Temperature	Duration	Cycles
Initial denaturation	95°C	30sec	1x
Denaturation	95°C	10sec	40x
Annealing	58°C	45sec	
Elongation	95°C	60sec	1x
Denaturation	58°C	30sec	1x
Melting curve	95°C	30sec	1x

### 3.2.11 Bromodeoxyuridine (BrdU) incorporation assay

The assay was carried out using the Cell Proliferation ELISA, BrdU (colorimetric) kit (Roche Diagnostics, Germany), in accordance with the manufacturer's instructions. DNA syntheses of HPASMCs were assessed by measuring the incorporation of 5- Bromo-2-deoxyuridine

(BrdU) into cellular DNA. The rate of DNA synthesis is considered as a marker for cell proliferation. The proliferation of cells was analyzed after 24 hours of the experiment. Briefly, synchronized cell cultures were treated with an inhibitor or stimulator for 24 hours in a 96 well plate and incubated with BrdU labeling solution for 18 hours at 37° C in a humidified atmosphere. After incubation with BrdU, cells were washed with PBS and subsequently fixed and DNA was denatured using a Fixing Solution provided by the manufacturer. Fixed cells were then treated with an anti-BrdU-POD antibody for 90 minutes at room temperature. Cells were then washed three times with PBS and incubation with substrate solution was performed at room temperature until color development. Signal intensity was measured with an ELISA plate reader (TECAN) at a wavelength of 370/492 nm.

### 3.2.12 Measurement of cell cytotoxicity

The assay was carried out using the Cytotoxicity Detection kit (LDH) (Roche Diagnostics, Germany), in accordance with the manufacturer's instructions. Briefly, HPASMCs were seeded in triplicates in a sterile 96 well tissue culture plate (5000 cells/well). After overnight incubation in an incubator (37°C, 5% CO<sub>2</sub>, 90% humidity), the cells were treated with 100 µl of their respective test substances at predetermined concentrations in serum-free media. After 24 hours, a multichannel was used to transfer 100 µl of supernatant from the top of all the wells of the experimental culture plate to the new sterile 96 well tissue culture plate. Care was taken not to disturb the cells or draw up any debris. Shortly before use, the cytotoxicity reagents were prepared according to the manufacturer's protocol and 100 µl of the reaction mixture was then added to each of the assay wells on top of the supernatant in rapid succession. The total volume in each well was 200 µl. The assay plates were then incubated for 30 minutes at room temperature in the dark. After that, the absorbance of the samples measured at 490 nm using a standard plate reader.

#### Overview of the controls:

Contents of the well	Background control	Low control	High control
Assay medium	200 µl	100 µl	-

Cells	-	100 µl	100 µl
TritonX-100 solution (2% in assay medium)	-	-	100 µl

### 3.2.13 Caspase-Glo 3/7 Assay

Apoptosis was detected biochemically by measuring the activation of caspase-3 and -7 using the Caspase-Glo-3/7 assay kit (Promega, USA). The assay provides a caspase 3/7 substrate, which contains the tetrapeptide sequence DEVD, in a reagent optimized for caspase activity and cell lysis. Adding caspase-3/7 reagent to cells results in cell lysis, which generates “glow-type” luminescent signal when cleaved by active caspase. Healthy and IPAH PASM cells were seeded in 96-well white luminometer assay plates at a density of 5000 cells per well and incubated at 37°C for 24 hrs. After that, cells were incubated with serum free media for 24 hours before treated with ruxolitinib for 24 hours. 100 µl caspase-Glo-3/7 reagents were added to each well including a well without cells (used as a negative control) and incubated for 30 min at room temperature. The luminescence intensity was measured using an ELISA plate reader (Tecan, Germany).

### 3.2.14 XTT-assay

Cell viability was assessed by using the Sodium 3-[1-(phenylaminocarbonyl)-3,4-tetrazolium]-bis (4-methoxy-6-nitro) benzene sulfonic acid hydrate (XTT) assay kit (Sigma-aldrich, Germany). It is a substrate for mitochondrial dehydrogenases resulting in the formation of an orange formazan dye in the living cells. The intensity of the colour is proportional to the number of viable cells and their metabolic activity. Healthy and IPAH PASM cells were seeded in 96-well plates at a density of 5000 cells per well and incubated at 37°C for 24 hrs. After that, cells were incubated with serum free media for 24 hours before treated with ruxolitinib for 24 hours. 50 µl XTT labeling mixture was added to each well including a well without cells (used as a negative control) and incubated for ~4 hour at 37°C. Absorbance at 450-500 nm was measured by using an ELISA plate reader (TECAN, Germany).

### **3.2.15 Transwell migration assay**

HPASMCs were serum-starved for 24 hours was used in the experiment. Cellular migration was assessed by a transwell migration assay, in which transwell plates, a modification of the Boyden chamber method, were used. Cell suspension (15000 cells in 100 µl) in basal media (BM) was pipetted into the insert, and preincubated with ruxolitinib for 1 hour before and throughout the assay. The wells of Transwell plates were filled with 400 µl of BM containing IL-6 (100 ng/ml). The Transwell plates were incubated in a humidified CO<sub>2</sub> incubator at 37°C during the migration (14-16 hours). After the incubation time, the media was aspirated from both inserts and wells. The cells on the top membrane surface were gently scraped with a cotton swab, and the cells on the bottom surface were fixed and stained with DAPI (4',6'-diamidino-2-phenylindole, 0.5µg/ml, Sigma, Germany) for 20 minutes. DAPI positive cells were counted under bright field microscopy at 40x magnification in five random fields of view. The cell migration percentage was calculated according to the manufacturer's instructions.

### **3.2.16 Animal experiments**

Animals (mice and rats) were purchased from Charles River Laboratories (Sulzfeld, Germany). All animal studies were conducted in accordance with the National Institute of Health Guidelines on the Use of Laboratory Animals. The study protocol (PH GI 20/10 Nr. G50/2016; JLU Nr. 818\_GP) was approved by both, the University Animal Care Committee and the Federal Authorities for Animal Research of the Regierungspräsidium Giessen (Hessen, Germany). The above-mentioned animal study protocols were written by Bruno Pöttker, Ingrid Henneke and Astrid Weiss. The following animal procedures and animal experiments were performed with the help of Christina Vroom and Baktybek Kojonazarov.

#### **3.2.16.1 Monocrotaline (MCT) induced pulmonary hypertension rat model**

Adult male Sprague-Dawley rats (300–350 g in body weight) were randomized and administered MCT (60 mg/kg body weight) by subcutaneous injection (s.c) to induce pulmonary hypertension or the same volume of saline as vehicle control. After 21 days, rats were separated into 4 groups: control group (n=6), MCT group (60 mg/kg, n=6), treatment 1 group (ruxolitinib 30 mg/kg, n=6), treatment 2 group (ruxolitinib 90 mg/kg, n=7). The ruxolitinib (Jak-2 inhibitor) or placebo was prepared in 1.5% methylcellulose and rats were fed once daily by oral gavage. Rats were examined after 14 days of treatment (on day 35).

### **3.2.16.2 Chronic hypoxic mouse model of pulmonary arterial hypertension**

Mice were randomized and exposed to chronic hypoxia (10% O<sub>2</sub>) in a ventilated chamber to develop pulmonary hypertension or control mice were kept under normoxia for the same period. After 21 days, mice were separated into 4 groups to receive daily either the ruxolitinib or placebo orally by gavage: control group (n=7), Hox group (n=6), treatment 1 group (ruxolitinib 60 mg/kg, n=5), treatment 2 group (ruxolitinib 180 mg/kg, n=10). The ruxolitinib (JAK-2 inhibitor) was prepared as described for rats.

### **3.2.17 Echocardiography**

Transthoracic echocardiography was performed to measure the right ventricular internal diameter (RVID), tricuspid annular plane systolic excursion (TAPSE), and cardiac output (CO) with a VEVO2100 (Visualsonics, Canada) system equipped with a 13-24-MHz transducer (MS250 and 400) as described previously (ref). Briefly, animals were exposed to isoflurane gas (3%) to induce anesthesia and maintained with 1.5% isoflurane in room air supplemented with 100% O<sub>2</sub>. Animals were positioned supine position on a heating platform with all legs taped to ECG electrodes for heart rate (HR) monitoring. Body temperature was monitored via a rectal thermometer (Indus Instruments, USA). The chest of each animal was shaved, and chemical hair remover was used to reduce ultrasound attenuation. A pre-warmed ultrasound gel was spread over the chest wall of the animals to provide a coupling medium for the transducer. To measure RVID, the apical four-chamber view was used to calculate the maximal distance from the RV free wall to the septum. To determine TAPSE in M-mode, the apical four-chamber view was used to measure the distance between end-diastole to end-systole. PA diameter was determined at the level of the pulmonary outflow tract during mid systole by superior angulation of the parasternal short-axis view. PA flow velocity-time integral (VTI) was measured by Pulsed-wave Doppler. CO value was derived by combining PA VTI, pulmonary artery area, and heart rate echocardiographically. The following formula was used to calculate the total pulmonary vascular resistance index: TPVRI = RVSP/CI, where RVSP is the right ventricular systolic pressure (mmHg) and the cardiac index (CI; ml min<sup>-1</sup> per 100 g body weight) is the cardiac output (CO; ml min<sup>-1</sup>) normalized to 100 g body weight.

### **3.2.18 Hemodynamic and right ventricular hypertrophy measurements**

Animals were anesthetized as described above to measure the hemodynamic parameters. After intubation, the animal was placed supine on a homeothermic plate (AD Instruments, Spechbach, Germany) and connected to a small-animal ventilator MiniVent type 845 (Hugo Sachs Elektronik, March-Hugstetten, Germany). The body temperature was controlled by the rectal probe connected to the control unit (AD Instruments, Spechbach, Germany) and was maintained at 37°C during the catheterization. To assess RVSP, the right external jugular vein was catheterized with a high-fidelity 1.4F micromanometer catheter (Millar Instruments, Houston, USA) and advanced into the right ventricle. Data were collected and analyzed using the PowerLab data acquisition system (MPVS-Ultra Single Segment Foundation System, AD Instruments, Spechbach, Germany) and LabChart 7 for Windows software.

### **3.2.19 Histology and pulmonary vascular morphometry**

For vascular morphometry, lungs were flushed with saline at a vascular pressure of 22 cm H<sub>2</sub>O and a tracheal pressure of 12 cm H<sub>2</sub>O before being fixed by vascular perfusion with Zamboni's fixative through the pulmonary artery. The left lung was stored in 4% paraformaldehyde (PFA) for the next 24 h and then in PBS before being dehydrated. The paraffin-embedded lung tissues were subjected to sectioning and 3- $\mu$ m thick samples were generated with a microtome. The degree of muscularization of small peripheral pulmonary arteries was assessed by double-staining the sections with an anti- $\alpha$ -smooth muscle cell actin antibody (dilution 1:900, clone 1A4, Sigma) and an anti-human von Willebrand factor antibody (dilution 1:900, Dako, Hamburg, Germany). Stained thin sections were examined by light microscopy, and the color along the perimeter of the vessel was analyzed using a computerized morphometric system (Qwin, Leica, Wetzlar, Germany) that differentiates the purple staining of the smooth muscle and the brown staining of the endothelial layer. At 40-fold magnification, 80-100 intra-acinar vessels accompanying either alveolar ducts or alveoli of 25 to 50  $\mu$ m were analyzed by an observer blinded to the treatment of the animals. Each vessel was categorized as either non-muscularized (less than 5% SMC actin around the vessel), partially muscularized (5 to 75% SMC actin around the vessel) or fully muscularized ( $\geq$  75% SMC actin around the vessel). The percentage of pulmonary vessels in each muscularization category was determined by dividing the number of vessels in that category by the total number counted in the same experimental group.

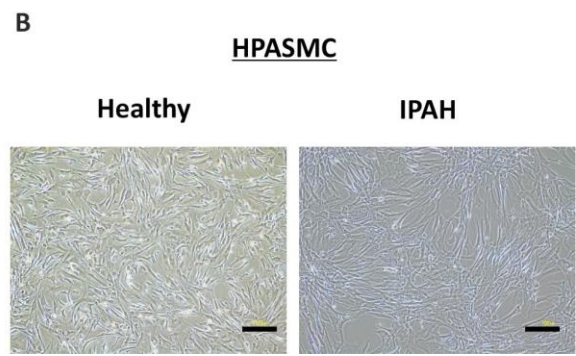
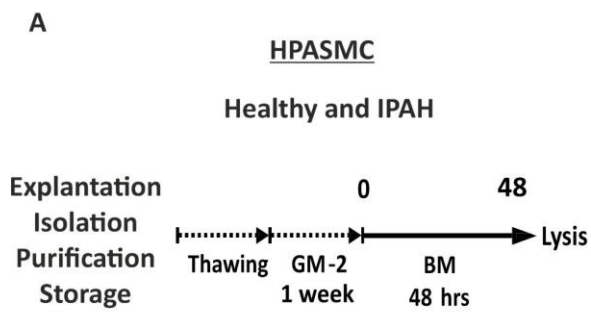
### **3.2.20 Statistical analysis**

Statistical analysis was performed with Prism 5 software (GraphPad, San Diego, CA). All data are presented as mean  $\pm$  standard error of the mean (SEM). Two-group comparisons were determined by the Mann-Whitney test or two tailed unpaired t-test. For multiple group comparisons, one-way ANOVA with Dunnett's post-hoc analysis or Tukey's post-hoc analysis was applied. All statistically significant P values were described in the figure legends.

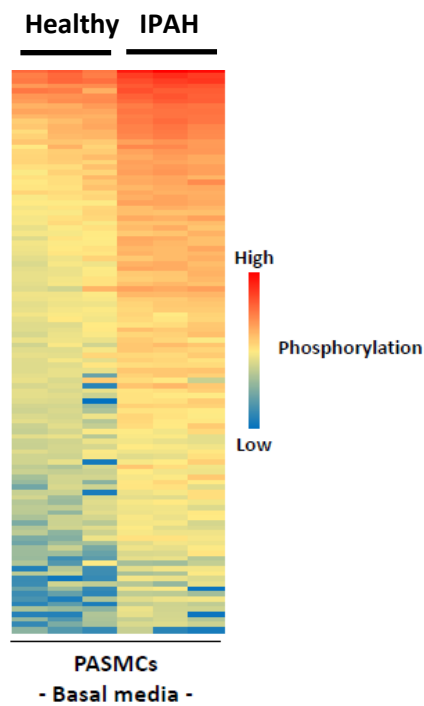
## 4. RESULTS

### 4.1 Pulmonary arterial smooth muscle cells (PASMC) from PAH-patients display increased JAK activity

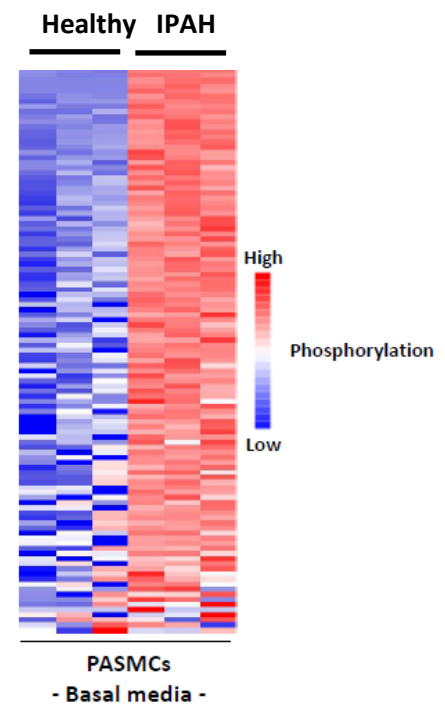
Human PASMCs from healthy individuals and PAH-patients were serum-starved for 48 hours in basal media (BM) without any multiple growth factor (MGF) supplements (Fig. 8A) prior to total protein lysis for peptide-based kinase activity measurements via the PamStation platform (Fig. 8C). This technology allows for the investigation of distinct kinase-mediated signaling signatures between two experimental conditions [75-77] e.g. in healthy and diseased states. I observed that there was a marked difference in the intensities of peptide phosphorylation between healthy PASMCs and PASMCs derived from PAH patients as shown in the heat map (Fig. 8D), indicating that certain signaling pathways driven by specific kinases was deregulated under disease condition. In a two-group comparison, the peptides are ranked by their correlation score (homogeneity within one group) with the most de-regulated peptide phosphorylation at the top (Fig. 8E). Based on those phosphorylation patterns, a computational upstream kinase analysis predicted an increased activity of JAK1, JAK2, and JAK3 kinases (amongst other tyrosine kinases) in the PASMCs isolated from PAH patients compared to PASMCs from healthy donors (Fig. 8F). As JAK2 was one of the most significantly de-regulated receptor tyrosine kinases in the human PASMCs tyrosine kinase analysis (Fig. 8F) and significantly upregulated in IPAH PASMCs, it was selected for further investigations.



**D** Heat map of log transformed raw data



**E** Two group comparison healthy versus IPAH



**F**

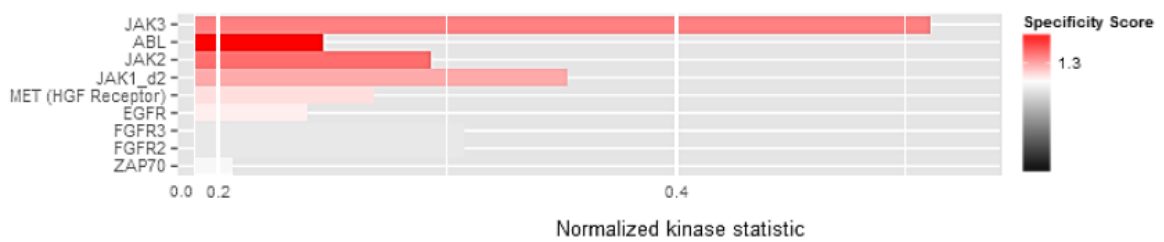


**Figure 8. Setup of cell culture conditions used to perform peptide-based kinase activity profiling of PSMCs from healthy individuals and IPAH patients.**

(A) Illustration of the PSMC culture experimental protocol. The cells were serum-starved in basal media (BM) for 48 hours and lysed for protein extraction. (B) Representative images of cultured PSMCs from healthy individuals and IPAH patients. Images were taken at adequate magnification with a scale bar of 100  $\mu\text{m}$ . (C) The workflow of peptide-based kinase activity profiling of PSMCs which revealed a differential kinase activity profile between PSMCs from healthy individuals (n=3) and IPAH patients (n=3) when cultured in basal media. (D) Heat map of log<sub>2</sub>-transformed mean values of raw data (i.e. signals of peptide phosphorylation determined by densitometry) displaying an increase in kinase activity in IPAH samples as compared to healthy controls (based on the pattern of their substrate peptide phosphorylation). (E) Two-group comparison using the two-sample t-test for all samples showing the overall difference in the tyrosine phosphorylation pattern between both PSMCs entities (i.e. healthy and IPAH) under basal media condition. Rows indicate peptides showing significant differences in phosphorylation between the two groups; columns represent individual samples from the two groups. (F) Bar chart displaying a predicted higher kinase activity in PSMCs derived from IPAH patients. Upstream kinase prediction is based on the differential pattern of substrate phosphorylation. Normalized kinase statistics indicating the relative kinase activity, calculated using a mathematical-based algorithm and the specificity score show the reliability and accuracy of the prediction. GM-2=growth media.

#### **4.2 Expression analyses for JAK2-STAT3 signaling in a human specimen and experimental models of PH**

To investigate if the elevated kinase activity is a consequence of a transcriptional or translational up-regulation on protein and mRNA level, Western blot and real-time PCR on JAK2, and its downstream effectors STAT3, c-MYC, CyclinD1 was performed.

##### **4.2.1 Protein expression of JAK2-STAT3 signaling molecules in human PSMCs**

Protein expression profiles were investigated in PSMCs from patients with IPAH compared to healthy PSMCs under basal media condition (Fig. 9A). Western blot analyses followed by densitometry quantification (Fig. 9B) (normalized to vinculin) demonstrated a significant increase in protein levels of P-JAK2 and P-STAT3 in IPAH PSMCs as compared to healthy PSMCs. c-MYC and Cyclin D1 did not show an increase in protein levels.

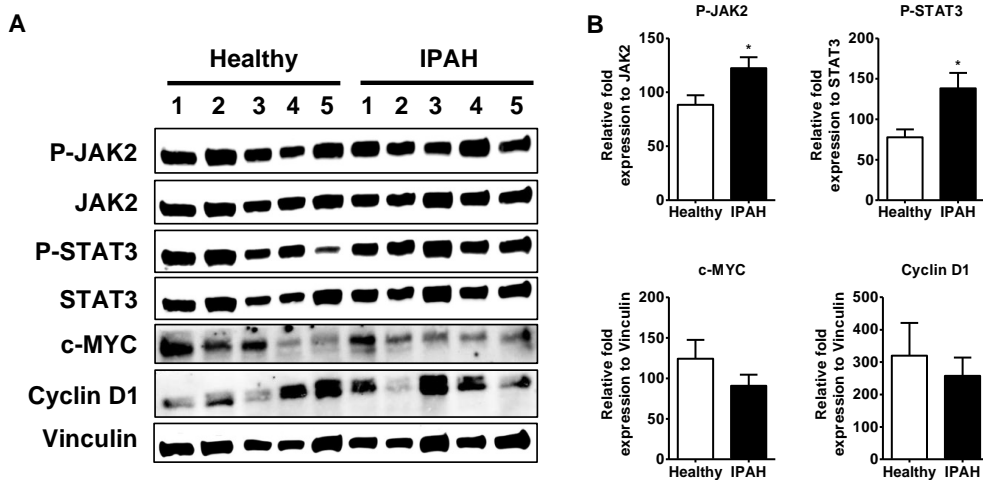


**Figure 9. Protein expression analyses for JAK2-STAT3 signaling molecules in human PSMCs.**

PASMCs obtained from the lungs of healthy individuals (n=5) and IPAH patients (n=5). After serum starvation, cells were cultured in BM for 24 hours. (A, B) Western blot analysis and subsequent densitometry quantification of members of the Jak2-Stat3 signaling axis in healthy and IPAH PSMCs. One representative experiment of three independent repetitions is shown. Vinculin served as a loading control. All data represent the mean  $\pm$  SEM of n-fold expression compared to healthy control. \*P < 0.05, Statistical analysis was performed using a Mann-Whitney t test.

#### 4.2.2 mRNA expression of JAK2-STAT3 signaling proteins in human PSMCs and in lung homogenates of experimental PH models

mRNA expression analysis of members of the JAK2-STAT3 pathway was performed in PASMCs from IPAH patients as well as in healthy PASMCs under basal media condition. In lung homogenates from experimental models of PH, similar studies were undertaken. JAK2, STAT3, Cyclin D1 and Bcl-2 showed a significant increase in mRNA expression in PASMCs from IPAH patients as compared to healthy PASMCs (Fig. 10A). A similar increase in JAK2, STAT3, Cyclin D1, Bcl-2 mRNA levels was detected in MCT-injected rats as compared to the healthy controls (Fig. 10B). In contrast, except Stat3 other genes did not show significant changes in hypoxia-exposed mice as compared to Nox controls (Fig. 10C).

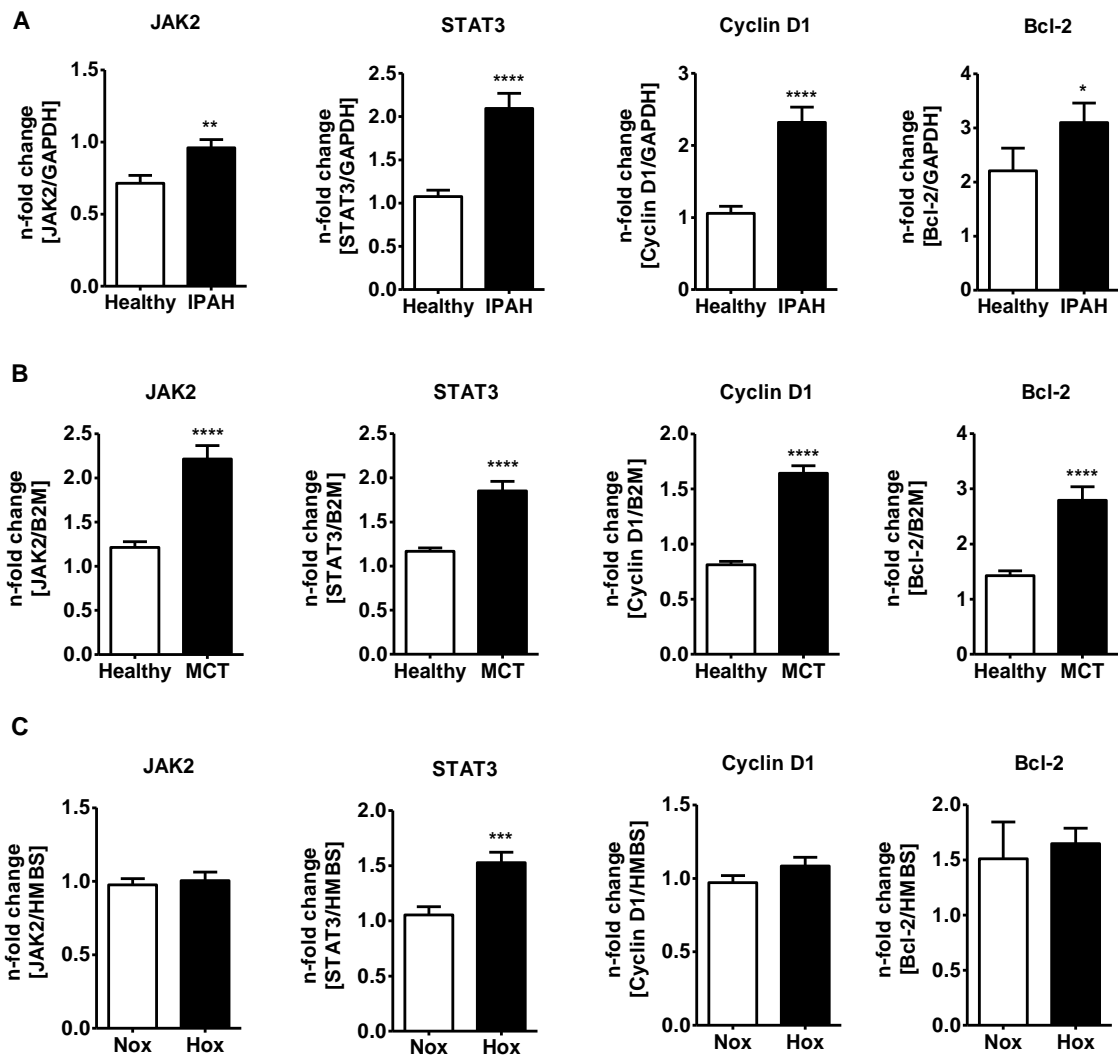


**Figure 10. mRNA expression of JAK2-STAT3 signaling molecules in human PSMCs and in lung homogenates of experimental PH models.**

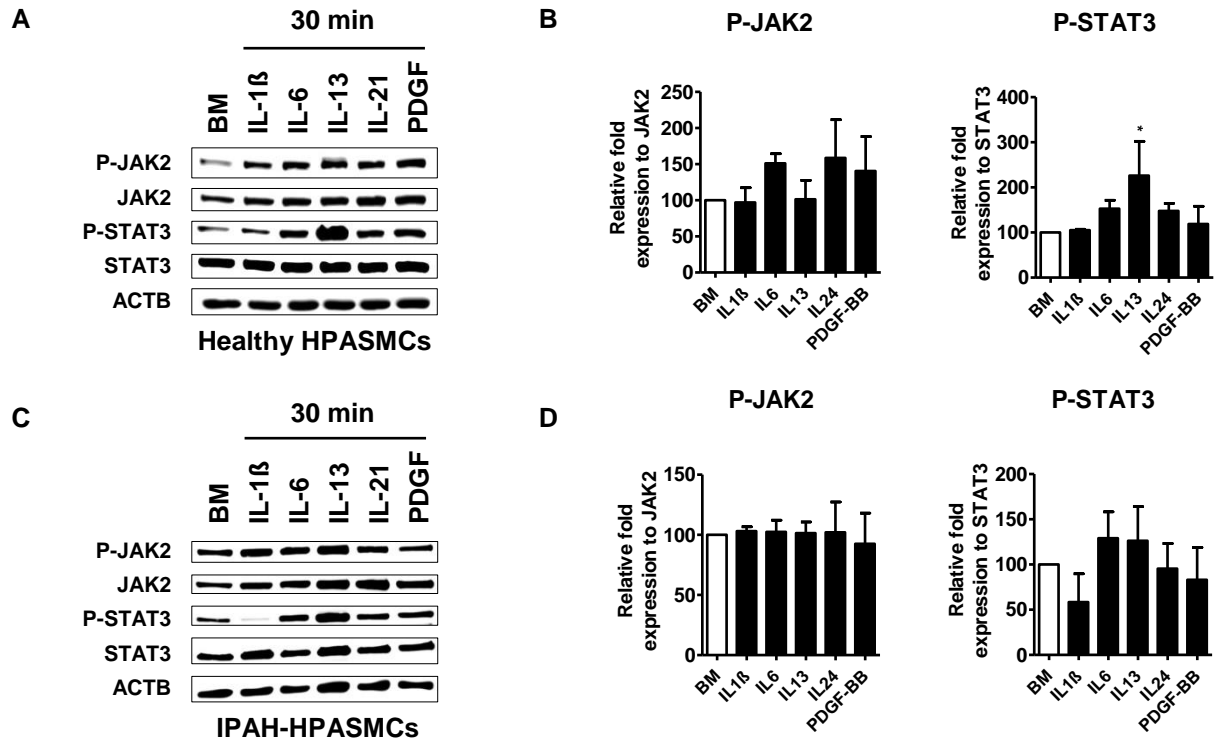
PASMCs obtained from the lungs of healthy individuals (n=5) and IPAH patients (n=5). After serum starvation, cells were cultured in BM for 24 hours. (A) mRNA expression analysis of JAK2, STAT3, Cyclin D1 and Bcl-2 in healthy and IPAH PASMCs. The mRNA expression was normalized to glyceraldehyde-3-phosphate dehydrogenase (GAPDH) as a reference gene. All data represent the mean  $\pm$  SEM of n-fold change ( $2^{-\Delta\Delta Ct}$ ) compared to healthy control. \*\*\*\*P < 0.0001, \*\*\*P < 0.001, \*\*P < 0.01, \*P < 0.05, Mann-Whitney test. 3 individual real-time PCR runs were performed in technical duplicates.

Analysis of JAK2, STAT3, Cyclin D1 and Bcl-2 mRNA expression in lung homogenates from (B) monocrotaline (MCT) treated rats and (C) chronic hypoxia (Hox) exposed mice. The mRNA expression from rat and mice samples normalized to  $\beta$ 2-microglobulin (B2M) and hydroxymethylbilane synthase (HMBS) as reference genes, respectively. All data represent the mean  $\pm$  SEM of n-fold change ( $2^{-\Delta\Delta Ct}$ ) compared to control column (Healthy or Nox). n=7-8 animals per group. Nox= normoxia. \*\*\*\*P < 0.0001, \*\*\*P < 0.001, \*\*P < 0.01, \*P < 0.05, two-tailed unpaired t-test. 3 individual real-time PCR runs were performed in technical duplicates.

### 4.3 Molecular analysis of the JAK2-STAT3 signaling axis in HPASMCs

#### 4.3.1. Stimulation (by interleukins and PDGF) of JAK2-STAT3 signaling in HPASMCs

One of the major ligands inducing the JAK2-STAT3 signaling pathway in HPASMCs is IL-6 [78]. To investigate whether other factors also contribute to the stimulation of the JAK2-STAT3 axis, starved PSMCs (healthy and IPAH) were incubated with various interleukins and PDGF for 30 minutes and 24 hours in basal media before protein lysis and subsequent western blotting. IL-6 treatment (30 minutes) in the presence of basal media conditions resulted in robust JAK2 and STAT3 phosphorylation demonstrating the activation of this signaling pathway in healthy PSMCs (Fig. 11A) and only P-STAT3 showed increase in protein levels in IPAH PSMCs (Fig. 11E). Long incubation with IL-6 (24 hours) did not show the activation of pathway in both healthy (Fig. 11C) and IPAH PSMCs (Fig. 11G). These observations have also been obtained after the addition of other interleukins or PDGF. We further continued only with IL-6 stimulated (30 minutes) PSMCs because all other interleukins tested (as well as PDGF) also act on multiple signaling networks leading to unwanted cellular stimulation independent of JAK2.



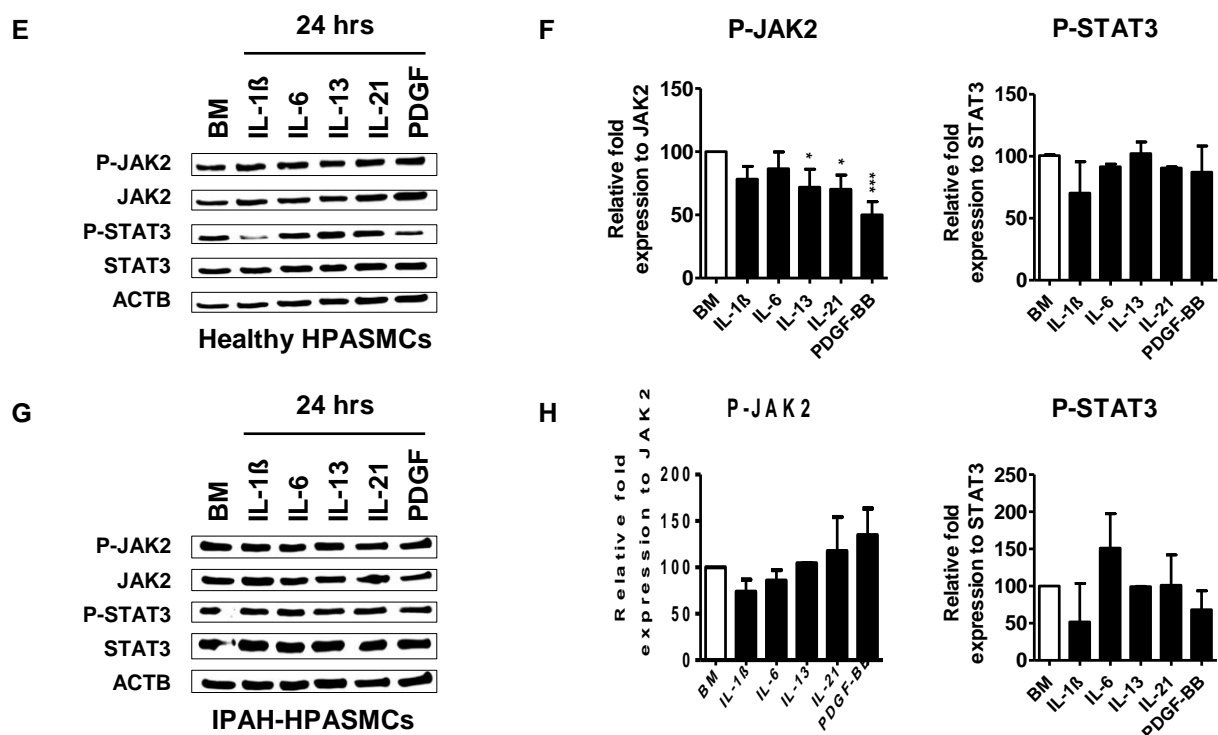


**Figure 11. Stimulation (by interleukins and PDGF) of JAK2-STAT3 signaling in HPASMCs.**

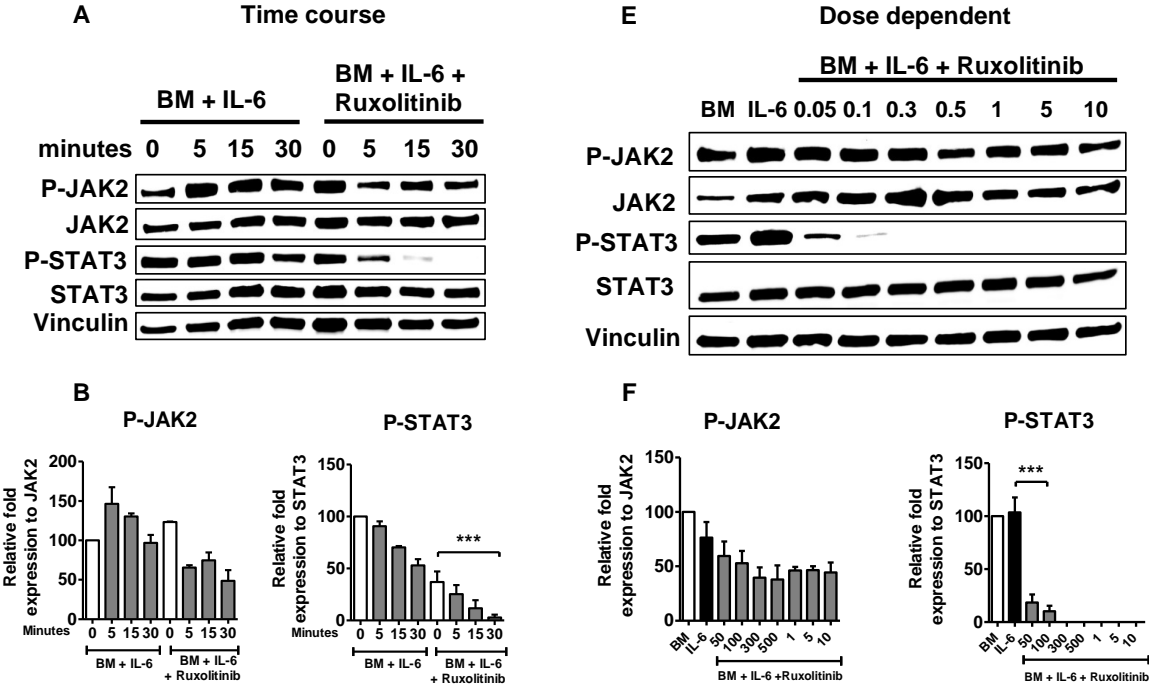
Cells were synchronized in BM for 24 hours. JAK2-STAT3 induction by interleukins, PDGF in healthy and IPAH PSMCs under BM condition. (A, C, E, G) Western blot analysis and (B, D, F, H) Subsequent densitometry quantification of phosphorylation of JAK2, STAT3 following 30 minutes (A-D) or 24 hours (E-H) stimulation in healthy (A, B, E, F) and IPAH (C, D, G, H) PSMCs. One representative experiment of three independent repetitions is shown. Beta-actin (ACTB) served as a loading control. All data represent the mean  $\pm$  SEM. one-way ANOVA with Dunnett's multiple comparison post-hoc test to compare all bars versus BM control. Interleukins were applied at 100 ng/ml and PDGF at 30 ng/ml concentrations. \*\*\* $P < 0.001$ , \* $P < 0.05$ . P values for distinct conditions were only given.

#### 4.3.2 Inhibition of JAK2-STAT3 signaling using JAK2 inhibitor ruxolitinib

Next, I investigated the response of HPASMCs to the treatment with and without ruxolitinib. In time-course experiments, HPASMCs were exposed to ruxolitinib (50 nM) for 2 hours prior to stimulation with IL-6 (100 ng/ml) for the indicated time points (5 to 30 minutes). Western blot analysis was performed to demonstrate the consequences of targeted JAK1/JAK2 inhibition on JAK2 and STAT3 phosphorylation. Here, protein levels of P-JAK2 and P-STAT3 were significantly reduced in the presence of ruxolitinib regardless of the duration of IL-6 stimulation in both the healthy (Fig. 12A) and IPAH (Fig. 12C) PSMCs. While the level of P-JAK2 was rapidly decreased already after 5 minutes and remained constant upon ruxolitinib exposure, the reduction of STAT3 phosphorylation was time-dependent with a complete blockage after 30 min of IL-6 treatment. To study dose-dependent effects of ruxolitinib on

JAK2-STAT3 signaling, pre-incubated PSMCs with indicated concentrations of ruxolitinib (0.05 to 10  $\mu$ M) for 60 minutes and stimulated the cells with IL-6 for subsequent 30 minutes. The IL-6 induced STAT3 phosphorylation was inhibited by ruxolitinib at all tested concentrations while levels of P-JAK2 remained unaffected in both the healthy (Fig. 12E) and IPAH PSMCs (Fig. 12G).

### Healthy PSMCs



## IPAH PSMCs

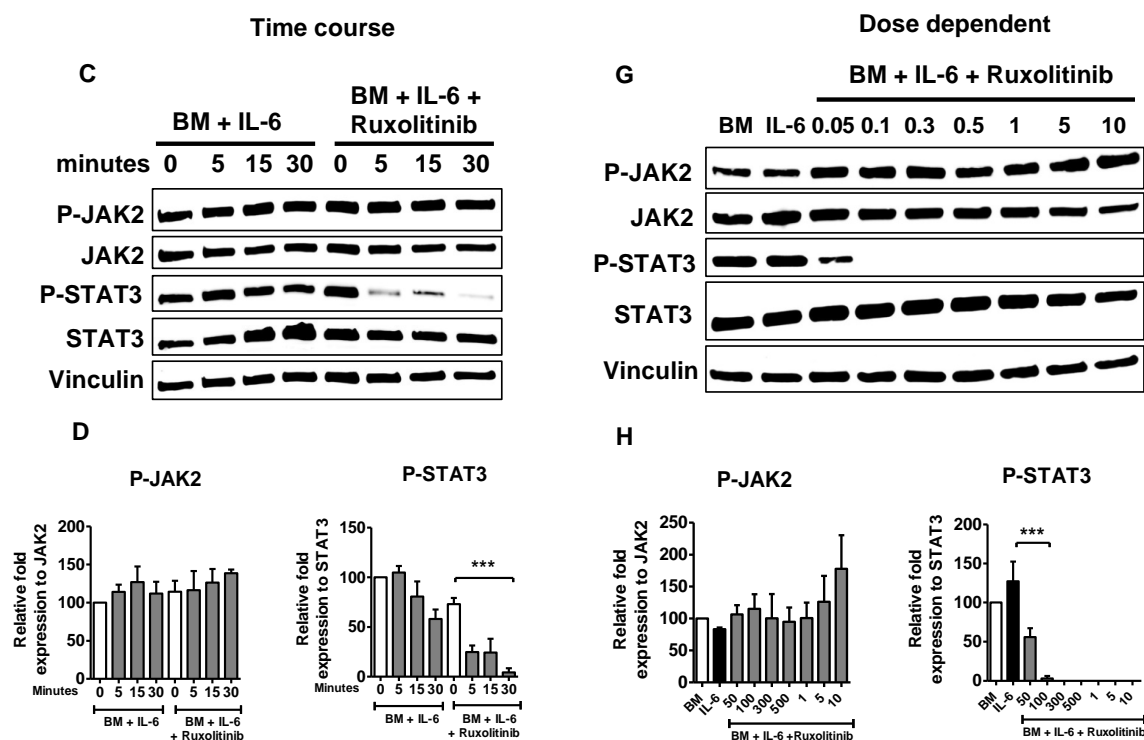


**Figure 12. Targeted inhibition of JAK-STAT signaling by ruxolitinib in HPASMCs.** Cells were pre-treated with the indicated concentration of ruxolitinib or DMSO as a control for 60 minutes before stimulation. Western blot analysis and Subsequent densitometry quantification for time (A-D) and dose-dependent (E-H) inhibition of JAK2 activity in healthy (A, B, E, F) and IPAH (C, D, G, H) PSMCs by ruxolitinib. Representative Western blots from PSMCs exposed to IL-6 and treated with vehicle (IL-6 + DMSO) or ruxolitinib (BM + IL-6 + Ruxolitinib) for the indicated times (given in minutes) with the indicated concentrations (given in  $\mu\text{M}$ ) for 30 minutes. Vinculin served as a loading control. Interleukins were applied at 100 ng/ml and PDGF at 30 ng/ml concentrations. All data represent the mean  $\pm$  SEM. \*\*\* $P < 0.001$ , one-way ANOVA with Dunnett's multiple comparison post-hoc test to compare all bars versus BM or IL-6 control.

### 4.4 Effects of ruxolitinib on downstream targets of JAK2 in healthy HPASMCs

To assess the effect of ruxolitinib on downstream targets of JAK2 and on PI3K signaling, cells were treated with indicated concentrations of ruxolitinib for 24 hours in BM. Western blot analysis demonstrated that phosphorylation of STAT3, PI3K and c-MYC were significantly reduced in response to ruxolitinib treatment (Fig. 13B). Long exposure to ruxolitinib did not affect the cell viability (Fig. 13A). This results further supported by the significant reduction in mRNA expression of STAT3 and c-MYC in HPASMCs (Fig. 13D).

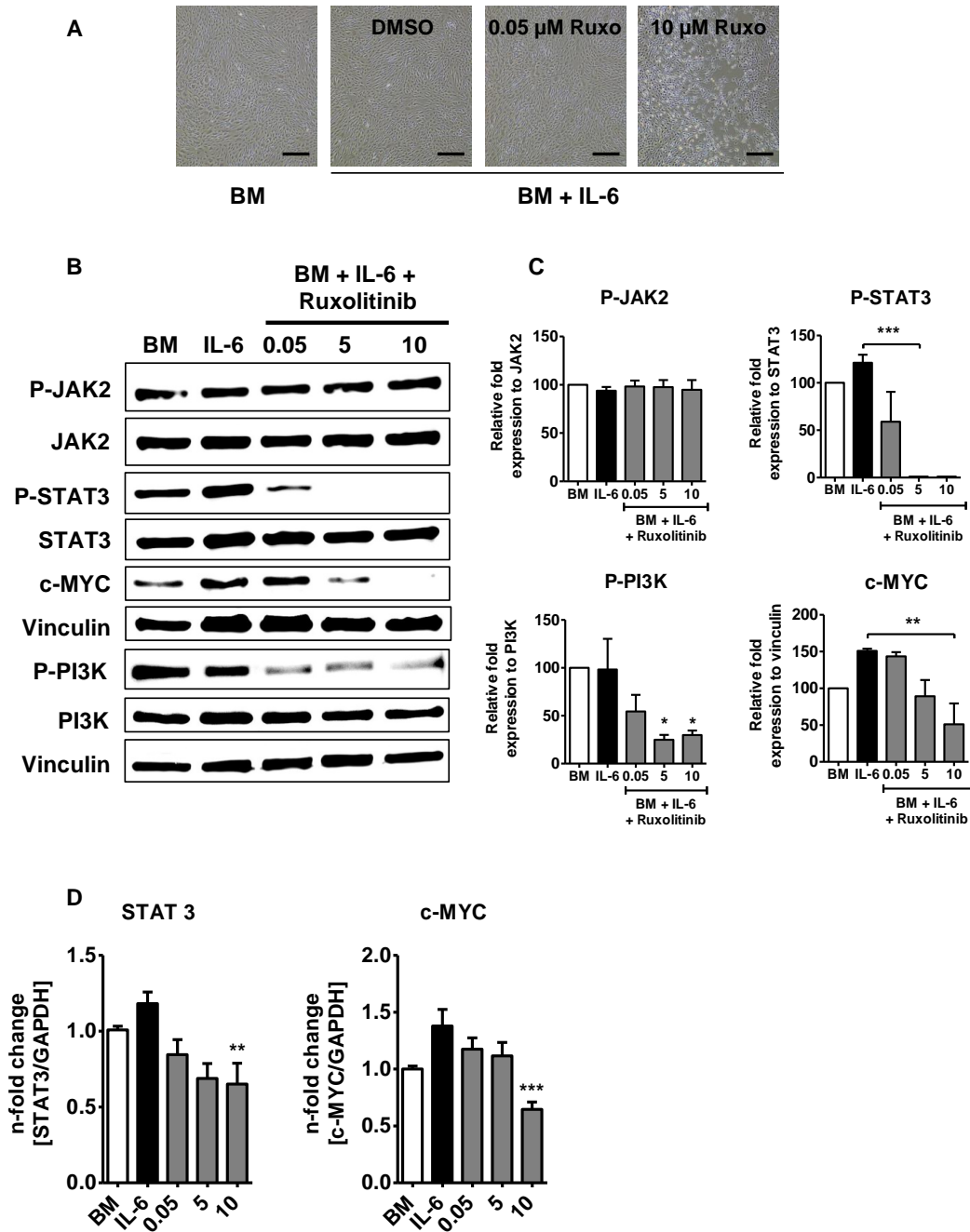


**Figure 13. Effects of ruxolitinib on downstream targets of JAK2 in healthy HPASMCs.**

Healthy PSMCs were synchronized in BM and exposed to IL-6 in the presence of DMSO (as a control) or ruxolitinib at the indicated concentrations (given in  $\mu\text{M}$ ) for 24 hours in BM. Cells were pre-treated with the indicated concentration of ruxolitinib or DMSO as a control for 60 minutes before stimulation. (A) Representative phase-contrast images of the studied cells at adequate magnification with a scale bar of  $100\ \mu\text{m}$ . (B) Western blot analysis and (C) subsequent densitometry quantification of P-JAK2, P-STAT3, c-MYC and P-PI3K in healthy HPASMCs. Vinculin served as a loading control. (D) The mRNA expression analysis of STAT3 and c-MYC was normalized to GAPDH as reference gene. 3 individual real-time PCR runs were performed in duplicates. All data throughout the figure represent the mean  $\pm$  SEM. \*\*\* $P < 0.001$ , \*\* $P < 0.01$ , \* $P < 0.05$ , one-way ANOVA with Dunnett's multiple comparison post-hoc test to compare all bars versus BM control or IL-6. IL-6 was applied at  $100\ \text{ng/ml}$  concentration.

#### 4.5 Effects of ruxolitinib on IL-6 induced proliferation of human HPASMCs

To study the functional effect of ruxolitinib on HPASMCs proliferation, serum starved PSMCs were treated with increasing concentrations of ruxolitinib (0.05 to 10  $\mu\text{M}$ ) in the presence and absence of IL-6 in basal media. IL-6 significantly induced cellular proliferation measured by BrdU incorporation which can be dose-dependently inhibited by ruxolitinib in both the stimulation conditions in healthy PSMCs (Fig. 14A-B). Similar results were obtained in IPAH PSMCs (Fig. 14C-D).

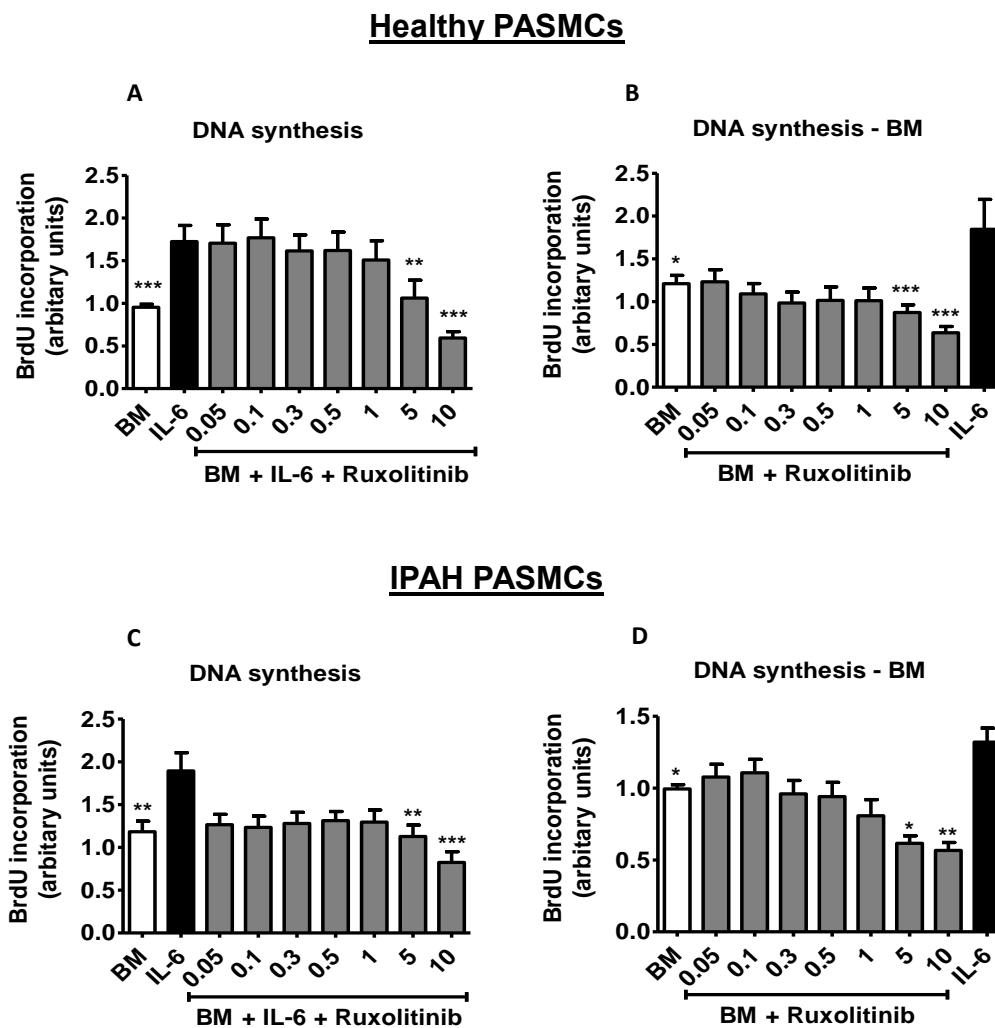


**Figure 14. Effects of ruxolitinib on IL-6 induced proliferation of HPASMCs.**

Healthy and IPAH PSMCs were synchronized in BM and exposed to IL-6 and BM in the presence of DMSO (as a control) or ruxolitinib at the indicated concentrations (given in  $\mu\text{M}$ ) for 24 hours in BM. Control cells were exposed to BM. After 18 hours of incubation with BrdU, cellular proliferation was determined by measuring BrdU incorporation (relative absorbance [ $A_{370\text{nm}}-A_{492\text{nm}}$ ]) in healthy (A-B) and IPAH (C-D) PSMCs. Data from each experiment normalized to BM (white). 3 independent cell culture experiments were performed in triplicates. The results were analyzed by one-way ANOVA with Dunnett's multiple comparison post-hoc test to compare all bars versus IL-6 control (black); \*\*\* $P < 0.001$ , \*\* $P < 0.01$ , \* $P < 0.05$ . P values for distinct conditions were only given. IL-6 concentration used 100 ng/ml.

#### 4.6 Effects of JAK2 inhibitor ruxolitinib on cytotoxicity of human HPASMCs

To study the role of ruxolitinib treatment on cytotoxicity of HPASMCs, cells were treated with increasing concentrations of ruxolitinib (0.05 to 10  $\mu\text{M}$ ) in the presence and absence of IL-6 in basal media. In healthy (Fig. 15A-B) PSMCs, the ruxolitinib treatment did not show any cytotoxicity as determined in an LDH release assay using 2% Triton-X100 as a positive control (PC). However, a slight but significant cytotoxicity was detected in IPAH PSMCs (Fig. 15C-D) at higher concentrations, i.e. 1-10  $\mu\text{M}$ .

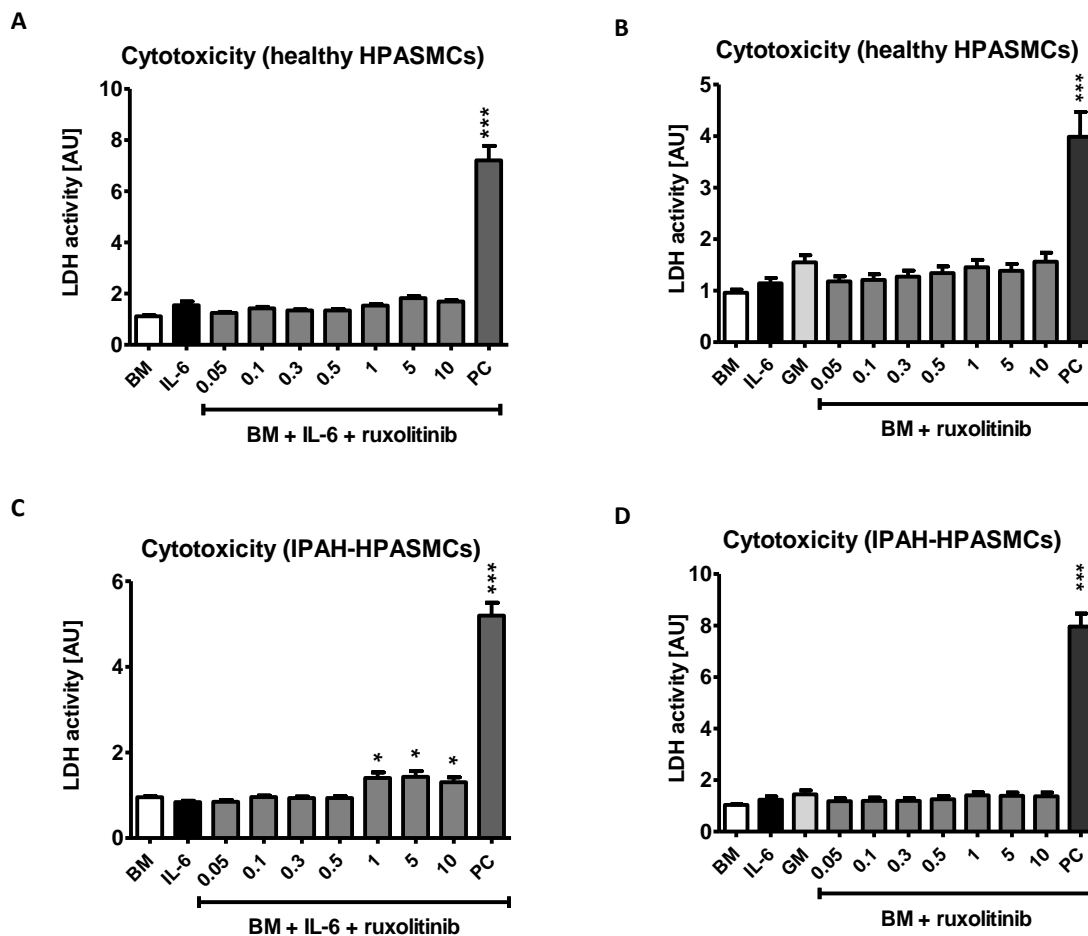


**Figure 15. JAK2 inhibitor ruxolitinib has not induced cytotoxicity of human HPASMCs.**

Cytotoxicity analysis of ruxolitinib. HPASMCs were incubated with and without IL-6 and different doses of ruxolitinib (0.05–10  $\mu\text{M}$ ) for 24 hours. The supernatant was removed and the release of active lactate dehydrogenase (LDH) was determined (relative absorbance [ $A_{492\text{nm}}-A_{620\text{nm}}$ ]) in healthy (B) and IPAH (D) PSMCs. Triton-X-100 was used as a positive control (PC) for cell death induction. Data from each experiment normalized to BM (white). 3 independent experiments were performed in triplicates. The results were analyzed by one-way ANOVA with Dunnett's multiple comparison post-hoc test to compare all bars versus IL-6 control (black); \*\*\* $P < 0.001$ , \* $P < 0.05$ . P values for distinct conditions were only given. IL-6 concentration used 100 ng/ml.

#### 4.7 Treatment with ruxolitinib has no effect on apoptosis and viability of human PSMCs

Human PSMCs were treated with increasing concentrations of ruxolitinib (0.05 to 10  $\mu$ M) in basal media for 24 hours. Apoptosis was measured by Caspase-Glo 3/7 assay (Fig. 16A-B) and cell viability was assessed by XTT assay (Fig. 16C-D). In both healthy and IPAH PSMCs, after the ruxolitinib treatment, no apoptosis induction was observed and also cell viability is not reduced.

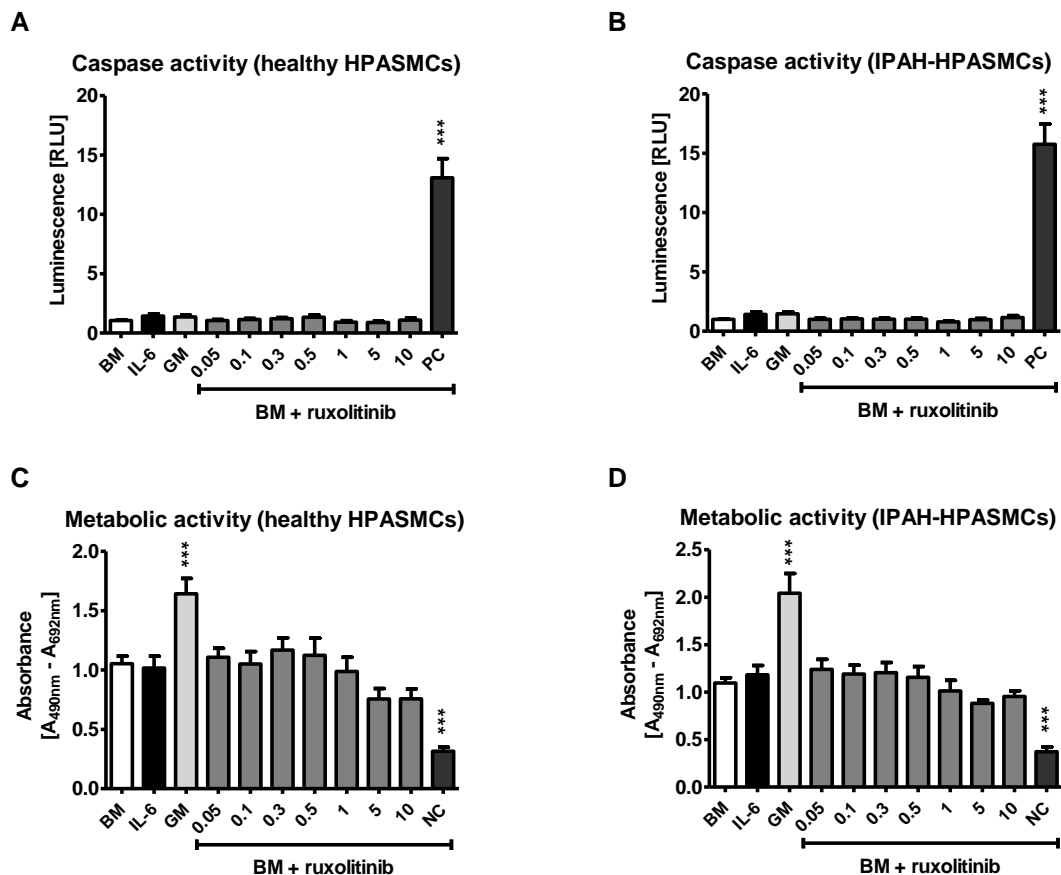


**Figure 16. Treatment with ruxolitinib has no effect on apoptosis and viability of human PSMCs.**

Healthy (n=4) and IPAH (n=4) PSMCs were synchronized in BM and exposed to BM in the presence of DMSO (as a control) or ruxolitinib at the indicated concentrations (given in  $\mu$ M) for 24 hours in BM. Control cells were exposed to BM. Caspase-Glo 3/7 assay analysis showing ruxolitinib effect in healthy (A) and IPAH (B) PSMCs. Cell viability was determined by the XTT assay after 4 hours of incubation (relative absorbance [ $A_{490nm} - A_{692nm}$ ]) in healthy (C) and IPAH (D) PSMCs. Staurosporine served as positive control (PC) for (A, B) and negative control for (C, D). Data from each experiment normalized to BM (white). 4 independent cell culture experiments were performed in triplicates. The results were analyzed by one-way ANOVA with Dunnett's multiple comparison post-hoc test to compare all bars versus BM control (white); \*\*\* $P < 0.001$ . P values for distinct conditions were only given. IL-6 concentration used 100 ng/ml.

#### 4.8 Effects of ruxolitinib on IL-6 induced migration of human PSMCs

Next, I examined the effect of ruxolitinib on HPASMCs migration in a modified transwell chamber assay. Cells were treated with ruxolitinib for 18 and 6-hours. The decrease in the percentage of cells migrated through the membrane was significant already at the lowest dosage of 50 nM ruxolitinib compared to IL-6 induced control cells after 18 hours (Fig. 17A). No difference in cell migration was observed after 6-hour time point (Fig. 17B). Taken together, our data demonstrate that ruxolitinib inhibits PSMCs proliferation at the highest concentrations of 5 to 10  $\mu$ M but exerts an anti-migratory potential already at a low dose of 0.05  $\mu$ M without showing signs of cytotoxicity, induction of apoptosis and reduction of cell viability.

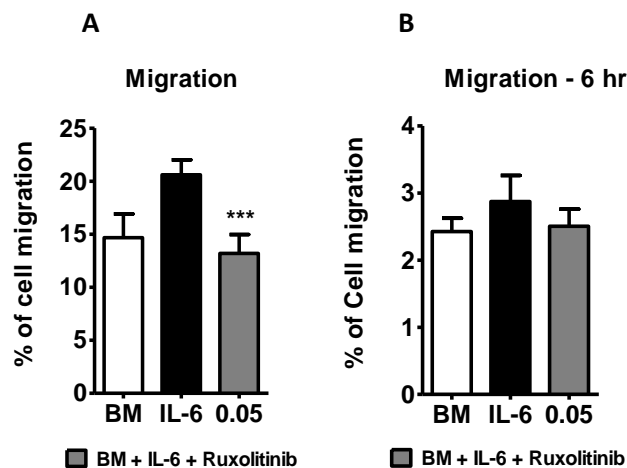


**Figure 17. Effects of ruxolitinib on IL-6 induced migration of human HPASMCs.**

Effects of ruxolitinib on IL-6 induced migration of healthy PSMCs was investigated by Transwell assay. After 24 hours of starvation in BM, cells treated with either IL-6 or ruxolitinib (0.05  $\mu$ M) for 18 (A) and 6 hours (B). 3 independent experiments were performed. The results were analyzed by one-way ANOVA with Dunnett's multiple comparison post-hoc test to compare all bars versus IL-6 control (black); \*\*\* $P < 0.001$ . P values for distinct conditions were only given. IL-6 concentration used 100 ng/ml.

#### 4.9 Ruxolitinib improves cardio-pulmonary functions in MCT-induced PAH

I determined the consequences of targeted JAK/JAK2 inhibition of ruxolitinib in the MCT-induced rat model of PAH. 21 days after MCT injection, rats were treated with either placebo or ruxolitinib at a daily dose of 30 mg/kg or 90 mg/kg body weight (BW) by oral gavage for 14 days (Fig. 18A). Improvement of cardio-pulmonary functions was assessed by echocardiography and hemodynamic measurements. Several parameters indicate that ruxolitinib was able to reverse the disease-associated phenotype at a higher dosage of 90 mg/kg BW. Right ventricular systolic pressure (RVSP, Fig. 18B), Fulton index (Fig. 18C), right

ventricular inner diameter (RVID, Fig. 18D), and total pulmonary vascular resistance index (TPVRI, Fig. 18G) were reduced due to ruxolitinib compared to the placebo group (MCT). In line with this stroke volume index (SVI, Fig. 18H), cardiac index (CI, Fig. 18E), and tricuspid annular plane excursion (TAPSE, Fig. 18F) were restored in ruxolitinib treated rats at 90 mg/kg BW compared to MCT placebo animals; without affecting the systolic blood pressure (SBP, Fig. 18I).

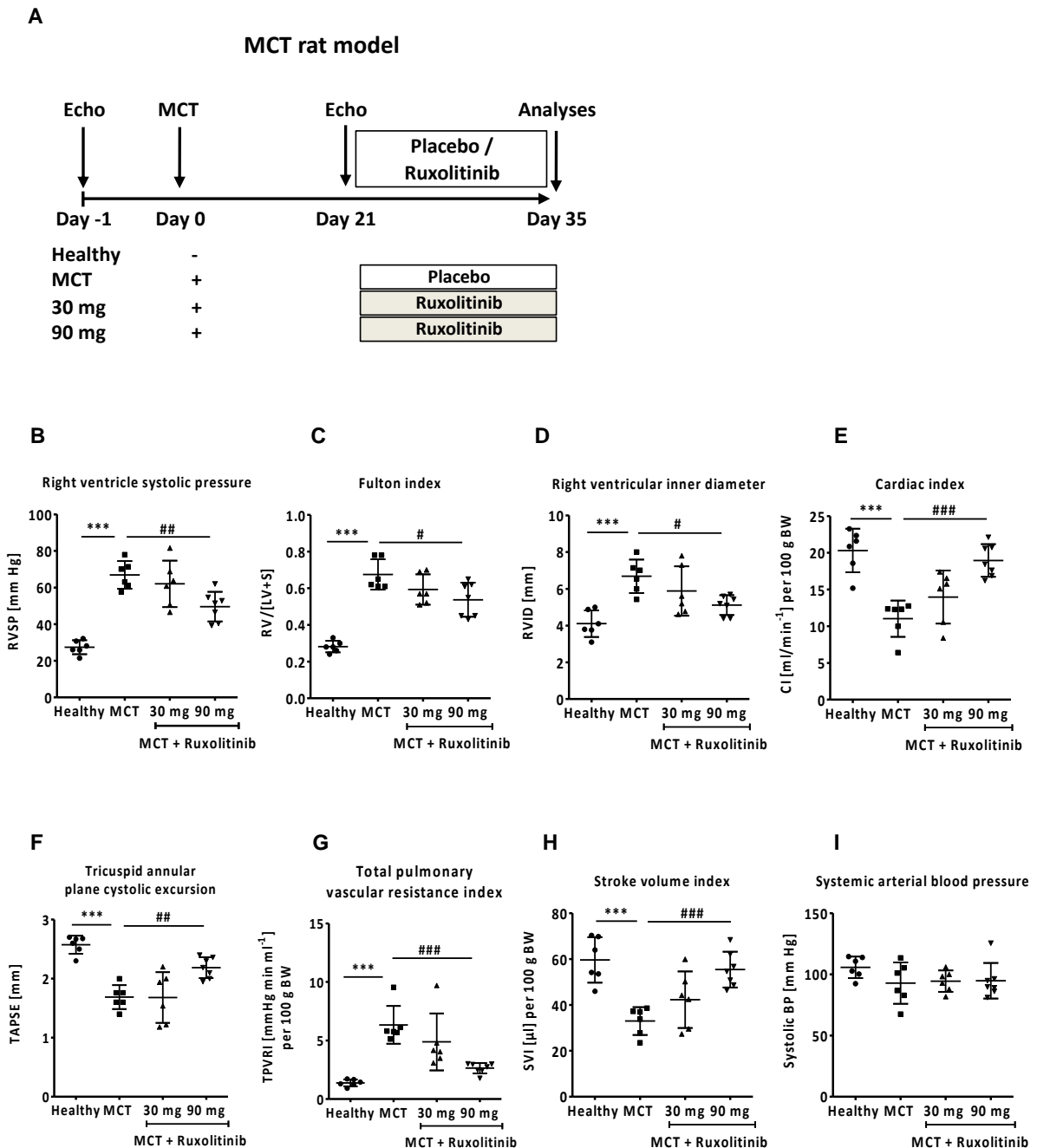


**Figure 18. Effects of ruxolitinib on cardio-pulmonary functions in rats with monocrotaline (MCT) induced pulmonary hypertension.**

(A) Diagram showing the experimental timeline for *in vivo* ruxolitinib administration in the MCT induced rat model of PAH. Animals are grouped into the following categories: Healthy (without MCT injection; n=6), MCT (Placebo treated; n=6) and rats treated with 30 mg/kg bodyweight ruxolitinib (MCT + 30 mg Ruxolitinib; n=6), 90 mg/kg bodyweight ruxolitinib (MCT + 90 mg Ruxolitinib; n=7) every day from day 21 to day 35. (B) Right ventricular systolic pressure (RVSP) [mmHg]. (C) RV hypertrophy measured as the ratio of RV to left ventricular (LV) wall plus septum [RV/ [LV+S]]. (D) Right ventricular internal diastolic diameter (RVID) [mm]. (E) Cardiac output (CI) [ml/min<sup>-1</sup>] per 100 g bodyweight. (F) Tricuspid annular plane systolic excursion (TAPSE) [mm]. (G) Total pulmonary vascular resistance index (TPVRI) [mmHg min ml<sup>-1</sup>] per 100 g body weight. (H) Stroke volume (SV) [μl]. (I) Systemic arterial blood pressure (Systolic BP) [mmHg]. Data represent the mean ± SEM and statistical analysis performed using one-way ANOVA with Dunnett's multiple comparison post-hoc test to compare all groups versus MCT. \*\*\**P* < 0.001 for MCT versus Healthy; ####*P* < 0.001, ##*P* < 0.01, #*P* < 0.05 for MCT+Ruxo 90mg versus MCT. This experiment performed with the help of ECCPS *in vivo* platform.

**4.10 MCT induced pulmonary vascular remodeling in rats**

Next, I examined the effect of ruxolitinib on pulmonary vascular remodeling by counting the number of gradually muscularized small pulmonary arteries based on immunohistological staining for smooth muscle actin and von Willebrand factor. Lung morphometry clearly demonstrated that ruxolitinib treatment with 90 mg/kg BW significantly reduced the percentage of fully muscularized small pulmonary arteries (Fig. 19A). These results demonstrate that ruxolitinib reverses pulmonary vascular remodeling (Fig. 19B) and thereby improves right ventricular function including a reduction in right ventricular hypertrophy in the MCT rat model of PAH *in vivo*. Furthermore, I analyzed a small panel of pro-(IL-1β, IL-6) (Fig. 19C) and anti-inflammatory (IL-10, IL-13) (data not shown) cytokines but ruxolitinib did not change the mRNA levels of any of these factors compared to the MCT group.

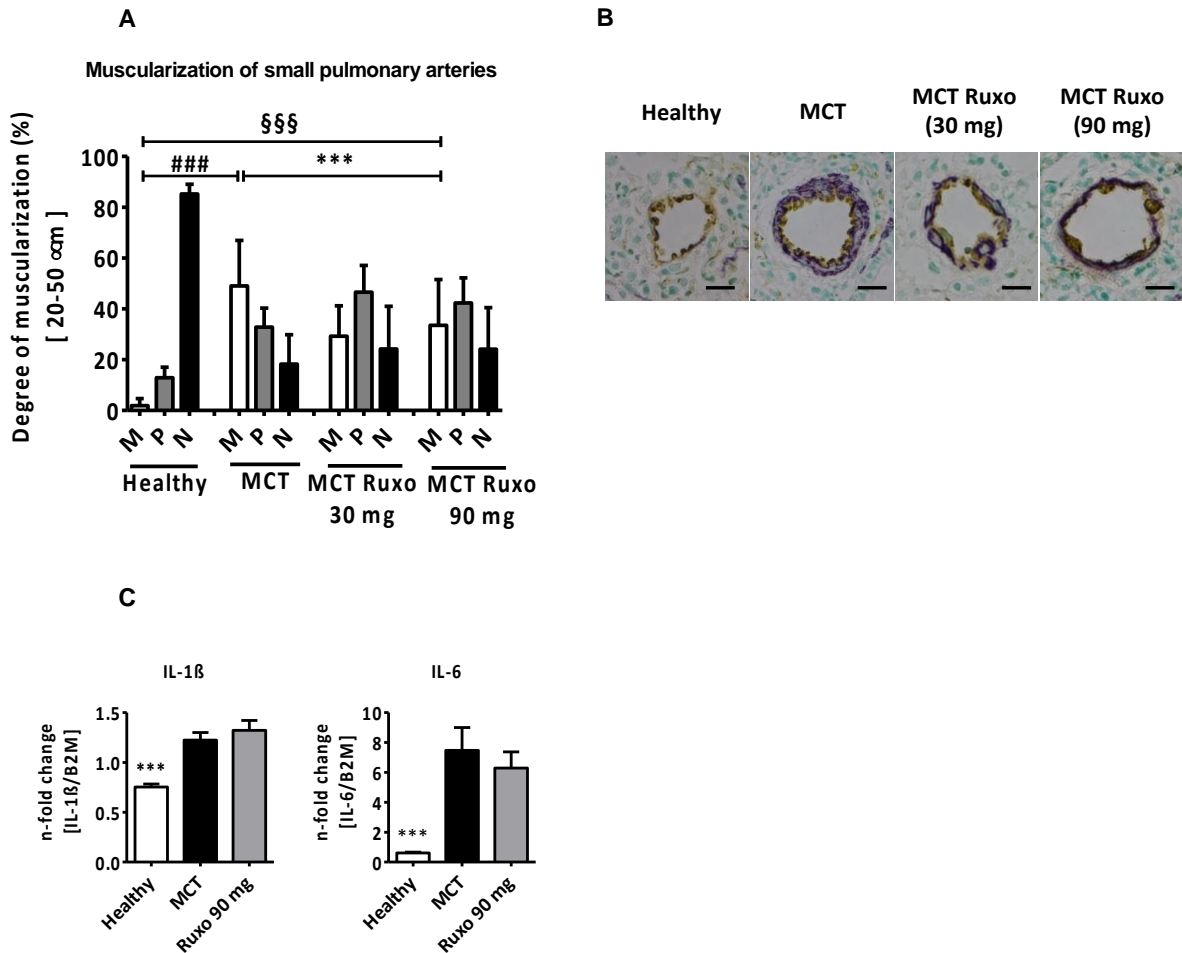


**Figure 19. Effect of ruxolitinib on vascular remodeling in rats with MCT induced pulmonary hypertension.**

**(A)** Bar chart showing the degree of muscularization of small pulmonary arteries (diameter 20-50  $\mu$ m) as measured by immunohistological staining of lung sections for vWF (brown) and  $\alpha$ -SMA (violet) together with methyl green for counterstaining in rats. M: fully muscularized; P: partially muscularized; N: non-muscularized. Data from all individual animals (Healthy n=9; MCT n=7, MCT+ Ruxo 30mg n=9, MCT+ Ruxo 90mg n=8) are presented as mean  $\pm$  SEM of 80–100 counted vessels and statistical analysis was performed using one-way ANOVA with Tukey's post-hoc test for multiple comparisons; \*\*\* $P$  < 0.001 for MCT Ruxo 90 mg versus Healthy; ###  $P$  < 0.001 for MCT versus Healthy; §§§  $P$  < 0.001 for MCT Ruxo 90 mg versus MCT. This experiment performed with the help of ECCPS *in vivo* platform **(B)** Representative photomicrographs for all 4 study groups are shown. Scale bar = 20  $\mu$ m. **(C)** RNA isolated from lung homogenates was analyzed for IL-1 $\beta$  and IL-6 mRNA expression (normalized to B2M as reference gene) in all three experimental groups. All data represent the mean  $\pm$  SEM of n-fold change ( $2^{-\Delta\Delta Ct}$ ) compared to healthy control rats. (Healthy n=9; MCT n=7; Ruxo 90mg n=8). Statistical analysis was performed using one-way ANOVA with Dunnett's multiple comparison post-hoc test to compare all bars versus MCT; \*\*\* $P$  < 0.001. 3 individual real-time PCR runs were performed in technical duplicates. Ruxo=Ruxolitinib.

#### 4.11 Ruxolitinib restores right ventricular function in chronic hypoxia-induced PH in mice

I also examined the effect of ruxolitinib in a second model of experimental PH. Chronic (21 days) hypoxia (Hox) exposed mice were treated with either placebo or ruxolitinib at a daily dose of 90 mg/kg or 180 mg/kg BW by oral gavage for subsequent 14 days in hypoxia (Fig. 20A). The ruxolitinib treatment resulted in a significant decrease in RVSP (Fig. 20B) and RV hypertrophy (Fig. 20C) as well as TPVRI (Fig. 20G). The function of the right ventricle was improved as shown by a significant decrease in RVID (Fig. 20D), increased SVI (Fig. 20H), cardiac index (CI) (Fig. 20E), and improved TAPSE (Fig. 20F) in ruxolitinib treated mice compared with control group (Hox). Ruxolitinib had no effect on SBP (Fig. 20I).

A

#### Hypoxia mouse model

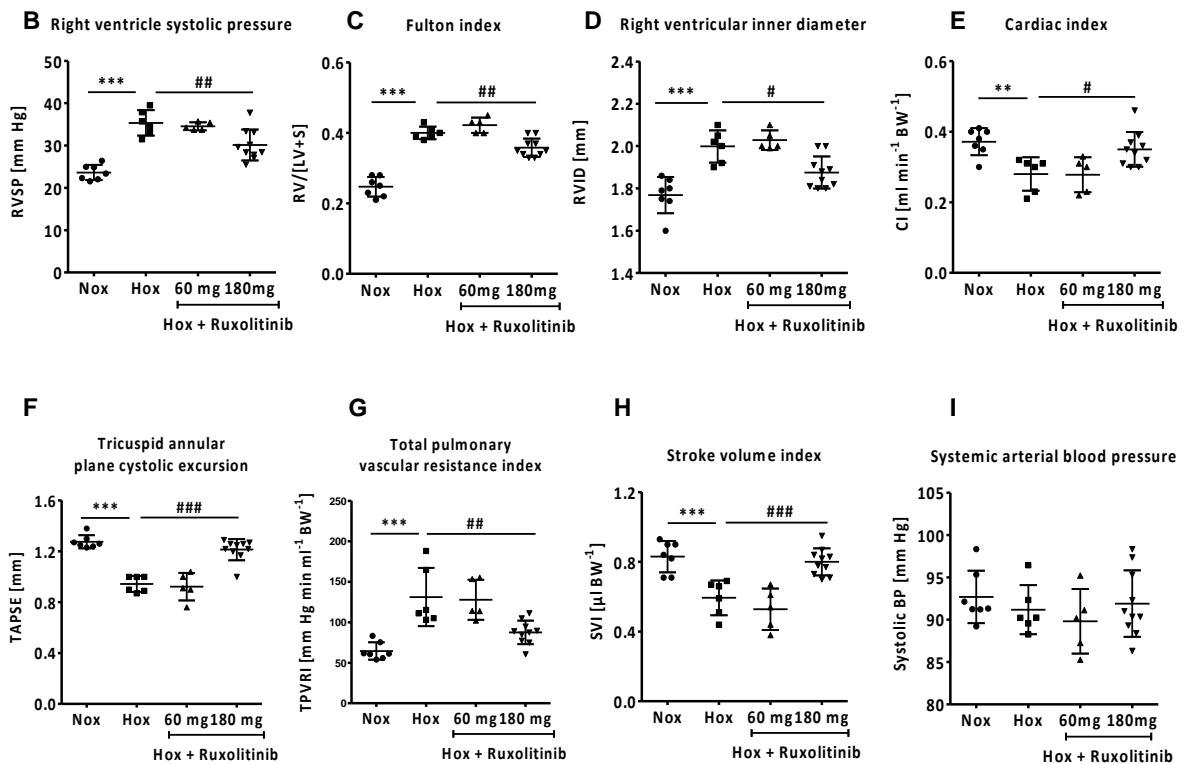
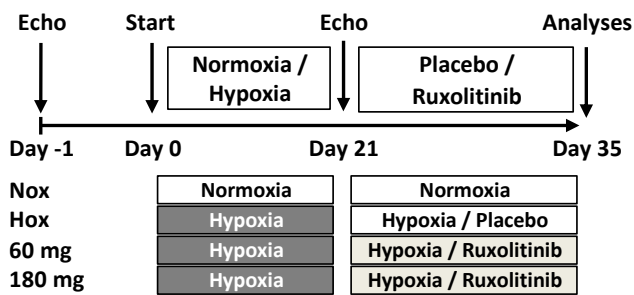
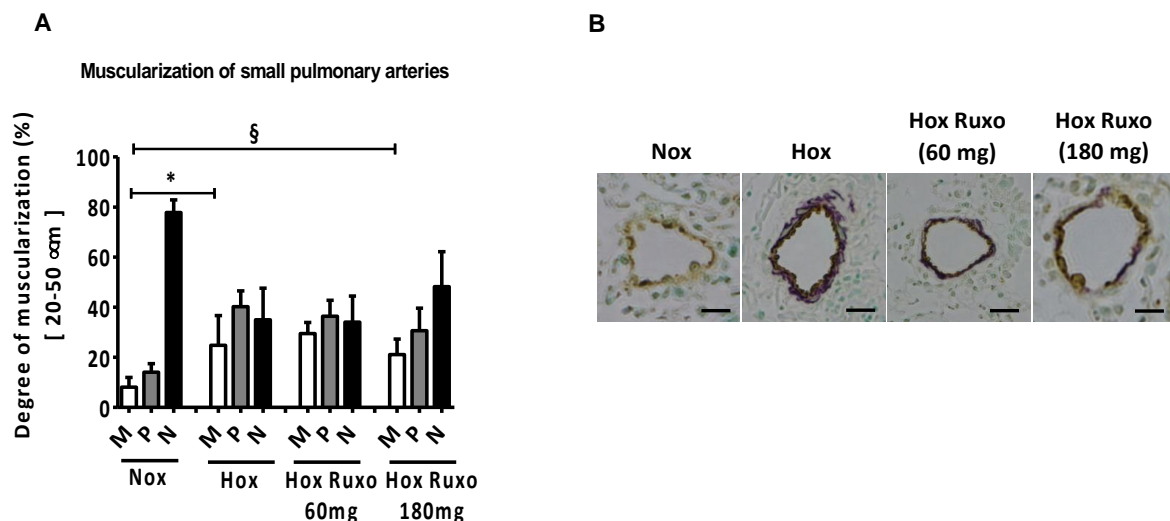


**Figure 20. Effects of ruxolitinib on cardio-pulmonary functions in mice with chronic hypoxia (Hox) induced pulmonary hypertension.**

**(A)** Diagram showing the experimental timeline for *in vivo* ruxolitinib administration in the chronic hypoxia-induced mouse model of PAH. Animals are grouped into the following categories: Nox (n=7), Hox (Placebo treated; n=6) and mice treated with 60 mg/kg bodyweight ruxolitinib (Hox + 60 mg Ruxolitinib; n=5), 180 mg/kg bodyweight ruxolitinib (Hox + 180 mg Ruxolitinib; n=10) every day from day 21 to day 35. **(B)** RVSP [mmHg]. **(C)** Fulton index [RV/ [LV+S]]. **(D)** RVID [mm]. **(E)** CI [ml/min<sup>-1</sup>] per bodyweight. **(F)** TAPSE [mm]. **(G)** TPVRI [mmHg min ml<sup>-1</sup>] per body weight. **(H)** SVI [μl] per body weight. **(I)** Systolic BP [mmHg]. Data represent the mean ± SEM and statistical analysis performed using one-way ANOVA with Dunnett's multiple comparison post-hoc test to compare all groups versus Hox. \*\*\**P* < 0.001, \*\**P* < 0.01 for Hox versus Nox; ###*P* < 0.001, ##*P* < 0.01, #*P* < 0.05 for Hox + Ruxo 180 mg versus Hox. This experiment performed with the help of ECCPS *in vivo* platform

**4.12 Chronic hypoxia-induced pulmonary vascular remodeling in mice**

*Ex vivo* lung morphometry analysis showed that ruxolitinib treatment did not significantly reduce the percentage of any of the sub-groups (fully, partial, none) of the muscularized small pulmonary arteries compared to the Hox mice (Fig. 21A). These results indicate that ruxolitinib treatment significantly improves right ventricular function without a reversal of pulmonary vascular remodeling in chronic hypoxia-induced PH mice (Fig. 21B). The mRNA expression levels of both pro-inflammatory cytokines namely IL-1β and IL-6 were significantly reduced upon ruxolitinib administration when compared to placebo-treated (Hox) mice (Fig. 21C).



C

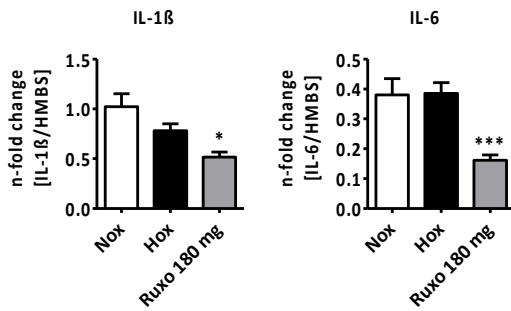


**Figure 21. Effect of ruxolitinib on vascular remodeling in mice with Hox induced pulmonary hypertension.**

**(A)** Bar chart showing the degree of muscularization of small pulmonary arteries (diameter 20-50  $\mu\text{m}$ ) as measured by immunohistological staining of lung sections for vWF (brown) and  $\alpha$ -SMA (violet) together with methyl green for counterstaining in mice. M: fully muscularized; P: partially muscularized; N: non-muscularized. Data from all individual animals (Nox, n=7; Hox, n=7; Hox + Ruxo 60 mg, n=5; Hox + Ruxo 180 mg, n=10) are presented as mean  $\pm$  SEM of 80–100 counted vessels and statistical analysis was performed using one-way ANOVA with Tukey's post-hoc test for multiple comparisons;  $\$P < 0.05$  for Hox + Ruxo 180 mg versus Nox,  $*P < 0.05$  for Hox versus Nox. This experiment performed with the help of ECCPS *in vivo* platform **(B)** Representative photomicrographs for all 4 study groups are shown. Scale bar = 20  $\mu\text{m}$ . **(C)** RNA isolated from lung homogenates was analyzed for IL-1 $\beta$  and IL-6 mRNA expression (normalized to HMBS as reference gene) in all three experimental groups. All data represent the mean  $\pm$  SEM of n-fold change ( $2^{-\Delta\Delta\text{Ct}}$ ) compared to Nox control mice. (Nox n=7; Hox n=7; Ruxo 180 mg n=10). Statistical analysis was performed using one-way ANOVA with Dunnett's multiple comparison post-hoc test to compare all bars versus Hox;  $***P < 0.001$ ,  $*P < 0.05$ . Three individual real-time PCR runs were performed in technical duplicates. Ruxo=Ruxolitinib.

Taken together, these results show that ruxolitinib efficiently blocks the JAK2-STAT3 signaling pathway in the progression of PH in two experimental models - the MCT rat and chronic hypoxia mouse model. IL-6 induced JAK2 activation and subsequent STAT3 phosphorylation was inhibited by ruxolitinib, leading to reduced proliferation (at highest dosages) and migration (at lowest dosage) that finally interferes with the structural remodeling in the pulmonary vasculature (Fig. 22).

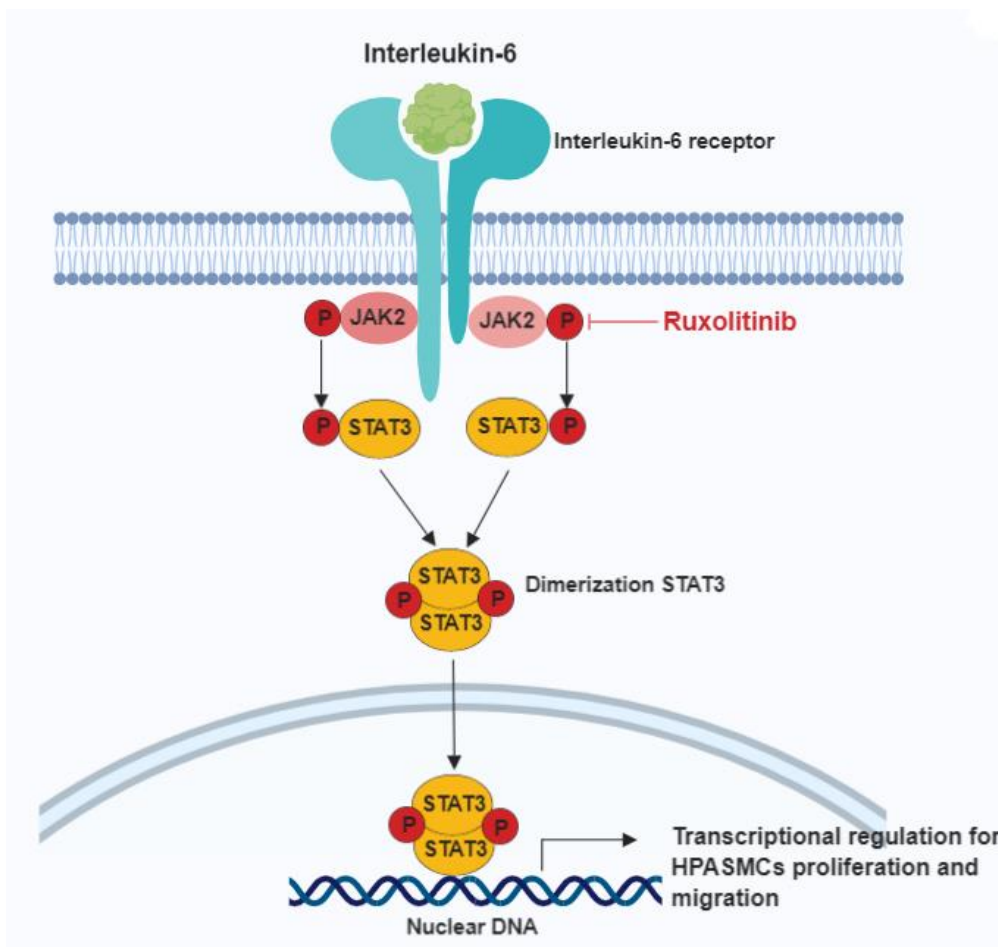


**Figure 22. Schematic representation of the ruxolitinib mode of action in HPASMCs in PAH.**

Interleukin-6 induces the activation of the JAK2-STAT3 pathway and leads to the proliferation and migration of PSMCs. Ruxolitinib is a selective inhibitor for JAK2 kinase activity which results in decreased phosphorylation of the downstream transcription factor STAT3. As a consequence, the expression of STAT3 target genes involved in survival and migration of PSMCs are inhibited. Thereby, ruxolitinib exerts anti-remodeling properties in vitro and in the pulmonary vasculature in experimental models of PH in vivo.

## 5. DISCUSSION

Currently, there are no approved PAH therapies targeting pulmonary vascular remodeling by reversing proliferative changes in the pulmonary circulation. However, anti-proliferative drugs like imatinib have been studied for their use in PAH [79] and our group recently showed that CDK inhibitors are effective in reducing disease symptoms in preclinical models [38].

The objective of this study was to identify and validate new drug targets for an anti-proliferative treatment of PH. Although the role of JAK2-STAT3 signaling in pulmonary hypertension is still not clearly defined, it is generally reported to play an important role in the development of PH. Moreover, very few studies reported on the JAK2-STAT3 signaling

pathway involvement in pulmonary hypertension. In this present study, the impact of ruxolitinib on the IL-6 induced JAK2-STAT3 pathway and its consequences on HPASMC function were investigated. In addition to that, this study is the first to demonstrate the effects of the JAK1/JAK2 inhibitor ruxolitinib in two well-characterized animal models of PH e.g. the MCT rat model of PAH and the chronic hypoxia model of PH in mice.

### **5.1 Tyrosine kinase analysis of human PSMCs**

Tyrosine kinase analysis was performed in PSMCs from the lungs of IPAH patients and healthy individuals. Significant differences were observed in peptide phosphorylation in PSMCs from IPAH patients as compared to healthy counterparts under basal media conditions. Among the family of tyrosine kinases, JAKs were found to be over-activated using a peptide-based kinase activity assay to screen this key cell type responsible for medial hypertrophy in PAH [80]. JAKs, especially JAK2, play an important role in vascular cell proliferation and migration [81], making JAK2 an attractive drug target. Some studies reported that JAK2 over-expression has been noted in IPF [82] and PAH patients [62]. Growth factors and cytokines play a central role in PSMC proliferation by activating signaling pathways like JAK2-STAT3 and promoting proliferation and migration [83, 84]. These results support further testing of targeted JAK2-STAT3 inhibition in PSMCs *in vitro* and in experimental PH models *in vivo*.

### **5.2 Expression of JAK-STAT signaling molecules in human and experimental PH**

The expression analysis on protein and mRNA levels was performed in PSMCs from IPAH patients and healthy counterparts under basal media conditions. Western blot analysis showed a significant increase in protein expression of P-JAK2 and P-STAT3 in IPAH-PSMCs as compared to healthy (Fig. 9A). The JAK2, and its downstream effectors STAT3, Cyclin D1, and Bcl-2 mRNA levels were significantly upregulated in IPAH-PSMCs as compared to healthy (Fig. 10C). This result along with tyrosine kinase profiling indicates that JAK2-STAT3 signaling is upregulated in IPAH-PSMCs and this is predominantly caused by enhanced protein expression of phosphorylated JAK2 (P-JAK2) and STAT3 (P-STAT3).

In experimental models of PH, a similar increase was observed in lung homogenates of MCT-treated rats and only STAT3 mRNA was upregulated in lungs of hypoxia-exposed mice. This might be because of differences in disease induction mechanisms, such as PAH in MCT rat

model is characterized by the increased proliferation of PASMCs, increased apoptosis of ECs and resistance of PASMCs to apoptosis and genes such as HIF-1 $\alpha$ , BMPR-2 and eNOS play a vital role in chronic hypoxia induced PH [85]. However, western blot analysis did not show significant differences in JAK2, STAT3 at protein levels (data not shown). Some studies have indicated the overexpression of JAK2 mRNA levels in rats with hypoxia-induced PH [82]. However, other studies failed to show increased JAK2 protein expression in IPAH-HPASMC compared with healthy PASMCs [86].

This shows the difference between transcription and translational regulation mechanisms of JAK2, STAT3 proteins and should be investigated in the future.

### **5.3 Molecular analysis of JAK2-STAT3 signaling in human PASMCs**

In the present study, JAK2 kinase activity and expression were increased in PASMCs derived from patients with IPAH. Dysregulated JAK2-STAT3 signaling is implicated in many human diseases including proliferative disorders and cancers [87]. This led me to study the ruxolitinib as a potent therapeutic option for PAH. Inhibition of JAK2 signaling achieved by ruxolitinib has been approved for the treatment of myeloproliferative disorder, polycythemia vera and GVHD. Additionally, ruxolitinib therapy could also be potentially relevant for vascular and cardiac conditions associated with JAK2 pathway malfunction, including vascular remodeling. Ruxolitinib acts through the inhibition of STAT3 phosphorylation and JAK2 activation in cancer cells [88]. In this study, i demonstrated that ruxolitinib treatment reduced IL-6 induced JAK2-STAT3 activation by inhibiting the JAK activity, i.e. the phosphorylation of STAT3, of both healthy and IPAH PASMCs in time and dose dependent manner.

### **5.4 Effect of ruxolitinib on IL-6 induced proliferation and migration of human PASMCs**

The pro-inflammatory cytokine IL-6 is known to stimulate the hyper-activation of JAK2-STAT3 pathway and leads to various cellular activities including proliferation and migration [89]. In order to examine the functional effect of JAK2 inhibition, ruxolitinib was applied on healthy and IPAH HPASMCs and the cellular phenotype, i.e. proliferation and migration, was assessed. Ruxolitinib has significantly reduced the IL-6 induced proliferation of both types of HPASMCs in a dose-dependent manner. In healthy HPASMCs, ruxolitinib was well-tolerated, showed no cytotoxicity and did not affect cell morphology. Interestingly, IPAH HPASMCs

appeared to be more sensitive towards cell growth arrest induced by ruxolitinib which indicates that IPAH HPASMCs might be easily targeted by ruxolitinib. In line with these findings, results from apoptosis and cell viability experiments showed that ruxolitinib treatment did not induce the apoptosis and not affected the viability of healthy and IPAH HPASMCs. Additionally, at the lower concentration ruxolitinib effectively inhibited the IL-6 induced migration of HPASMCs. These results indicate that the impact of ruxolitinib on PSMCs phenotype is mediated by inhibition of JAK2-STAT3 signaling. Based on these results, ruxolitinib might provide a therapeutic option for experimental PH.

### **5.5 Effect of ruxolitinib in experimental PH models**

Until now the potential effects of Jak inhibition in PAH in vivo have been unclear. But over-activation of Il6-mediated Jak2-Stat3 signaling has been shown to drive PH disease progression in several pre-clinical models and has reached clinical translation [60]. Although there are other studies using different strategies interfering with the IL6-Jak2-Stat3 signaling pathway, the present study focused on investigating the consequence of ruxolitinib application in two established animal models of PH. The MCT rat model of PAH is a common model to perform preclinical testing of potentially new drugs as PSMCs strongly contribute to the hyper-proliferative pathobiological phenotype (PH group 1) [90]. In order to investigate the effect of ruxolitinib in PH due to different etiology, i further studied the JAK2 inhibition in chronic hypoxia-induced mice model of PH. Per definition, the hypoxia-induced PH mouse model resembles PH group 3 and is mainly characterized by highly muscularized small pulmonary arteries, represented mainly by proliferation of PSMCs, fibroblasts and no or very less endothelial cell proliferation [91].

Nevertheless, both models are often used to complement each other. Firstly, the structural remodeling processes in the pulmonary vasculature are slightly different as mentioned before. This means anti-proliferative effects of ruxolitinib are best seen in the MCT model compared to the hypoxia mouse model.

In the chronic hypoxia model, a vasodilatory rather than a reverse remodeling mode of action could be observed which as a conclusion shows the multiple aspects can be addressed with these different experimental models of P(A)H. Secondly, both models allow investigations of right ventricular function and hypertrophy as a process of adaptation to the increased pressure overload in the cardio-pulmonary circulation.

I hypothesize that the cellular mechanism by which ruxolitinib is reversing pulmonary vascular remodeling in PH *in vivo* is probably due to inhibition of the JAK2-STAT3 axis in PASMCs. The pathological role of JAKs and Stat's in oncology has been extensively reviewed [60]. Although the role of JAK2-STAT3 in the pathogenesis of PAH has been described, the molecular mechanisms that induce JAK2-STAT3 activation are currently unknown.

Previous studies have indicated that pro-inflammatory cytokines like IL-1 $\beta$  and IL-6 may play a role in the development of pulmonary hypertension [92, 93]. The contribution of an anti-inflammatory impact of ruxolitinib could be monitored best in the MCT rat model which is also driven by inflammation due to the reactive MCT metabolite monocrotaline pyrrole (MCTP) that initiates pulmonary vascular cell injury.

In the present study, rats treated with MCT displayed increased expression of IL-1 $\beta$  and IL-6 mRNA in the lung tissue. In contrast to that, chronic hypoxia exposed mice lungs showed no such increased expression. Ruxolitinib treatment inhibits the development of pulmonary hypertension and right heart hypertrophy in both animal models of PH but a reduction in the expression of IL-1 $\beta$  and IL-6 mRNA was only observed in chronic hypoxia exposed mice.

In the present study, it indeed became clear that ruxolitinib did not affect muscularization at the level of significance (only with a trend) in the mild mouse model of PH (i.e. hypoxia induced PH) but in the more severe model (i.e. in MCT exposed rats).

Despite evidence suggesting the beneficial effect of ruxolitinib treatment, it was able to lead to an exacerbation of PAH in a myelofibrosis patient for a yet unknown reason [94]. But it has to be mentioned that this is a single case and by the withdrawal of ruxolitinib the symptoms of PAH were resolved. Very recently, a second publication described a decrease in systolic function of the left ventricle after ruxolitinib treatment which further raises the question of adverse events [95]. Although the study has some limitations, it addresses an important fact which is the exact (patho) physiological condition of the heart at the time of ruxolitinib therapy. It has been shown that functional Jak2-Stat3 axis is crucial for proper cardiac function and recovery after stress i.e. a myocardial infraction to prevent heart failure. To the contrary, in another clinical study with 15 myelofibrosis patients, ruxolitinib decreased the plasma levels of several PH biomarkers, led to improvements in echocardiographic findings and to a marked increase in NO levels whereas no changes were noted with conventional therapies [96]. However, no side effects were observed in the

present study. This demonstrates that ruxolitinib is, in principle, able to reverse the PAH associated phenotype.

This data confirm that the JAK2-STAT3 signaling pathway contributes to the disease onset and progression of PH. To my knowledge, this is the first study that demonstrates a therapeutic benefit of JAK2 inhibition by ruxolitinib in preclinical models of PH by improving cardio-pulmonary function. The anti-proliferative effect of this FDA-approved pharmacologic drug underscores the importance of further investigation of its therapeutic potential in PH patients.

## 6. SUMMARY

Pulmonary arterial hypertension (PAH) is characterized by an excessive vascular remodeling, which accounts for the obliteration of the lung vasculature resulting an increase in vascular resistance and mean blood pressure in the pulmonary arteries ultimately leading to right heart failure and death. Vascular remodeling involves increased proliferation of cells in all three layers of the vessels; intimal-endothelial, medial-smooth muscle and adventitial-fibroblast cells. Deciphering the molecular details of aberrant signaling in pulmonary vascular cells in P(A)H is fundamental for the development of new therapeutic strategies.

I aimed to identify tyrosine kinases as new potential drug targets that are dysregulated in PAH by means of a peptide-based kinase activity assay. I performed a tyrosine kinase dependent phosphorylation assay using 144 selected microarrayed kinase substrate peptides. The differential signature of phospho-peptides was used to predict alterations in tyrosine kinase activities in pulmonary arterial smooth muscle cells (HPASMCs) from IPAH patients compared to healthy control cells. Thereby, i observed an over-activation and an increased expression of Janus kinase 2 (Jak2) in HPASMCs from IPAH patients. In line with this finding, increased expression of Jak2 and it's downstream target Stat3 was observed in HPASMCs from IPAH patients as compared to donors. Furthermore, similar upregulation was observed in lung homogenates from MCT rats as compared to healthy rats.

I demonstrated a decrease in proliferation and migration of HPASMCs from healthy individuals as well as from IPAH patients upon exposure to the FDA-approved Jak2-inhibitor ruxolitinib.

*In vivo* experiments were performed in two established experimental models of pulmonary hypertension – MCT rats and chronic hypoxia mice. I demonstrated, ruxolitinib dose-dependently attenuated elevated pulmonary arterial pressure, reduced right heart hypertrophy and restored cardiac index in hypoxia-induced PH in mice and monocrotaline-induced PAH in rats. No adverse events of ruxolitinib on cardiac function could be detected. These results suggest that ruxolitinib is a novel therapeutic agent in PAH by effectively blocking Jak2-Stat3 mediated signaling pathways.

## 7. ZUSAMMENFASSUNG

Die pulmonale arterielle Hypertonie (PAH) ist durch eine abnorme Umwandlung der Pulmonalgefäße gekennzeichnet, welche für die Obliteration dieser Blutgefäße verantwortlich ist. Diese führt zu einem Anstieg des Gefäßwiderstands und des Blutdrucks in den Lungenarterien, was letztlich zur Rechtsherzinsuffizienz und dem vorzeitigen Tod führt. Die Umwandlung der Blutgefäße geht mit einer verstärkten Proliferation der Zellen in allen drei Schichten der Gefäße einher; intimal- Endothelzellen, medial- glatte Muskelzellen und adventitial- Fibroblasten. Die Entschlüsselung der molekularen Details der veränderten Signalübertragung in den Zellen der Pulmonalgefäße in der P(A)H ist essentiell für die Entwicklung neuer therapeutischer Strategien.

Ziel dieser Arbeit war es, durch einen Peptid-basierten Kinaseaktivitätstest, in der PAH deregulierte Tyrosinkinase als neue potenzielle Wirkstoffziele zu identifizieren. Ich habe einen Tyrosinkinase-abhängigen Phosphorylierungstest mit 144 ausgewählten, auf einem Microarray Chip fixierten Kinase-Substrat-Peptiden durchgeführt. Die unterschiedliche Signatur der Phosphopeptide wurde verwendet, um Veränderungen der Tyrosinkinaseaktivitäten in pulmonal arteriellen glatten Muskelzellen (HPASMCs) von IPAH-Patienten, im Vergleich zu gesunden Kontrollzellen, zu prognostizieren. Dabei beobachteten ich eine Überaktivierung und eine erhöhte Expression der Janus-Kinase 2 (Jak2) in HPASMCs von IPAH-Patienten. In Übereinstimmung mit diesen Ergebnissen konnte eine erhöhte Expression von Jak2 und seinem nachgeschalteten Zielprotein Stat3 in HPASMCs von IPAH-Patienten, im Vergleich zu HPASMCs von gesunden Probanden, beobachtet werden. Dieselbe Hochregulation trat auch in Lungenhomogenisaten von MCT Ratten, verglichen mit gesunden Ratten, auf.

Durch die Behandlung mit dem von der FDA zugelassenen Jak2 Inhibitor Ruxolitinib konnten ich eine Abnahme der Proliferation und Migration von HPASMCs von gesunden Probanden, sowie von IPAH-Patienten, zeigen. Die *in vivo* Experimente wurden in zwei etablierten experimentellen Modellen der pulmonalen Hypertonie durchgeführt, MCT-Ratten und chronisch hypoxischen Mäusen. Ich zeigte, dass Ruxolitinib dosisabhängig den pulmonalen arteriellen Druck verringert, die Hypertrophie des rechten Herzens reduziert und den Herzindex, in Hypoxie induzierter PH in Mäusen und in der Monocrotalin induzierten PAH in Ratten, wiederherstellt. Zudem konnten keine Nebenwirkungen von Ruxolitinib auf die Herzfunktion identifiziert werden. Diese Ergebnisse legen nahe, dass Ruxolitinib, ein neuartiges therapeutisches Mittel für die PAH ist, indem es Jak2-Stat3-vermittelte Signalwege effektiv blockiert.

## 8. REFERENCES

1. Simonneau, G., et al., *Haemodynamic definitions and updated clinical classification of pulmonary hypertension*. Eur Respir J, 2019. **53**(1).
2. Hensley, M.K., et al., *Emerging therapeutics in pulmonary hypertension*. Am J Physiol Lung Cell Mol Physiol, 2018. **314**(5): p. L769-L781.
3. Hoeper, M.M., et al., *A global view of pulmonary hypertension*. Lancet Respir Med, 2016. **4**(4): p. 306-22.
4. Simonneau, G., et al., *Updated clinical classification of pulmonary hypertension*. J Am Coll Cardiol, 2013. **62**(25 Suppl): p. D34-41.
5. Sysol, J.R. and R.F. Machado, *Classification and pathophysiology of pulmonary hypertension*. Continuing Cardiology Education, 2018. **4**(1): p. 2-12.
6. Humbert, M., et al., *Pathology and pathobiology of pulmonary hypertension: state of the art and research perspectives*. Eur Respir J, 2019. **53**(1).
7. Frid, M.G., et al., *Inflammation, immunity, and vascular remodeling in pulmonary hypertension; Evidence for complement involvement?* Glob Cardiol Sci Pract, 2020. **2020**(1): p. e202001.
8. Huber, L.C., H. Bye, and M. Brock, *The pathogenesis of pulmonary hypertension--an update*. Swiss Med Wkly, 2015. **145**: p. w14202.
9. Mandegar, M., et al., *Cellular and molecular mechanisms of pulmonary vascular remodeling: role in the development of pulmonary hypertension*. Microvasc Res, 2004. **68**(2): p. 75-103.
10. Deanfield, J.E., J.P. Halcox, and T.J. Rabelink, *Endothelial function and dysfunction: testing and clinical relevance*. Circulation, 2007. **115**(10): p. 1285-95.
11. Budhiraja, R., R.M. Tuder, and P.M. Hassoun, *Endothelial dysfunction in pulmonary hypertension*. Circulation, 2004. **109**(2): p. 159-65.
12. Hughes, J.M., *Hypoxic pulmonary vasoconstriction: clinical implications*. Eur Respir J, 2016. **47**(1): p. 31-4.
13. Schermuly, R.T., et al., *Mechanisms of disease: pulmonary arterial hypertension*. Nat Rev Cardiol, 2011. **8**(8): p. 443-55.
14. Johnson, S.R., J.T. Granton, and S. Mehta, *Thrombotic arteriopathy and anticoagulation in pulmonary hypertension*. Chest, 2006. **130**(2): p. 545-52.
15. Lannan, K.L., R.P. Phipps, and R.J. White, *Thrombosis, platelets, microparticles and PAH: more than a clot*. Drug Discov Today, 2014. **19**(8): p. 1230-5.

16. Humbert, M., et al., *Cellular and molecular pathobiology of pulmonary arterial hypertension*. J Am Coll Cardiol, 2004. **43**(12 Suppl S): p. 13S-24S.
17. Tuder, R.M., *Pulmonary vascular remodeling in pulmonary hypertension*. Cell Tissue Res, 2017. **367**(3): p. 643-649.
18. Tuder, R.M., et al., *Pathology of pulmonary hypertension*. Clin Chest Med, 2007. **28**(1): p. 23-42, vii.
19. Archer, S.L., E.K. Weir, and M.R. Wilkins, *Basic science of pulmonary arterial hypertension for clinicians: new concepts and experimental therapies*. Circulation, 2010. **121**(18): p. 2045-66.
20. Sartore, S., et al., *Contribution of adventitial fibroblasts to neointima formation and vascular remodeling: from innocent bystander to active participant*. Circ Res, 2001. **89**(12): p. 1111-21.
21. Stenmark, K.R., et al., *Role of the adventitia in pulmonary vascular remodeling*. Physiology (Bethesda), 2006. **21**: p. 134-45.
22. Mitchell, J.A., et al., *Role of prostacyclin in pulmonary hypertension*. Glob Cardiol Sci Pract, 2014. **2014**(4): p. 382-93.
23. Said, S.I., *Mediators and modulators of pulmonary arterial hypertension*. Am J Physiol Lung Cell Mol Physiol, 2006. **291**(4): p. L547-58.
24. Lan, N.S.H., et al., *Pulmonary Arterial Hypertension: Pathophysiology and Treatment*. Diseases, 2018. **6**(2).
25. Naeije, R. and S. Eddahibi, *Serotonin in pulmonary arterial hypertension*. Am J Respir Crit Care Med, 2004. **170**(3): p. 209-10.
26. Antoniu, S.A., *Targeting PDGF pathway in pulmonary arterial hypertension*. Expert Opin Ther Targets, 2012. **16**(11): p. 1055-63.
27. Schermuly, R.T., et al., *Reversal of experimental pulmonary hypertension by PDGF inhibition*. J Clin Invest, 2005. **115**(10): p. 2811-21.
28. Kherbeck, N., et al., *The role of inflammation and autoimmunity in the pathophysiology of pulmonary arterial hypertension*. Clin Rev Allergy Immunol, 2013. **44**(1): p. 31-8.
29. Sprague, A.H. and R.A. Khalil, *Inflammatory cytokines in vascular dysfunction and vascular disease*. Biochem Pharmacol, 2009. **78**(6): p. 539-52.
30. Lau, E.M.T., et al., *Epidemiology and treatment of pulmonary arterial hypertension*. Nat Rev Cardiol, 2017. **14**(10): p. 603-614.
31. Humbert, M. and H.A. Ghofrani, *The molecular targets of approved treatments for pulmonary arterial hypertension*. Thorax, 2016. **71**(1): p. 73-83.
32. Perrin, S., et al., *New pharmacotherapy options for pulmonary arterial hypertension*. Expert Opin Pharmacother, 2015. **16**(14): p. 2113-31.

33. Roskoski, R., Jr., *Properties of FDA-approved small molecule protein kinase inhibitors*. Pharmacol Res, 2019. **144**: p. 19-50.
34. Godinas, L., et al., *Tyrosine kinase inhibitors in pulmonary arterial hypertension: a double-edge sword?* Semin Respir Crit Care Med, 2013. **34**(5): p. 714-24.
35. Alexander, S.P., et al., *THE CONCISE GUIDE TO PHARMACOLOGY 2017/18: Transporters*. Br J Pharmacol, 2017. **174 Suppl 1**: p. S360-S446.
36. Milara, J., et al., *JAK2 mediates lung fibrosis, pulmonary vascular remodelling and hypertension in idiopathic pulmonary fibrosis: an experimental study*. Thorax, 2018. **73**(6): p. 519-529.
37. Weiss, A., et al., *Kinases as potential targets for treatment of pulmonary hypertension and right ventricular dysfunction*. Br J Pharmacol, 2019.
38. Weiss, A., et al., *Targeting cyclin-dependent kinases for the treatment of pulmonary arterial hypertension*. Nat Commun, 2019. **10**(1): p. 2204.
39. Villarino, A.V., Y. Kanno, and J.J. O'Shea, *Mechanisms and consequences of Jak-STAT signaling in the immune system*. Nat Immunol, 2017. **18**(4): p. 374-384.
40. Thomas, S.J., et al., *The role of JAK/STAT signalling in the pathogenesis, prognosis and treatment of solid tumours*. Br J Cancer, 2015. **113**(3): p. 365-71.
41. Wilks, A.F., *The JAK kinases: not just another kinase drug discovery target*. Semin Cell Dev Biol, 2008. **19**(4): p. 319-28.
42. Heinrich, P.C., et al., *Interleukin-6-type cytokine signalling through the gp130/Jak/STAT pathway*. Biochem J, 1998. **334 ( Pt 2)**: p. 297-314.
43. Banerjee, S., et al., *JAK-STAT Signaling as a Target for Inflammatory and Autoimmune Diseases: Current and Future Prospects*. Drugs, 2017. **77**(5): p. 521-546.
44. Babon, J.J., et al., *The molecular regulation of Janus kinase (JAK) activation*. Biochem J, 2014. **462**(1): p. 1-13.
45. Levy, D.E. and J.E. Darnell, Jr., *Stats: transcriptional control and biological impact*. Nat Rev Mol Cell Biol, 2002. **3**(9): p. 651-62.
46. Pencik, J., et al., *JAK-STAT signaling in cancer: From cytokines to non-coding genome*. Cytokine, 2016. **87**: p. 26-36.
47. Heinrich, P.C., et al., *Principles of interleukin (IL)-6-type cytokine signalling and its regulation*. Biochem J, 2003. **374**(Pt 1): p. 1-20.
48. Quintas-Cardama, A. and S. Verstovsek, *Molecular pathways: Jak/STAT pathway: mutations, inhibitors, and resistance*. Clin Cancer Res, 2013. **19**(8): p. 1933-40.
49. Li, W.X., *Canonical and non-canonical JAK-STAT signaling*. Trends Cell Biol, 2008. **18**(11): p. 545-51.

50. Welsch, K., et al., *Targeting JAK/STAT signalling in inflammatory skin diseases with small molecule inhibitors*. Eur J Immunol, 2017. **47**(7): p. 1096-1107.
51. Tsurumi, A., C. Zhao, and W.X. Li, *Canonical and non-canonical JAK/STAT transcriptional targets may be involved in distinct and overlapping cellular processes*. BMC Genomics, 2017. **18**(1): p. 718.
52. Hixson, K.M., et al., *Evidence for a non-canonical JAK/STAT signaling pathway in the synthesis of the brain's major ion channels and neurotransmitter receptors*. BMC Genomics, 2019. **20**(1): p. 677.
53. Yu, H., et al., *Revisiting STAT3 signalling in cancer: new and unexpected biological functions*. Nat Rev Cancer, 2014. **14**(11): p. 736-46.
54. Groner, B. and V. von Manstein, *Jak Stat signaling and cancer: Opportunities, benefits and side effects of targeted inhibition*. Mol Cell Endocrinol, 2017. **451**: p. 1-14.
55. O'Shea, J.J., S.M. Holland, and L.M. Staudt, *JAKs and STATs in immunity, immunodeficiency, and cancer*. N Engl J Med, 2013. **368**(2): p. 161-70.
56. Bourgeais, J., et al., *Oncogenic STAT5 signaling promotes oxidative stress in chronic myeloid leukemia cells by repressing antioxidant defenses*. Oncotarget, 2017. **8**(26): p. 41876-41889.
57. Zimmers, T.A., M.L. Fishel, and A. Bonetto, *STAT3 in the systemic inflammation of cancer cachexia*. Semin Cell Dev Biol, 2016. **54**: p. 28-41.
58. Cracowski, J.L., et al., *Proinflammatory cytokine levels are linked to death in pulmonary arterial hypertension*. Eur Respir J, 2014. **43**(3): p. 915-7.
59. Grote, K., M. Luchtefeld, and B. Schieffer, *JANUS under stress--role of JAK/STAT signaling pathway in vascular diseases*. Vascul Pharmacol, 2005. **43**(5): p. 357-63.
60. Paulin, R., J. Meloche, and S. Bonnet, *STAT3 signaling in pulmonary arterial hypertension*. JAKSTAT, 2012. **1**(4): p. 223-33.
61. Wang, G.S., et al., *[Changes of interleukin-6 and Janus kinases in rats with hypoxic pulmonary hypertension]*. Zhonghua Jie He He Hu Xi Za Zhi, 2003. **26**(11): p. 664-7.
62. Christmann, R.B., et al., *Interferon and alternative activation of monocyte/macrophages in systemic sclerosis-associated pulmonary arterial hypertension*. Arthritis Rheum, 2011. **63**(6): p. 1718-28.
63. McMurtry, M.S., et al., *Gene therapy targeting survivin selectively induces pulmonary vascular apoptosis and reverses pulmonary arterial hypertension*. J Clin Invest, 2005. **115**(6): p. 1479-91.
64. Padma, R. and L. Nagarajan, *The human PIM-1 gene product is a protein serine kinase*. Cancer Res, 1991. **51**(9): p. 2486-9.

65. Bousoik, E. and H. Montazeri Aliabadi, *"Do We Know Jack" About JAK? A Closer Look at JAK/STAT Signaling Pathway*. Front Oncol, 2018. **8**: p. 287.
66. Vainchenker, W., et al., *JAK inhibitors for the treatment of myeloproliferative neoplasms and other disorders*. F1000Res, 2018. **7**: p. 82.
67. Mascarenhas, J. and R. Hoffman, *Ruxolitinib: the first FDA approved therapy for the treatment of myelofibrosis*. Clin Cancer Res, 2012. **18**(11): p. 3008-14.
68. Shi, J.G., et al., *The pharmacokinetics, pharmacodynamics, and safety of orally dosed INCB018424 phosphate in healthy volunteers*. J Clin Pharmacol, 2011. **51**(12): p. 1644-54.
69. Shilling, A.D., et al., *Metabolism, excretion, and pharmacokinetics of [14C]INCB018424, a selective Janus tyrosine kinase 1/2 inhibitor, in humans*. Drug Metab Dispos, 2010. **38**(11): p. 2023-31.
70. Verstovsek, S., et al., *Safety and efficacy of INCB018424, a JAK1 and JAK2 inhibitor, in myelofibrosis*. N Engl J Med, 2010. **363**(12): p. 1117-27.
71. Aittomaki, S. and M. Pesu, *Therapeutic targeting of the Jak/STAT pathway*. Basic Clin Pharmacol Toxicol, 2014. **114**(1): p. 18-23.
72. Firth, A.L., J. Mandel, and J.X. Yuan, *Idiopathic pulmonary arterial hypertension*. Dis Model Mech, 2010. **3**(5-6): p. 268-73.
73. Jasmin, J.F., et al., *Effectiveness of a nonselective ET(A/B) and a selective ET(A) antagonist in rats with monocrotaline-induced pulmonary hypertension*. Circulation, 2001. **103**(2): p. 314-8.
74. Stenmark, K.R., et al., *Animal models of pulmonary arterial hypertension: the hope for etiological discovery and pharmacological cure*. Am J Physiol Lung Cell Mol Physiol, 2009. **297**(6): p. L1013-32.
75. Arsenault, R., P. Griebel, and S. Napper, *Peptide arrays for kinome analysis: new opportunities and remaining challenges*. Proteomics, 2011. **11**(24): p. 4595-609.
76. Anderson, J.C., et al., *Correction: Kinomic Profiling of Electromagnetic Navigational Bronchoscopy Specimens: A New Approach for Personalized Medicine*. PLoS One, 2016. **11**(8): p. e0161986.
77. Anderson, J.C., et al., *High Throughput Kinomic Profiling of Human Clear Cell Renal Cell Carcinoma Identifies Kinase Activity Dependent Molecular Subtypes*. PLoS One, 2015. **10**(9): p. e0139267.
78. Tamura, Y., et al., *Ectopic upregulation of membrane-bound IL6R drives vascular remodeling in pulmonary arterial hypertension*. J Clin Invest, 2018. **128**(5): p. 1956-1970.
79. Ghofrani, H.A., et al., *Imatinib in pulmonary arterial hypertension patients with inadequate response to established therapy*. Am J Respir Crit Care Med, 2010. **182**(9): p. 1171-7.

80. Liu, T., et al., *Regulation of S100A4 expression via the JAK2-STAT3 pathway in rhomboid-phenotype pulmonary arterial smooth muscle cells exposure to hypoxia*. Int J Biochem Cell Biol, 2012. **44**(8): p. 1337-45.
81. Zhang, L., et al., *Inhibition of PDGF-BB-induced proliferation and migration in VSMCs by proanthocyanidin A2: Involvement of KDR and Jak-2/STAT-3/cPLA2 signaling pathways*. Biomed Pharmacother, 2018. **98**: p. 847-855.
82. Milara, J., et al., *The JAK2 pathway is activated in idiopathic pulmonary fibrosis*. Respir Res, 2018. **19**(1): p. 24.
83. Courboulin, A., et al., *Kruppel-like factor 5 contributes to pulmonary artery smooth muscle proliferation and resistance to apoptosis in human pulmonary arterial hypertension*. Respir Res, 2011. **12**: p. 128.
84. Helkin, A., K.G. Maier, and V. Gahtan, *Thrombospondin-1, -2 and -5 have differential effects on vascular smooth muscle cell physiology*. Biochem Biophys Res Commun, 2015. **464**(4): p. 1022-1027.
85. Maarman, G., et al., *A comprehensive review: the evolution of animal models in pulmonary hypertension research; are we there yet?* Pulm Circ, 2013. **3**(4): p. 739-56.
86. Courboulin, A., et al., *Role for miR-204 in human pulmonary arterial hypertension*. J Exp Med, 2011. **208**(3): p. 535-48.
87. Yoshikawa, T., et al., *JAK2/STAT3 pathway as a therapeutic target in ovarian cancers*. Oncol Lett, 2018. **15**(4): p. 5772-5780.
88. Quintas-Cardama, A., et al., *Preclinical characterization of the selective JAK1/2 inhibitor INCB018424: therapeutic implications for the treatment of myeloproliferative neoplasms*. Blood, 2010. **115**(15): p. 3109-17.
89. Wang, S.W. and Y.M. Sun, *The IL-6/JAK/STAT3 pathway: potential therapeutic strategies in treating colorectal cancer (Review)*. Int J Oncol, 2014. **44**(4): p. 1032-40.
90. Sztuka, K. and M. Jasinska-Stroschein, *Animal models of pulmonary arterial hypertension: A systematic review and meta-analysis of data from 6126 animals*. Pharmacol Res, 2017. **125**(Pt B): p. 201-214.
91. Lee, Y.S., et al., *Monocrotaline-induced pulmonary hypertension correlates with upregulation of connective tissue growth factor expression in the lung*. Exp Mol Med, 2005. **37**(1): p. 27-35.
92. Rabinovitch, M., et al., *Inflammation and immunity in the pathogenesis of pulmonary arterial hypertension*. Circ Res, 2014. **115**(1): p. 165-75.
93. Groth, A., et al., *Inflammatory cytokines in pulmonary hypertension*. Respir Res, 2014. **15**: p. 47.

94. Low, A.T., et al., *Pulmonary arterial hypertension exacerbated by ruxolitinib*. *Haematologica*, 2015. **100**(6): p. e244-5.
95. Miyawaki, H., et al., *Long-term Effects of the Janus Kinase 1/2 Inhibitor Ruxolitinib on Pulmonary Hypertension and the Cardiac Function in a Patient with Myelofibrosis*. *Intern Med*, 2020. **59**(2): p. 229-233.
96. Tabarroki, A., et al., *Ruxolitinib leads to improvement of pulmonary hypertension in patients with myelofibrosis*. *Leukemia*, 2014. **28**(7): p. 1486-93.

## 9. DECLARATION

I declare that I have completed this dissertation on my own without the unauthorized help of a second party and only with the assistance acknowledged therein. I have appropriately acknowledged and referenced all text passages that are derived literally from or are based on the content of published or unpublished work of others, and all information that relates to verbal communications. I have abided by the principles of good scientific conduct laid down in the charter of the Justus Liebig University of Giessen in carrying out the investigations described in the dissertation.

Giessen, November 6<sup>th</sup> 2020

---

(Yerabolu Naga Dinesh Reddy)

## 10. ACKNOWLEDGEMENTS

I would like to thank everyone who contributed to the successful outcome of this work.

First and foremost, I would like to thank my supervisor, **Prof. Dr. Ralph Schermuly**, for providing me with an opportunity to work in his lab and learn under his supervision.

His outstanding counseling and the intriguing discussions helped me during my research and the writing of this thesis.

I would like to express my sincere gratitude to **Prof. Dr. Reinhard Dammann** of the Institute of Genetics for his insightful comments and encouragements as well as his willingness to participate as my external supervisor. Additionally, my sincere appreciation goes to **Prof. Dr. Norbert Weissmann**, and **Prof. Dr. Sandra Hake** who support me as members of my thesis committee.

I would especially like to express my gratitude to, **Dr. Astrid Weiss**, for her scientific guidance and support, whenever I had questions regarding this and other topics.

I would also like to thank **Dr. Baktybek Kojonajarov, Christina Vroom and Sophia Hattesoehl** for helping me with the animal experiments. Very special thanks to **Beate Schlueter** for writing the German translation of my thesis summary.

I would also like to thank all my lab mates. I especially appreciate the time spent with **Dr. Mario Böhm, Beate Schlueter, Mona Hoeret, Kerstin Gernert** as colleagues. They created a great work atmosphere and supporting me during the last five years.

Last but not least, I want to thank my parents, **Satyanarayana Reddy** and **Sailaja**, my wife **Himabindu**. All of them supported me considerably in the completion of this work and guided me throughout my Ph.D. years by giving me the moral support I need to keep going.

I dedicate this work to my father and grandmother **Seetharavamma**.